ANALYSIS OF CORTICAL AND THALAMIC CONTRIBUTORS TO FUNCTIONAL ORGANIZATION OF PRIMATE PRIMARY VISUAL CORTEX (V1)

By

Ilya Khaytin

Dissertation

Submitted to the Faculty of the

Graduate School of Vanderbilt University

in partial fulfillment of the requirements

for the degree of

DOCTOR OF PHILOSOPHY

in

Neuroscience

May, 2008

Nashville, Tennessee

Approved:

Professor Jon H. Kaas

Professor Anna W. Roe

Professor A. B. Bonds, III

Professor Vivien A. Casagrande

Professor John Gore

ACKNOWLEDGEMENTS

I would like to thank my parents. My mom believed in me. Without her selfless efforts to guide my education I would not even be writing these words. My father left his whole life behind in Russia, so that I could get best education.

I would like to express my gratitude to Vivien Casagrande. She helped me through thick and thin. She taught me how to do research and think critically. She pushed me beyond my comfort zone and helped me combat some of my fears. All these years, she has been a wonderful adviser, teacher, and mentor. With her every day work, she set an example for me of being a scientist and a person. Thank you, Vivien.

I would also like to express my gratitude to Julie Mavity-Hudson. She kept me sane, during tough times and went above and beyond call of duty to help me when I needed it. She helped me with experiments, English, and advice. She was a real friend. Thank you, Julie.

I would like to thank my collaborators. Ralph Siegel, who, between reminding me about my Jewish roots, helped me understand fine points about the methods that I used. I would like to thank Gopathy Purushothaman, who demonstrated the level of clarity in his thoughts and writing, which I am still learning to achieve. I would like to thank Xin Chen who was a friend for all these years. He stayed with me all those imaging nights and helped me keep going. I would also like to thank David Royal. His ideas made me think more critically of what I do, and his advice made sailing these waters a bit easier. I would like to thank Xiangmin Xu, who introduced me to optical imaging, gave me first lessons of research and made my first experiments mysteriously

productive. I would like also to thank Christine Collins. She was expecting a baby and still was willing to take shifts in imaging.

I would like to thank Walter Jermakowicz, my fellow MSTP, who helped me when I needed and kept me company during experiments. I also thank him for helping me proof much of my writing. I also would like to thank Roan Marion for all his time. I thank Octavio Ruiz who challenged my thinking.

I would like to thank Mary Early-Zald for all the candies that she let me 'borrow.' She worked to keep me on track and going toward this point. I thank Shirin Pulous for all the reminders that she sent. I thank all the people who worked in our lab, David Godlove, Maria Tamborski, Soo Ryum Yang and many others.

I would like to thank Dan Shima for helping with imaging set up, and making sure my stimuli worked. I would like to thank David Schaffer for help with making injectrodes and being willing to tolerate my sudden appearances. I would like to thank Mary Feurtado for making sure my monkeys live and making sure they are ready for my experiments. I would like to thank Robert Friedman for help with optical imaging. I would like to thank all the veterinarians and animal care technicians for keeping my animals happy. I would like to thank Maria Couppis, Erik Emeric, and Corrie Camalier taking time to talk to me.

Finally, I would like to thank my thesis committee, AB Bonds, Anna Roe, Jon Kaas and John Gore. They challenged me to become better scientist and asked questions that I needed to be asked.

TABLE OF CONTENTS

Page

ACKNOWLEDGEMENTS ii

LIST OF FIGURES vii

LIST OF TABLES x

Chapter

I. PREFACE 1

II. BACKGROUND 4
Organization of lateral geniculate nucleus 5
Functional organization of V1 6
Parsing geniculate input to V1 9
Effects of feedback inputs on functional properties of V1 10
The overall goals of this thesis 12

III. ANIMAL MODELS AND INVESTIGATIVE TECHNIQUE 13
Animal models 13
Bush baby as a model organism 13
Owl monkey as a model organism 18
Optical imaging 19
Advantages of optical imaging 20
Sources of imaging signals 22
Analysis methods 25
Verifying optical imaging credibility 29
Conclusion 31

IV. FUNCTIONAL ORGANIZATION OF TEMPORAL FREQUENCY SELECTIVITY IN PRIMATE VISUAL CORTEX 35
Introduction 36
Methods 38
Animals 38
Surgery and perfusion 40
Histology and Alignment 41
Optical imaging 44
Analysis 46
Results 51
Mapping V1 and aligning images 51
Responses at different temporal frequencies 53

Structure of single condition maps at different temporal frequencies 55
Structure of differential maps at different temporal frequencies using sine-wave gratings 57
Quantification of center of mass locations 61
Invariance of orientation domains with respect to temporal frequency changes 62
Automatic classification of z-normalized images 65
Absence of visible temporal frequency preference domains 66
Quantification of response strength at different temporal frequencies 69
CO domain dependence of temporal frequency tuning 70
Discussion 73
Mapping of visual features in bush baby 77
Functional maps in other species 78
Are feature maps stable? 80

V. THE EFFECT OF REMOVING P OR M LGN INPUT ON FUNCTIONAL MAPS IN V1 OF BUSH BABY 82
Preface 82
Introduction 82
Methods 86
Animals 86
Surgery and perfusion 86
Muscimol injection 87
Histology and alignment 90
Optical imaging 90
Analysis 92
Results 92
Effect of blocking the P channel 92
Response to the moving sinusoidal grating 95
Signal strength before and after block 96
Orientation preference with and without P layer input 97
Spatial frequency preference with and without P layer input 97
Effects of the M layer block on activity in V1 102
Discussion 107
The classical model 108
Support of the modified classical model 109
Mystery of the M block effects 110
Role of the LGN inputs in function of V1 111

VI. THE ORGANIZATION OF THE MIDDLE TEMPORAL (MT) AREA IN OWL MONKEYS 115
Preface 115

Part 1: Background 116
Connections of MT 116
Functional properties of MT 118

Part 2: The Middle Temporal (MT) Visual Area: What rules apply to its retinotopic organization? 119
Introduction....119
Methods....120
Animals....120
Surgery and histology....121
Imaging....122
Analysis....123
Results....124
Retinotopic organization of Owl Monkey area MT....124
Cortical Magnification factor (CMF) calculations....126
Comparison with other primates....127
Relationship between V1 and MT....127
Discussion....132
What can account for the organization in area MT?....132
Scaling across parallel pathways....133

Part 3: Unequal representation of visual space in area MT....135
Introduction....135
Methods....137
Results....138
Discussion....141

VII. EEFFECT S OF BLOCKING V1 AND MT: FUNCTIONAL TESTS OF FEEDFORWARD AND FEEDBACK PATHWAYS....143
Preface....143

Part 1: Optical imaging of visually evoked responses in the middle temporal area after deactivation of primary visual cortex in adult primates....144
Introduction....144
Methods....145
Results....147
Discussion....149

Part 2: Effect of blocking middle temporal area in bush baby on activity in V1 151
Introduction....151
Methods....154
Results....155
Discussion....158

VIII. CONCLUSIONS....161
Summary of results....161
Future directions....164

REFERENCES....166

LIST OF FIGURES

Figure		Page
3-1	Nissl stained section of bush baby LGN	16
3-2	Dorso-lateral view of the bush baby brain with major visual areas marked	17
3-3	Differential images of orientation preference in bush baby V1	32
3-4	Demonstration of the effect of low-pass filtering on the final orientation preference map	33
3-5	Quantification of the number of pinwheels per mm^2 in relationship to the average size of filter	34
4-1	Three predictions concerning the relationship between temporal frequency and orientation preference domains	39
4-2	Histological alignment and activation from one case (06-07)	43
4-3	Pixel-wise linear fit	50
4-4	Single condition activation patterns	54
4-5	Analysis of low magnification single condition maps at different temporal frequencies (case 06-07)	58
4-6	Analysis of high magnification single condition maps at different temporal frequencies (case 06-07)	59
4-7	Differential images at different temporal frequencies acquired using sine wave gratings	60
4-8	Locations of centers of mass of domains identified in Figures 4-5 and 4-6	63
4-9	Cross-correlation coefficient as a function of independent random shift of activation domains	64
4-10	Dendrogram showing similarity between sixteen z-normalized conditions	67
4-11	Orientation and temporal frequency preference images	68
4-12	Response strengths at different temporal frequencies	71

4-13 Example of thresholding method to separate CO compartments in V1 (case 06-07)....72

4-14 Response strength at different temporal frequencies in blob and interblob subdomains....74

4-15 Comparison of activation domains different temporal frequencies to average orientation domains....75

5-1 A schematic indicating some of the main intrinsic and extrinsic connections of V1 in primates....84

5-2 Photomicrograph of the tip if the injectrode....88

5-3 Schematic diagram of the LGN layer blocking experiment....91

5-4 Bush baby LGN....93

5-5 Responses of bush baby V1 to stimuli at four orientations and four spatial frequencies before block....94

5-6 Effect of blocking the Pc layer of LGN....98

5-7 Example of orientation preference domains in V1 before and after P channel block....99

5-8 Example of spatial frequency preference domains in V1 before and after P channel block....100

5-9 Spatial frequency (SF) preference in V1 before and after P channel block....101

5-10 Image of bush baby LGN showing injection into the contralaterally innervated M layer....103

5-11 Orientation preference responses before and after M channel block....104

5-12 Winner-take-all (WTA) maps of spatial frequency preference before and after M channel block....105

6-1 Activation of MT by 0/90 degree gratings inside a circular window centered on the *area centralis*....125

6-2 Cortical magnification factor curve in owl monkey MT....128

6-3 Plot of CMF curves for four primate species....129

6-4 Unequal representation of cardinal and oblique orientations in owl monkey MT....139

6-5 Point spread activation produced from circular stimulus patches 140

7-1 Effect of blocking part of V1 on the activity in MT 148

7-2 Effect of blocking retinotopically matching part of MT on activity in V1.....156

7-3 Quantification of the activation in owl monkey V1 before and after blocking MT.....157

LIST OF TABLES

Table Page

6-1 Summary data of cortical magnification factors and surface areas in V1 and MT across four primates 131

CHAPTER I

PREFACE

Recent decades have seen tremendous advances in our understanding of the organization and function of primary visual cortex (V1). Since the early work of Hubel and Wiesel (1962; 1968; 1969), it has become clear that the visual cortex of primates and carnivores is organized into functional domains. For example, extensive electrophysiological (Berardi et al., 1982; Berman et al., 1987; Hubel and Wiesel, 1977; Maffei and Fiorentini, 1977; Tolhurst et al., 1981; Tolhurst and Thompson, 1982; Tootell et al., 1981) and functional (Malach et al., 1997; Tootell et al., 1988a; 1988b; 1988c; 1988d; 1988e) studies in visual cortex have shown that cells are clustered into domains according to their principle properties such as ocular dominance, orientation preference, and spatial frequency preference. Anatomical studies (see Casagrande and Kaas, 1994 for review) have demonstrated that primary visual cortex has a complex internal structure and extensive connections to extrastriate cortical areas such as the medial temporal (MT) visual area and multiple subcortical structures such as the lateral geniculate nucleus (LGN) of thalamus. Moreover, the LGN sends information to V1 along at least three separate pathways, the magnocellular (M), parvocellular (P), and koniocellular (K), with the M and P pathways providing the bulk of visual information. These three pathways carry information about visual features by coding different spatial and temporal frequencies, and contrast (Casagrande and Norton, 1991). Although information from the three input pathways to V1 from LGN is combined in different ways within V1 some

have argued that the signatures of the input pathways can be recognized in V1 and that they are utilized in different ways by different cell groups (Casagrande and Kaas, 1994; Casagrande and Xu, 2004).

Although a lot is understood about the properties and potential roles of the feedforward pathways to V1 much less is understood about the massive feedback that this area also receives. Interestingly, electrophysiological experiments seem to show that the latency of this feedback is so short (Hupe et al., 2001) that it can affect the functional properties of V1 even before some of the information arrives via the feedforward pathways. The question that remains to be answered is how this varied array of feedforward and feedback projections affect the overall functional organization of V1.

The present work is organized as follows. In addition to this chapter, the second chapter provides background on the functional and anatomical organization of the visual system relevant to the specific questions addressed in this thesis. The third chapter reviews the methodology of optical imaging of intrinsic signals, the primary method of data collection used in this thesis. This chapter reviews issues concerning the measurement of optical signals as an indicator of brain activity, and outlines the reasons for using optical imaging in the species I have chosen for my work, namely owl monkeys and bush babies. The fourth chapter focuses on examining whether different temporal frequencies are mapped as separate domains in primary visual cortex (V1). This work, which has already been published, was carried out to fill in a missing piece of information concerning the representation of sensory features in V1. This study showed that, unlike spatial frequency and orientation, temporal frequency is not mapped in separate domains. The fifth chapter is concerned with the roles of the primary

feedforward channels to V1, namely the M and P channels, in setting up functional maps. Although the data here are still preliminary, they confirm that orientation domain structure is not dependent on either the M or P pathway, but that the map of spatial frequency is altered by removal of one LGN channel. The sixth and seventh chapters address the role of feedback from one extrastriate area, the middle temporal (MT) visual area, on the functional organization of V1. In chapter six, the organization of MT is shown to have an orderly visuotopic map in owl monkeys. Then the question of anisotropies in the visual space representations in MT is addressed. Finally, in chapter seven the issue of interdependence of MT and V1 on each others' inputs is investigated. MT's dependence on V1 for its main drive is considered, and evidence is presented that blocking feedback from MT can alter both the magnitude of V1 responses and the temporal frequency profile of V1 populations. In the final chapter, the summary of my main results and directions for future research are provided.

CHAPTER II

BACKGROUND

Primates critically depend upon vision for their survival. Inspection of flattened cortices in various primate species shows that areas devoted to the analysis of visual stimuli occupy a significant proportion of cortex (see Kaas, 1996 for review). Felleman and Van Essen (1991) proposed, based on previous electrophysiological and anatomical studies, that the macaque visual system includes at least 32 visual areas. Although there is debate as to the exact number of visual areas that exist (Kaas and Lyon, 2001), more recent fMRI studies tend to agree that humans have even more areas (Stiers et al., 2006).

Data also support the idea that these visual areas are densely interconnected (Gattass et al., 2005). In fact, the average number of area-to-area connections is almost equal to the total number of areas squared (Changizi and Shimojo, 2005). Moreover, contrary to the accepted "textbook" version of cortical organization and processing, the feedback connections far outnumber the feedforward hierarchical connections (Bullier et al., 2001). Therefore, it is hard to imagine that processing of visual information in one area is not influenced by the input from all of the other cortical and subcortical areas to which it is connected. This may seem like a trivial and obvious point but emphasis over the past decades has been placed heavily on the contributions of feedforward pathways with much less emphasis on what feedback and lateral connections provide.

The overarching hypothesis uniting the series of studies described below is that the basic functional organization of primary visual cortex (V1) is influenced by combined

input from *both* lower and higher visual areas. More specifically, the studies in this thesis were designed to investigate how inputs from lateral geniculate nucleus (LGN) and middle temporal (MT) visual area impact the functional maps in V1. This chapter reviews relevant background information that places the following studies in the broader framework of current knowledge. First, general information concerning the anatomical and functional organization of LGN, V1 and MT are reviewed, and then background relevant to each specific study is examined in turn.

Organization of the lateral geniculate nucleus

The primate dorsal lateral geniculate nucleus receives its driving input from several distinct classes of retinal ganglion cells, the two major classes being midget and parasol cells (for review see Casagrande and Norton, 1991; Casagrande and Xu, 2004). The latter project to the two major subdivisions of LGN, namely, the parvocellular (P) and magnocellular (M) layers, respectively. The other subdivision of the LGN includes the koniocellular (K) layers which receive input from several classes of retinal ganglion cells (Dacey et al., 2003). In all primates each layer of the LGN receives input from only one half of the retina, either the nasal retina from the opposite eye (contralateral) or the temporal retina from the eye on the same side (ipsilateral). Therefore, the standard primate LGN pattern consists of at least one P and one M cellular layer for each ocular input. In some primates the portion of the P layers representing central vision can split into 2 layers creating 4 P layers, however, in primates that are the subject of this thesis, bush babies and owl monkeys, only the standard 2 P and 2 M layer pattern is observed (Casagrande et al., 2007; Kaas et al., 1978).

The major geniculate subdivisions are segregated not only anatomically, but also functionally. Geniculate cells retain the same basic receptive field structure as their afferent ganglion cell inputs (for review see Casagrande and Norton, 1991). In comparison to P cells, M cell receptive fields are larger at the same retinotopic representation. M cells, on average, respond to stimuli at lower contrast, lower spatial frequencies and higher temporal frequencies than P cells. Their response is more phasic and they conduct at a faster rate than P cells. Responses of K cells lie somewhere between those two extremes, although the majority of K cells have conduction velocities even slower than those of P cells. In some primates K cells (and in trichromaic primates also P cells) can carry chromatic signals. Based on differences between P and M cells it has been speculated that the P pathway to V1 is designed to carry information relevant to object vision while the M pathway is better suited to carrying information relevant to motion vision (Livingstone and Hubel, 1988). However, studies involving lesions of the M or P pathway do not support such a simplistic view (Merigan and Maunsell, 1990; Schiller et al., 1990). We will return to the issue of the potential roles of theses pathways below.

Functional organization of V1

The primary visual cortex (V1) combines LGN afferent inputs to produce several emergent properties. Unlike the majority of the geniculate neurons, which respond to stimuli from only one eye, many neurons in V1 respond to input from both eyes (Casagrande and Ichida, 2002). Another important property of V1 neurons is orientation preference. Although some studies in primates have shown that a subset of LGN cells

show a bias for stimuli presented at one orientation, geniculate cells still respond well at all other orientations (Xu et al., 2002). The majority of primate V1 cells are, however, sharply tuned for orientation and do not respond to stimuli at the orthogonal orientations (Reid and Alonso, 1996 for recent review). Yet another emergent property of cortical cells is direction sensitivity, that is, cells strongly respond to a grating moving in one direction and not the other. Like geniculate neurons, cortical neurons have spatial and temporal frequency preferences; however, for most cortical neurons the preferred frequencies seem to be different than the average seen in LGN (DeBruyn et al., 1993).

Such a variety of novel properties presents a problem of representation over the surface of V1. If any particular property is important it needs to be represented at every retinotopic location in V1, as argued originally by Hubel and Wiesel (1977). The way most primates solve this coverage problem is by organizing properties into domains. In their original studies, Hubel and Wiesel (1962; 1968; 1969) found that in electrode penetrations made perpendicular to the surface all of the cells showed roughly the same functional preferences. In other words, cells within a single vertical column shared properties. Moving the electrode parallel to the surface produced smooth changes in orientation preference with occasional discontinuities. Later, combined histological and functional studies (Hubel and Wiesel, 1977) demonstrated that ocular dominance and orientation preference are organized into orderly domains, with all the cells within an individual functional domain having roughly the same functional preference.

Finding multiple functional properties organized as domains raised a question of how many functional dimensions can be clustered without breaking the coverage requirement (i.e., the need to represent each property at each retinotopic location without

leaving gaps or holes). In a series of computational studies, using data from cat area 17, Swindale and colleagues (Swindale et al., 2000; Swindale, 2004) investigated this question. They used modeling to find that it was possible to have 6-8 binary properties, such as ocular dominance, arranged into clusters without breaking retinotopic coverage in V1. The number of possible periodic properties, such as orientation preference, was found to be less, approximately 4. Finally, Swindale (2004) concluded from their modeling attempts that very few (1-2) scalar properties such as spatial or temporal frequency could be represented as clusters in V1 without causing retinotopic "holes". Given their model, it becomes important to understand how basic functional properties are represented in V1 of primates and whether they follow the rules suggested by the Swindate et al. (2004) model.

Until the advent of optical imaging it was difficult to appreciate exactly how individual properties are organized with respect to retinotopy and with respect to each other in V1. Investigations suggest that all studied primates have maps of orientation preference (Lu and Roe, 2008; Roe et al., 2005; Ts'o et al., 2001; Xu et al., 2004a; 2005). Ocular dominance appears to vary in organization across species but the reasons for this remain unclear given that this binary property should be easy to represent in V1 without interfering with the overall map. Maps of other properties have only been investigated very recently. Data collected in owl monkey and bush baby suggest that domains exist for spatial frequency but not for direction selectivity yet the existence of domains for spatial frequency remains controversial with some investigators showing evidence for clustering of spatial frequency representations and others reporting no such map (Basole et al., 2003; Issa et al., 2000; Sirovich and Uglesich, 2004; Xu et al., 2007; Hubener et al.,

1997; Shoham et al., 1997). One requirement of this thesis was to have a more complete set of data on the organization of V1 attributes in order to determine more clearly the effect of manipulating inputs. Therefore, considerable effort was expended to add temporal frequency mapping to the existing data set since this is a key property used to define visual features. Chapter 4, below, directly compares the organization of temporal frequency with spatial frequency and orientation in maps of V1.

Parsing geniculate input to V1

As was mentioned earlier, geniculate inputs to V1 are segregated anatomically and provide information about somewhat different aspects of visual stimuli. Nevertheless, perhaps because the experiments are so technically challenging, direct investigations of the contributions of different LGN channels to primate V1 organization are sparse. Two key studies, one in macaques (Nealey and Maunsell, 1994) and one in bush babies (Allison et al., 2000) demonstrated that the vast majority of V1 neurons receive inputs from both M and P layers of LGN. Yet, Allison et al. (2000) also found that blocking M LGN layers virtually abolishes responses to low contrast stimuli in V1. Moreover, when looking at the densities of the geniculate inputs normalized by the cortical magnification factor (CMF) in V1, Schein and de Monasterio (1987) have found that CMF in V1 closely follows the density of P inputs, but not of M inputs at least for macaque monkeys, again reinforcing the idea that functional properties of V1 may depend differentially on inputs from P and M LGN channels. In fact, there is evidence that M and P contributions extend beyond V1. Latency studies conducted by Munk et al. (1995) clearly demonstrated that signatures of the geniculate inputs could be identified in

V2, indicating that LGN influences were retained across at least two synapses. There is also evidence that M and P pathways contribute to the activity in both MT and V4 (Maunsell et al., 1990; Ferrera et al., 1994). All of these data were collected using single and multiunit electrophysiological recording, which leaves the question of how the map domains representing different properties in V1 are affected by feedforward LGN inputs. In the study described in Chapter 5, M or P LGN pathways were blocked individually and the maps of orientation and spatial frequency preference were compared.

Effects of feedback inputs on functional properties of V1

As mentioned above, the role of feedback projections from higher visual areas back to V1 is even less well understood. Feedback projections far outnumber the feedforward projections (Bullier et al., 2001). So why have there been so few studies examining the role of feedback in the visual system? The most likely explanation is that feedback connections are difficult to drive independent of feedforward connections so it has been difficult to parse the relative contributions of these pathways. In this thesis, the level of activity in area MT was manipulated and the population response in area V1 examined using optical imaging under the assumption that such manipulations might be easier to appreciate when the organization of many thousands of neurons were examined simultaneously.

Since we wanted to see the effect of MT blocking on activity in V1, it was important to know the functional properties of MT itself. MT was first described by Allman and Kaas (1971) in the owl monkey. Since then MT has been found in all studied primates and, in fact, seems to be one of the few areas that everyone appears to agree on

in primates outside of visual areas V1 and V2 (Kaas, 1996). One of the most significant functional characteristics of MT is that the majority of neurons in this area are sensitive to the direction of motion (for review see Ponce et al., 2008). Imaging studies of MT showed that both orientation and direction selectivity are organized into domains (Xu et al., 2004b) in bush babies, the species used in this thesis. MT neurons have much larger receptive field sizes than those of V1 neurons and have lower preferred spatial frequency selectivities.

Even though MT is one of the most extensively studied visual areas, there are still aspects of MT organization that need to be resolved. Originally, Allman et al. (1973) found that bush baby MT had a smooth retinotopic map on both local and global scales. A later study in macaques (Albright and Desimone, 1987) revealed that MT had retinotopy on a global scale, but on a local scale there were deviations from retinotopy. Other investigators also have noticed some 'irregularities' in the retinotopy of macaque MT (Gattass and Gross, 1981; Van Essen et al., 1981). All these studies were single unit electrophysiological studies and did not look at the overall population responses in MT. Chapter 6 is dedicated to a re-investigation of the problem of retinotopy in MT. This issue became an important prerequisite to our studies of feedback organization given that it was necessary to understand the visuotopy of both MT and V1 in order to be able to evaluate the effect of blocking input from one on the other.

What could be the function of MT feedback to V1? Hupe et al. (1998) found that MT participates in figure-background segregation in areas V1, V2 and V3 in macaque monkeys based on electrophysiological MT blocking experiments. Galuske et al. (2002) blocked the middle suprasylvian cortex in cat, an area that is responsible for processing

motion in that species, and discovered that all direction selectivity in area 18 was completely disrupted. These data would indicate that feedback can be involved in several aspects of processing in early visual areas. The question becomes whether feedback is fast enough to participate in the formation of functional maps in V1. Again, some propositions have been made. Hupe et al. (2001) demonstrated that feedback from MT in macaque can influence activation in V1 as early as 10ms after onset of responses. If MT feedback is that fast, it would indicate that MT can participate in the formation not only of functional properties of single neurons in V1, but also potentially functional maps of different attributes in that area. That is exactly what we tested (see Chapter 7).

The overall goals of this thesis

In summary, a number of previous studies, using a variety of experimental techniques, have demonstrated that area V1 has well organized functional maps of several properties, such as ocular dominance, orientation preference or spatial frequency preference. Moreover, those studies have shown that different classes of geniculate inputs may have significant and different roles in the formation of those maps. Additionally, feedback from MT also could be involved in the formation of those maps. Therefore, the overall goal of the series of studies described in this thesis was to parse out the role of these inputs in the final arrangement of the maps in V1.

CHAPTER III

ANIMAL MODELS AND INVESTIGATIVE TECHNIQUE

This chapter details the rationale for our choice of primate species and the technique we chose to use, optical imaging, for the studies to be described below.

Animal models

Bush baby as a model organism

In the majority of studies described in this thesis the bush baby was used as a model primate species. This primate was selected as an animal model because its visual system is well studied, as described in more detail below, and because all the visual cortical areas are accessible to optical imaging on the cortical surface.

Bush babies (*Otolemur garnetti)* are prosimian primates that are native to continental Africa. All of the animals used for our studies came from a long standing bush baby colony at Vanderbilt University, TN. Bush babies are small primates about the size of a small cat, and like cats they are nocturnal animals. Their adaptations to the nocturnal lifestyle include a tapetum, a rod dominated retina with a single cone type (Jacobs et al., 1996; Kawamura and Kubotera, 2004; Wikler and Rakic, 1990), the existence of a fovea in only 1 out of 9 members of the species and low ganglion cell density (DeBruyn et al., 1980; Walls, 1953). From the standpoint of our experiments, the presence of the tapetum provided additional benefit since it allowed back-reflection of

retinal landmarks onto our screen. Such landmarks included each optic disk is located 20 deg into the temporal hemifield and 5 deg into the upper hemifield from *area centralis* or fovea.

The bush baby's LGN exhibits the general primate pattern with the majority of the LGN having four main layers, two P and two M layers, as described in the background. As in the vast majority of primates, the contralaterally innervated layers lie at the top and bottom of the nucleus with the ipsilaterally innervated layers more centrally located. In addition, there are K cells that receive input from each eye that lie between the two P layers (Kaas et al., 1978; Norden, 1979; Norton and Casagrande, 1982). As is typical of all nocturnal primates the ratio of P to M cells is less than in diurnal primates which likely reflects the fact that nocturnal species have a lower resolution visual system with more convergence of receptors to ganglion cells and consequently larger receptive fields (Casagrande and DeBruyn, 1982; Ionescu and Hassler, 1968). The posterior part of the nucleus, which corresponds to central vision, is tipped slightly dorsally (Casagrande and Joseph, 1980). As a result, straight dorso-ventral penetrations can sometimes enter the very central part of the contra eye's M layer without entering the corresponding P layers (Figure 3-1). Additionally, as can be seen in Figure 3-1, the contralaterally innervated P layer lies more than 1.5 mm from the contralaterally innervated M layer, making inactivation of only a single pathway less technically challenging. Norton et al. (1988) have characterized the functional properties of bush baby LGN. As in other species, different classes of bush baby LGN cells have quite distinct preferences. They found that preferred spatial frequencies for M and P cells were 0.2 and 0.8 c/deg, respectively, with corresponding cut offs being 1.2 and 2.5 c/deg. The optimal temporal frequencies were

much closer for the two major cell classes, being 3.3 (11.0) and 3.8 (12.7) Hz (numbers in parenthesis are cut offs). Another interesting property that Norton et al. (1988) found was that some of the cells had elongated receptive fields, indicating that at the level of the LGN, there already was an emergence of orientation selectivity. This is important for the studies described in this thesis, since it can indicate that LGN inputs can participate in the setup of the initial functional maps in V1.

There have been a number of anatomical and functional studies of primary visual cortex in bush babies over the last few decades. One reason that we and others find the bush baby model attractive is that these animals have a relatively lissencephalic brain with a large portion of V1 exposed on the posterior edge of the occipital lobe (Figure 3-2). Up to twenty degrees of visual space representation can be visualized from the posterior-lateral approach. The remainder of V1 is on the medial aspect of the hemisphere and is not visible from the exposed brain. Extensive electrophysiological and optical imaging studies have been undertaken to investigate the functional properties of bush baby V1 at the level of single cells and also for cell populations. DeBruyn et al. (1993) studied the functional properties of V1 in this species in detail. They found that, as in macaques (Hubel and Wiesel, 1968; Poggio and Fischer, 1977; Schiller et al., 1976), the majority of cells have some degree of ocular dominance. The spatial and temporal frequency preference of most cells were 0.4-0.8 c/deg (cut off 1.0-2.3 c/deg) and 2.3-3.6 Hz (cut off 9-13 Hz), respectively. Importantly, even though the values are similar to ones in LGN, the bandwidth of the tuning curves was significantly narrower in V1. DeBruyn et al. (1993) found that almost half of the cells from which they recorded had some degree of directional selectivity. Most of these cells were located in the lower

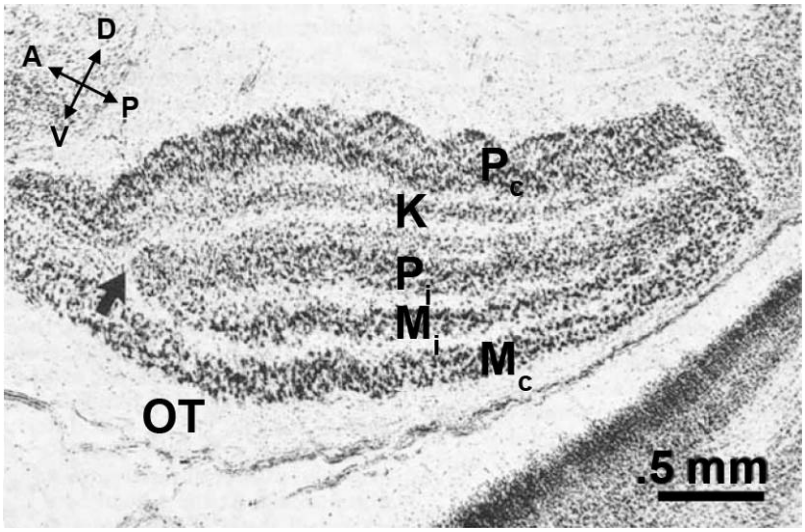

Figure 3-1. Nissl stained section of bush baby LGN. Pi and Pc are parvocellular layers receiving ipsilateral and contralateral retinal innervation. Mi and Mc are magnocellular layers receiving ipsilateral and contralateral retinal innervation. K refers to the two koniocellular layers. Central vision is represented in the posterior half of the nucleus. Black arrow marks the monocular/ binocular border. A- anterior, P - posterior, D - dorsal, V - ventral, OT - optic track. Modified from Casagrande and Joseph (1980), Fig 1 with permission.

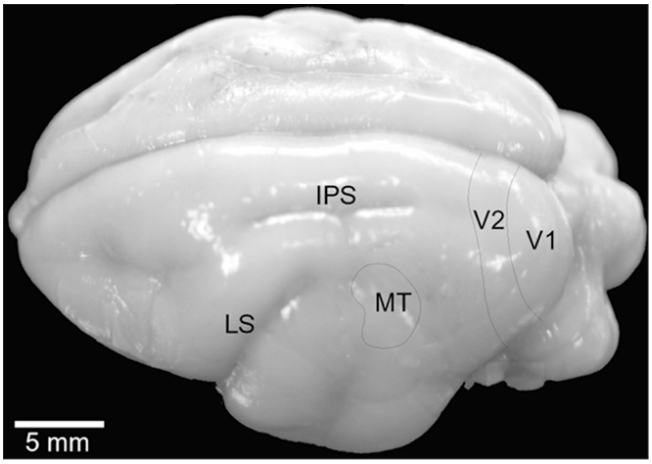

Figure 3-2. Dorso-lateral view of the bush baby brain with major visual areas marked. IPS – interparaetal sulcus, LS – lateral sulcus, MT – the middle temporal visual area, V1 – primary visual cortex, V2 – the second visual area. See text for details. Modified from Xu et al. (2005). Fig 1 with permission.

tier of layer 3 and upper tier of layer 4. Subsequently, Xu et al. (2005; 2007) investigated the functional properties of bush baby V1 using optical imaging. They found clear ocular dominance maps in bush baby V1 confirming previous anatomical studies, however, unlike that of macaque (LeVay et al., 1975), the map consisted of patchy domains, not stripes. Orientation preference maps in bush babies exhibited clear pinwheel and linear zone structures, common to other primates (Malach et al., 1994; Roe et al., 2005; Ts'o et al., 1990). Interestingly, Xu et al. (2005) found that bush babies had about twice as many pinwheels as cytochrome oxidase blobs, suggesting that pinwheels do not align precisely with CO blobs as had been suggested by others. Xu and colleagues showed that bush babies have a clear spatial frequency map (Xu et al., 2007), but they were not able to observe a directional selectivity map.

Owl monkey as a model organism

The second animal model used in the studies described below was the owl monkey (*Aotus trivirgatus).* Unlike bush babies, owl monkeys are New World simian primates and as such are more closely related to humans. Owl monkeys are also relatively small nocturnal primates. They have a single cone type, but do not have a tapetum. Like bush babies they have relatively lissencephalic brains, with the central 10-15 deg of primarily lower visual field representation exposed on the posterior-lateral aspect of each hemisphere. Both species are monochromatic, which allows for better comparison of functional maps between them, since there is no need to account for color sensitivity.

Like bush babies, owl monkeys have been very extensively studied using both electrophysiological and imaging techniques. O'Keefe et al. (1998) did an extensive study of *Aotus* LGN and V1 and found that both optimal spatial and temporal frequency in LGN were slightly higher but in V1 about the same as in bush babies. They also found that the majority of cells in owl monkey V1 were binocular. Xu et al. (2004a) and more recently Kaskan et al. (2007) made imaging studies of visual system organization in owl monkeys and found that they have typical primate pinwheel and linear zone organization of orientation preference. There is also evidence that they have direction selectivity maps in V1 (unpublished results).

In conclusion, bush babies and owl monkeys were chosen as our animal models because their primary visual cortices are well studied, which allowed us to ask further questions about feedback and feedforward contributions to the functional maps in these animals. Moreover, the smooth brain and exposed primary visual cortex provides easy access for the imaging studies.

Optical imaging

In choosing an investigative technique, we needed one which proved itself to be both reliable, and able to detect responses of large populations of neurons. As mentioned above, multiple methods have been used to study the visual system. One of the most widely used methods is electrophysiological recording of single or multiunit activity. This method provides very high temporal resolution of the activity in the brain and allows very detailed characterization of functional properties of individual neurons, however, electrophysiological recording suffers from an inability to sample large populations of

neurons, and there is a bias toward listening to larger diameter neurons since they have stronger signals. At the other extreme of the spectrum is functional magnetic resonance imaging (fMRI). This imaging technique allows visualizing of the whole brain activity; however, the temporal and spatial resolution of fMRI is still rather poor, being many minutes and in the range of a few millimeters, respectively. As a result, there is a need for a technique that balances the advantages and disadvantages of single electrode recording and fMRI. One such technique is optical imaging *in vivo* of intrinsic signals that relate to neural activity. The advantages of optical imaging, the source of its signal, and some analytical considerations will be described next and the recent controversy concerning the validity of imaging results will be described.

Advantages of optical imaging

Studying functional the organization of cortex requires the ability to visualize large populations of neurons. The 'ice cube' model, proposed by Hubel and Wiesel (1977), stated that there is a periodic arrangement of functional properties in visual cortex that repeats in iterated units composed of columns and slabs; however, testing their hypothesis concerning the details of this proposal with single unit recording was a challenge. The first real tests of the proposed arrangement in the 'ice cube' model were done using a metabolic imaging technique with 2-deoxyglucose (Hubel and Wiesel, 1977; Kennedy et al., 1976; Skeen et al., 1978). This technique, however, requires rapid freezing of a virtually unfixed brain and allows mapping of a maximum of two properties, one for each isotope used. As a result, mapping a range of orientations or any other properties with 2-deoxyglucose method in a single animal is impossible. The first

technique that allowed visualization of a whole range of properties was imaging with voltage sensitive dyes (Blasdel and Salama, 1986; Orbach et al., 1985). This imaging method allowed millisecond temporal resolution and submillimeter spatial resolution. However, the need to place dye on the exposed cortex had certain disadvantages, such as toxicity of the chemical used and photofading. An imaging method immune to this problem was needed.

Optical imaging of intrinsic signals overcame these problems. This method has several very important advantages when used to study the functional organization of cortex. First of all, it allows detailed study of large areas of visual cortex with resolution close to 100 microns. Second, like voltage sensitive dyes, optical imaging permits visualization of cortical functional features over the whole range of a given property in the same animal. Several different functional properties can be studied in one experiment. Third, unlike voltage sensitive dyes, optical imaging does not require application of any substances to visualize activity. As a result, longer sessions are possible; moreover, optical imaging allows subsequent imaging experiments on the same animal. Fourth, even though optical imaging is not as fast as voltage sensitive dye imaging, it still has much higher temporal resolution than other imaging techniques, such as PET or fMRI, and it has significantly higher spatial resolution. Finally, as discussed below, optical imaging of intrinsic signals permits visualization of subthreshold activity, therefore, allowing the study of not only excitatory but inhibitory neuronal interactions.

An additional advantage of optical imaging is that it has already been extensively used to study multiple functional properties in multiple species. This allows direct comparison of different functional maps. Optical imaging has been established as a

standard method to study such properties as ocular dominance (Blasdel, 1992; Orbach et al., 1985; Ts'o et al., 1990; Xu et al., 2005; Kaskan et al., 2007), orientation preference, and spatial frequency selectivity (Bonhoeffer et al., 1995; Das and Gilbert, 1995; Das and Gilbert, 1997; Xu et al., 2004b; Xu et al., 2004a). It has been used to study responses to complex stimuli (Basole et al., 2003; Mante and Carandini, 2005; Ramsden et al., 2001) and plasticity (Dragoi et al., 2000). All of these advantages made it a natural choice for our studies of various contributions to the functional maps in bush baby and owl monkey V1.

Sources of imaging signals

Unlike electrophysiological recording, optical imaging of intrinsic signals is an indirect functional imaging technique. It measures changes in reflectance of the area of cortex under investigation. There are several sources for this change. Grinvald and colleagues (Frostig et al., 1990; Malonek and Grinvald, 1996) have shown that the three major sources of the intrinsic signal are light scattering, changes in concentration of oxyhemoglobin, and overall changes in blood volume in the active area. Importantly, even though these three signals have different time courses and somewhat different spatial extents, they produce very similar functional maps. The light scattering and oxy-to-deoxyhemoglobin changes are fastest and more localized to the active area. The decrease in oxygenation of the brain tissue (resulting from the activity of local neurons) triggers the opening of capillary beds and the inflow of oxygenated blood to the area. This latter imaging component is not as restricted as the other two components (Frostig et al., 1990). The scattering component of the intrinsic signals can be best visualized when

a longer wavelength (e.g.,630 nm) is used to illuminate the cortex. Below that limit the hemoglobin components dominate the signal. The initial increase in deoxyhemoglobin concentration can be seen as a transient dip in the signal as soon as 200 ms after the onset of neural activation The increase in oxygenation due to increased blood volume follows by about 200-400 ms. The overall change in reflectance during stimulation has the following profile: upon onset of stimulus, and consequent increase in neural response, the absorbance decreases, producing an undershoot lasting 1.5 to 8 sec, depending on the duration of the stimulus. The undershoot is followed by an overshoot and eventual return to baseline, which can last more than 10 sec. Nevertheless, the most important consideration in using optical imaging of intrinsic signals is how well those signals correlate with spiking activity. Das and Gilbert (1995; 1997) and Toth et al. (1996) have shown that there is very good correlation between the spiking activity and optical imaging. However, they showed that optical imaging is capable of recording not only the spiking activity but also subthreshold activity that is associated with a surround signal due to lateral connections. In spite of this observation, all the studies in which single electrode recording was done in conjunction with optical imaging demonstrated that both are in very good agreement (Arieli and Grinvald, 2002)

One important issue that must be mentioned here is that the optical signal described above is very small. Depending on the wavelength used to visualize activity, the signal used to create functional maps is only 0.1-0.2% of the overall reflected light; therefore, it cannot be visualized directly and additional analysis is always necessary to extract it. Additionally, the changes in reflectance due to the neuronal activity ride on top of, in most cases, much larger biological and non-biological noise. The two largest

sources of biological noise are respiration and heart beat. Since the animal is usually paralyzed for the imaging experiments, instead of air filling the lungs under negative pressure created by rib expansion, air has to be pushed in by positive pressure. This creates oscillating modulation in blood pressure which affects the filling of brain blood vessels and can result in the brain surface moving. Similarly, the difference between systolic and diastolic pressure can result in changes in the optical signal. Another source of biological noise is the slow change in the physiological state of the animal. Imaging experiments are usually many hours long. During this time it is virtually impossible to maintain the plane of anesthesia and paralysis completely unchanged, and any changes in physiology are reflected in the imaging. The major non-biological source of noise relates to the pattern of illumination. The surface of the brain is never absolutely flat, even under a cover glass, which is usually used to minimize brain movement, described above. As a result, it is virtually impossible to place sources of light in such a way that the whole imaged area receives the same illumination. Areas that are poorly illuminated show decreased intrinsic signal strength and increased non-biological noise, namely electronic or "shot" noise. Moreover, because the brain is much denser than air, most of the light falling on the cortex is reflected from its surface, hiding much weaker internal reflectance changes. Finally, some degradation of the optical signal occurs due to optical properties of the system. The tandem lens assembly has intrinsic scatter. Additionally, the cortex is not a transparent substance and therefore there is some scatter occurring as the photons exit the cortex. This last point will be revisited latter in this chapter during discussion of the recent controversy regarding validity of the imaging.

Analysis methods

Very low relative amplitude of the desired signal coupled with multiple sources of noise requires significant processing to visualize the signal. Usually post-processing begins with averaging. Averaging is based on the assumption that the activity dependent signal should be reliably correlated with the stimulus presentation, whereas various biological and non-biological artifacts should be independent of the stimulus presentation. By obtaining data from multiple trials (sometimes as many as 60-80) and then averaging the trials together, it is possible to cancel out the effect of these artifacts.

The averaging is fairly good at eliminating artifacts due to camera shot noise, heart beat and breathing; however, it does not address the problem of the low relative magnitude of the relevant signal. In order to eliminate the vast majority of the surface reflectance while enhancing the functional signal, several baseline normalization techniques are used. The first, most commonly used technique is differential imaging. In this method, an image of average activity during a single stimulus presentation is subtracted from an image obtained during a different stimulus presentation. This method is extremely powerful in visualizing the imaging signal. However, as can be immediately appreciated, it requires prior knowledge that two stimuli activate different patches of cortex. This assumption is easily met for orientation stimuli, since electrophysiological studies demonstrate that most neurons in V1 fire significantly better when presented with preferred vs. orthogonally oriented stimuli. Similarly, direction selectivity of neurons is defined based on the increase of firing in response to one stimulus direction compared to the opposite stimulus direction. Another major deficiency of differential imaging is that it removes most of the signal that is common to both stimulus presentations, under

assumption that this is an artifact. Unfortunately, this assumption is not always valid. For instance, as was mentioned before, optical imaging is capable of detecting subthreshold activity. That activity often spans a much larger area than what is shown by differential imaging. Moreover, because this technique compares two signals to each other, it becomes impossible to understand the significance of the gray areas in the resulting images. Those areas may indicate that both stimuli did not activate a given patch of cortex, or it may indicate that both activated that patch to the same degree.

In order to overcome these last two problems, two blank normalization methods for post-processing were developed. The first one is a gray condition normalization. In this method, one or several of the presented stimuli is either a gray or black screen. In theory, these stimuli should either activate cortex uniformly or not at all, respectively. As a result, subtracting activity during gray/black screen presentations from the activity during the other stimulus presentations should leave only the stimulus related response, both sub and super threshold. This method is best suited for studying responses to stimuli without prior knowledge of underlying electrophysiological responses, or if there is not a clear cut 'orthogonal' condition, such as spatial frequency preference. The major drawback of the method is that it reintroduces into the signal artifacts related to slow changes in the physiological state of the animal. Since this blank response is always separated in time from the response due to actual stimuli, any changes in the state of the animal can shift the resulting baseline. Additionally, Kenet et al. (2003) demonstrated that the assumption that a blank response activates the cortex uniformly is not entirely correct. They saw a spontaneous response in the cat area 18 which was very similar to the evoked orientation response (it is worth noting that they used voltage sensitive dye

imaging, and, therefore, it is not clear whether such a result translates into intrinsic signal imaging). In order to reduce this state of the animal artifact, a second technique, a cocktail blank, can be employed. In this method, responses to all the stimuli are averaged together to create a cocktail blank The assumption behind this method is that by averaging all the responses, the average will have uniform activation of cortex and will represent average activity of the cortex during the presentation of all of the stimuli. This is a more powerful technique than using the gray blank, but it suffers from some of the same shortcomings as the first technique. For instance, using optical imaging, Bonhoeffer and Grinvald (1993) demonstrated that averaging together activation due to the presentation of eight oriented gratings did not produce a condition with uniform activation of cortex. They speculated that the non-uniformity was due to some patches of cortex responding to stimuli at different spatial frequencies, something that was confirmed in several subsequent studies (see above).

All three aforementioned normalization methods assume that by averaging across multiple trials, it is possible to eliminate most artifacts due to the changing state of the animal. Often that is not the case, especially when imaging less responsive animal models, or when studying more limited stimuli, such as a grating at one orientation, spatial and temporal frequency. In such cases a normalization method is needed in which baseline is more closely matched to the activity period in time. That is accomplished by doing first frame, or single condition, analysis. This method requires collecting several frames of brain activity before presenting each stimulus. These first frames are averaged and subtracted from the stimulus associated frames. This method has the same assumptions as the gray blank normalization procedure; however, unlike the former, the

blank is collected at the same time as the response, and as a result, it removes most of the artifacts associated with animal physiology.

It is necessary to mention that in addition to the described arithmetical methods of normalizing imaging data, several other methods have been recently developed. For instance, if the acquisition camera is capable of recording brain responses continuously, it is possible to dramatically reduce acquisition time by presenting periodic stimuli. In that case, Fourier transforming the recorded activity and only keeping responses accruing at the stimulus presentation rate allows rapid extraction of the signal associated with the stimulus. Of course, since the stimuli are always presented in the same order, it is assumed that the order of the stimuli does not affect the result (but see Dragoi et al., 2000). Another method of extracting the relevant signal is independent component analysis (Siegel et al., 2007). This method decomposes the acquired responses into separate components, some of which correspond to the changes due to the stimulus presentation.

Finally, extraction of the signal is often only the first step in the analysis. It is often necessary to summarize responses to different stimuli. For instance, vector averaging of orientation preference data allows quick visualization of the cortical distribution of orientation preference (Blasdel, 1992). In this method, responses to gratings at different orientations are assigned to the vectors of the same orientation as the stimuli with magnitude equal to the magnitude of the corresponding responses. Then the vectors are summed pixelwise to produce an orientation preference map.

In other instances it is necessary to compare responses under different conditions, as was done in the studies described below which required the use of non-parametric

measures. For instance, it is possible to calculate a 'distance' between two images of responses to different stimuli by placing those images into multi-dimensional space with the number of dimensions equal to the number of pixels in the image. This reduces an image to a point and then one of the multiple methods of calculating the distance between points can be used. Using such a distance measure, it is possible to create a dendrogram, which groups the images according to the similarity, which in turn is proportional to the 'distance' (see Khaytin et al., 2007). Another method that was just developed in our lab for use with optical images is a receiver operating characteristic (ROC) analysis. In this method, a histogram of the responses of each pixel during all the repetitions of the same stimulus is constructed and compared to the similar histogram in response to a different stimulus (Purushothaman et al., 2007). Then, the probability that the cortex that is represented by this pixel is activated best by one or the other stimulus given optimum criterion is calculated. This method has several advantages over traditional techniques. It does not require *apriori* assumptions about the nature of the response, it allows objective evaluation of the extent of activation of the cortex, and it allows direct comparison of multiple conditions using all of the available information in the data without averaging.

Verifying optical imaging credibility

As mentioned above, there are a few limitations to the imaging of intrinsic signals. As a result of those limitations, optical imaging was recently criticized as unable to correctly represent neural activity (Polimeni et al., 2005). The argument made by Polimeni et al. (2005) is that optical imaging is flawed due to intrinsic blurring which

results from the opacity of the cortex and the limitations of optics. They modeled the point spread image of the point size activation at different depths in the cortex and claimed that blurring in the system would make the point stimulus spread 250 μm. They also stated that such spread would introduce a systematic error in vector averaged data, such as orientation preference maps. However, orientation preference maps are always pre-processed using the differential imaging technique. This dramatically sharpens the resulting image (Bonhoeffer and Grinvald, 1993). Moreover, as was mentioned above, numerous optical imaging experiments were performed in conjunction with electrophysiological studies and in all cases activity recorded with imaging was corroborated by results of activity recorded with single electrodes. Still, to completely dismiss Polimeni et al's (2005) claims would require careful investigation of the optical properties of the cortex and lenses, and how different normalization techniques affect the resultant resolution.

Polimeni et al. (2005) additionally claim that one of the steps in post-processing further distorts the activation data. They base that claim on modeling the imaging results and introducing white noise to mimic artifacts. That assumption that white noise can be used to model image artifacts is blatantly incorrect. There is very little if any white noise left in the images after averaging. The noise that is seen in the images is a high frequency noise created by the normalization techniques, and probably relates to the functional properties of the cortical vasculature. This noise makes the resultant differential or single condition images look grainy (see Figure 3-3). Note that the graininess makes the borders of the domains harder to see, but it does not actually change the placement of the pinwheels. To demonstrate this, we used real data and applied a

series of averaging disk filters to the differential data prior to calculating the orientation maps (Figure 3-4). As can be seen from this figure, it is quite possible to qualitatively see the location of the pinwheels in the image without filtering, but applying a strict 'all orientations present around pinwheel' rule would indicate that there are no pinwheels at all in the image. This is a very erroneous conclusion considering that simple animation of the differential images by arranging the four orientation responses into frames of a movie demonstrates that orientation activation domains move in circles around pinwheels even in unfiltered data. Filtering with a disk of 3-5 pixels in diameter almost completely removes the high frequency artifacts from the images and allows clear visualization of the pinwheels. Only when the size of the averaging disk becomes comparable to the size of a single orientation activation domain can we see dramatic movement and annihilation of the pinwheels (Figure 3-4, 3-5) as predicted by Polimeni et al. (2005). Therefore, we can conclude that optical imaging is a very powerful and valid technique.

Conclusion

This chapter has described the functional and anatomical attributes of bush babies and owl monkeys that make them ideal animal models for the studies described in subsequent chapters. The theory behind optical imaging of intrinsic signals and various methods of analysis were described. The next chapter will present data on temporal frequency tuning in the bush baby V1. That information is a critical missing piece in the functional maps of V1 without which it is not possible to fully investigate the effects of feedback and feedforward information on the organization of V1.

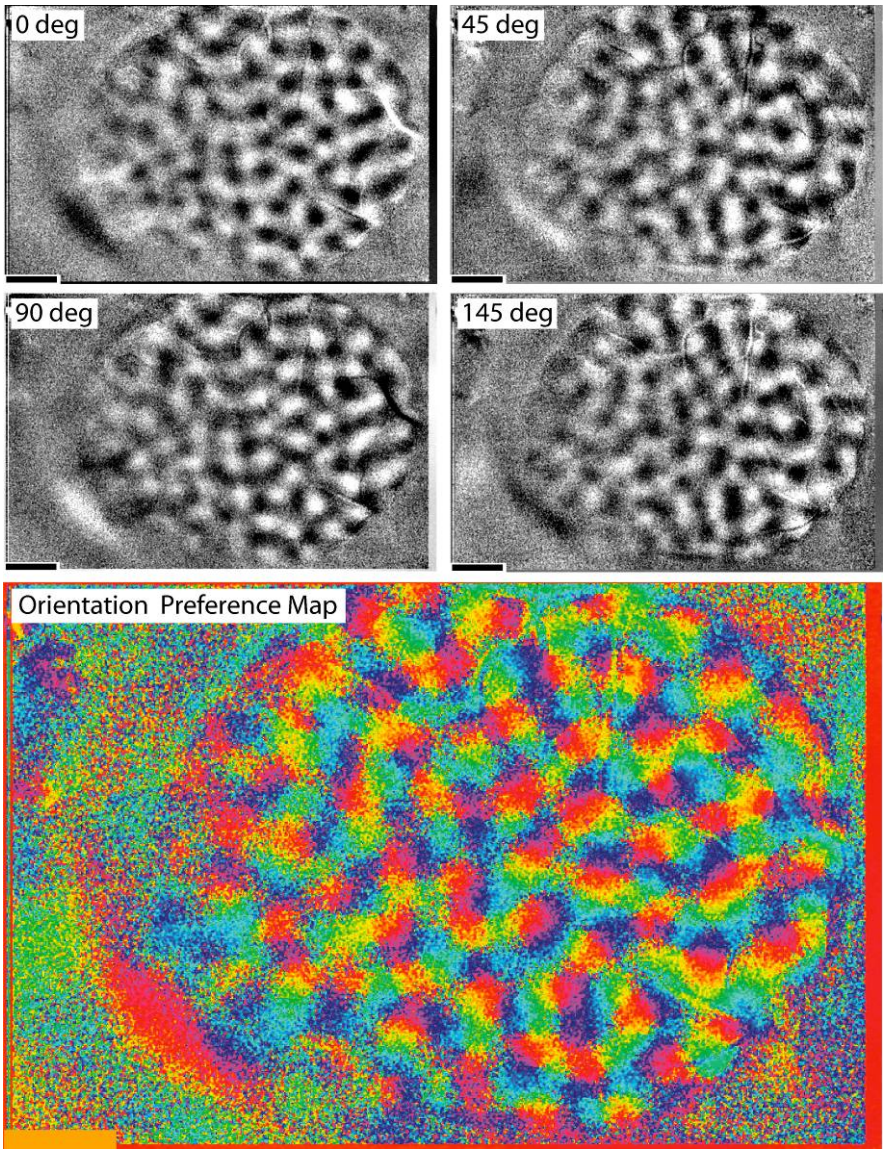

Figure 3-3. Differential images of orientation preference in bush baby V1. The upper grayscale images depict differential images of responses to moving gratings at four orientations. The dark and white areas correspond to zones of activity in response to the stimuli. There is clear activation in all four images, however, the 'graininess' of unfiltered differential images is apparent. The lower color coded image is a vector orientation preference map in which each color represents preference for a different orientation of the cortex underneath the corresponding pixel. The 'graininess' is even more apparent in this image. In spite of this graininess, the familiar pinwheels and linear zones of the map are apparent.

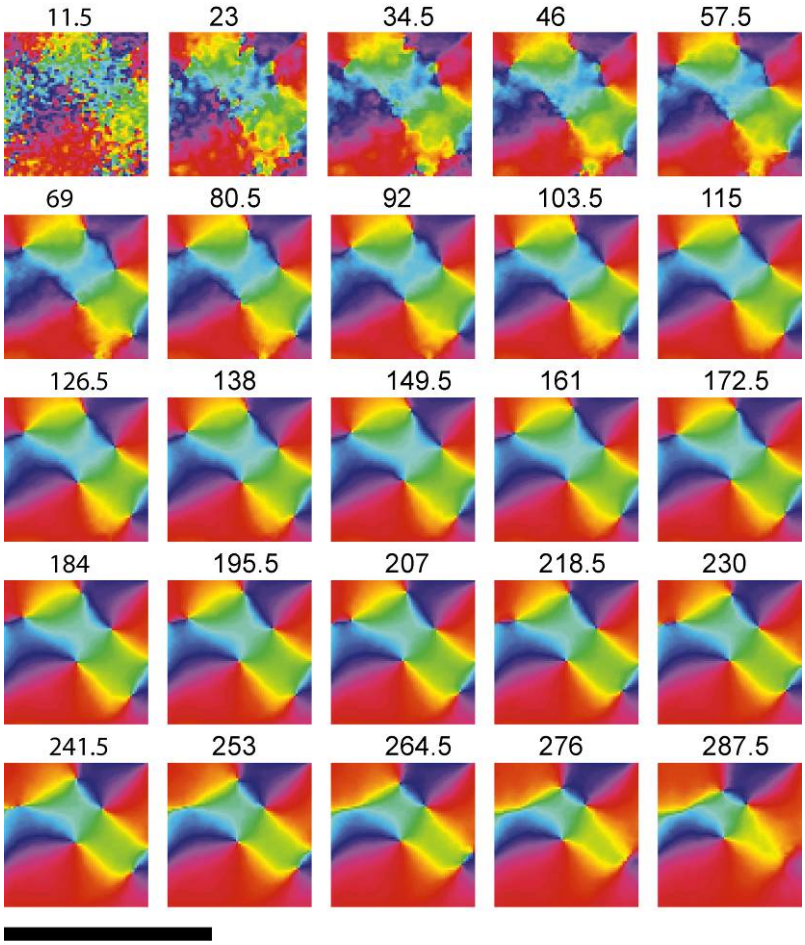

Figure 3-4. Demonstration of the effect of low pass filtering on the final orientation preference map. A one square millimeter region of interest was taken and low pass disk filters of various sizes were applied to it before creating orientation preference maps. The values above each panel are the diameter of the disk in microns. Note that the diameter of one pixel is ~11.5 μm. Therefore, the first image is the result of no filtering. The sequence clearly demonstrates that, (a) the overall structure of the map does not change much until filters of large diameter are used and (b) without filtering the map is too grainy to define pinwheel locations using the 'all orientations must be present' rule. Nevertheless, the locations of pinwheels can be visually determined and correspond to the location seen with a higher degree of filtering.

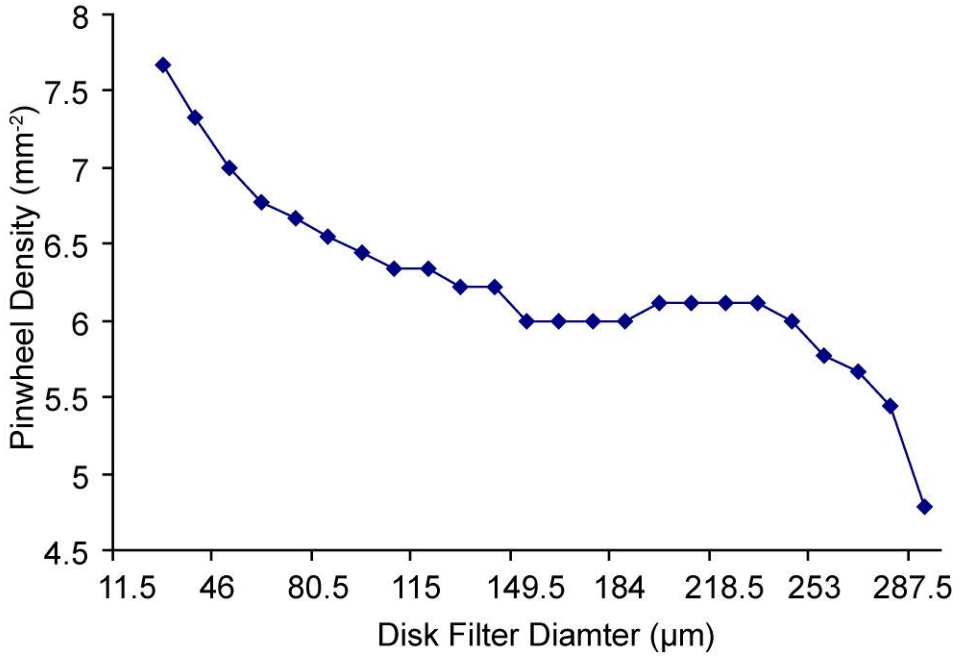

Figure 3-5. Quantification of the number of pinwheels per mm^2 in relationship to the average size of the filter. As can be seen after the filter reaches 3-5 pixels in diameter (35-60 µm) the density of pinwheels does not change much until the size of the filter approaches the size of individual orientation preference domains (~250 µm). Therefore, the usual amount of low pass filtering found in most optical imaging studies does not affect the density of pinwheels to any significant extent. See text for details.

CHAPTER IV

FUNCTIONAL ORGANIZATION OF TEMPORAL FREQUENCY SELECTIVITY IN PRIMATE VISUAL CORTEX

The study described in this chapter was published and reproduced below without alterations:

Khaytin I, Chen X, Royal DW, Ruiz O, Jermakowicz WJ, Siegel R, Casagrande VA. (2007) Functional organization of temporal frequency selectivity in primate visual cortex. Cerebral Cortex. Advance Access. doi:10.1093/cercor/bhm210

One of the defining characteristics of MT is motion sensitivity. Therefore, it was important to investigate functional organization of motion related properties in V1 before blocking MT. In the last several years, our lab has conducted a series of optical imaging studies on both bush babies and owl monkeys designed to facilitate our understanding of the functional organization of their V1 and higher visual areas (Xu et al., 2004a; 2004b; 2005; 2006; 2007). This work provides an important background to the studies proposed in this thesis. However, a previous optical imaging study (Xu et al., 2005) did not find direction sensitivity map in bush baby V1. Therefore, we concentrated our efforts on determining whether, like spatial frequency selectivity, temporal frequency selectivities were organized into domains.

Introduction

Based on their pioneering investigations of neuronal response properties in primary visual cortex (V1), Hubel and Wiesel (Hubel and Wiesel, 1974a) proposed the well-known "ice cube" model to explain how fundamental visual features are represented in the brain. This model posits that a small patch of the cortex is devoted to systematically representing all relevant sensory information from a small region of the sensory environment and that adjacent patches of the cortex represent adjacent regions of visual space. According to their model, which has largely been confirmed for primates using both single unit recording and optical imaging (Blasdel, 1992; Bonhoeffer and Grinvald, 1991; Bonhoeffer et al., 1995; Hubel and Wiesel, 1962; 1968; 1974b; Hubener et al., 1997; Issa et al., 2000; LeVay and Nelson, 1991; Shoham et al., 1997; Xu et al., 2004a; 2005), different sensory attributes such as ocular dominance, orientation selectivity and spatial frequency selectivity are represented systematically in domains or columns in which neurons that are tuned to similar preferences, representing the same part of visual space, lie adjacent.

As more and more columnar systems have been discovered, it has become increasingly important to establish if there are common rules that govern the geometric relationships between different column systems, particularly those which are key to the representation of features of the visual scene such as orientation, spatial and temporal frequency. For example, in all primates examined including the bush baby (the subject of the current study), different orientation preferences are grouped into "domains", i.e., patches of the cortex that run along smoothly varying contours. Some of these feature domains are locally orthogonal to each other and a discontinuity in one domain occurs in

the smoothest part of the others (Everson et al., 1998; Hubener et al., 1997; Weliky et al., 1996; Xu et al., 2005; 2007). A similar pattern is seen in most other species with the exception of rodents where orientation preferences curiously show no domain structure, suggesting that a different set of rules apply (Van Hooser et al., 2005; Van Hooser et al., 2006). For spatial frequency selectivity, domain-like structures also have been identified in the bush baby and in the cat, but whether this is the rule has been the subject of some controversy (Berardi et al., 1982; Bonhoeffer et al., 1995; Everson et al., 1998; Issa et al., 2000; Shoham et al., 1997).

Thus far the only optical imaging study that measured temporal frequency selectivity was done in the cat visual cortex, and that study did not systematically study the distribution of temporal frequency preferences (Shoham et al., 1997). Using single unit recording, DeAngelis et al. (1999) found some evidence to suggest that there may be clustering of neurons with similar temporal frequency preference. Surprisingly, however, no data are available in any species that have directly addressed the issue of how temporal frequency selectivity is mapped across visual cortex and if temporal frequency selectivity is organized into domains, how such domains are organized. Given the importance of both spatial and temporal frequencies as attributes defining the visual scene, it is critical to know whether common rules govern their organization and if not, how temporal frequency tuning is mapped in relationship to other sensory properties. Specifically, in this study, we quantitatively examined whether temporal frequency tuning, like spatial frequency tuning, ocular dominance and orientation preference (Xu et al., 2003; 2005; 2007), is organized into domains in the prosimian bush baby. If so, how do the maps of temporal frequency selectivity relate to other anatomical markers or

modules proposed to represent different functions, such as cytochrome oxidase (CO) blobs?

We had three predictions which are outlined in Figure 4-1. First, if temporal frequency preference is inseparable from orientation preference, then both the location and size of orientation preference domains should change depending on the fundamental temporal frequency of the stimulus (Figure 4-1A). Second, if temporal frequency preference is independent of orientation but the former is arranged into domains, we should see shifts in the location of maximal response within the same orientation domain at different temporal frequencies (Figure 4-1B). Finally, if temporal frequency preference is uniformly distributed across V1, we should see no change in orientation domain locations or in their sizes. In the latter case, the most significant difference in response would be a change in response magnitude with different temporal frequencies (Figure 4-1, see also DeBruyn et al., 1993).

Methods

Animals

Seven bush babies (*Otolemur garnetti*) of both sexes, which were raised in our colony, were used in these experiments. They were housed and handled according to approved protocols from the Institutional Animal Care and Use Committee (IACUC) at Vanderbilt University. Of these animals, four were used in acute experiments and three had initial surgery and then retinotopic optical mapping and temporal frequency mapping done in separate survival sessions before the final acute experiment during which the bulk of data were collected. A total of seven hemispheres were imaged.

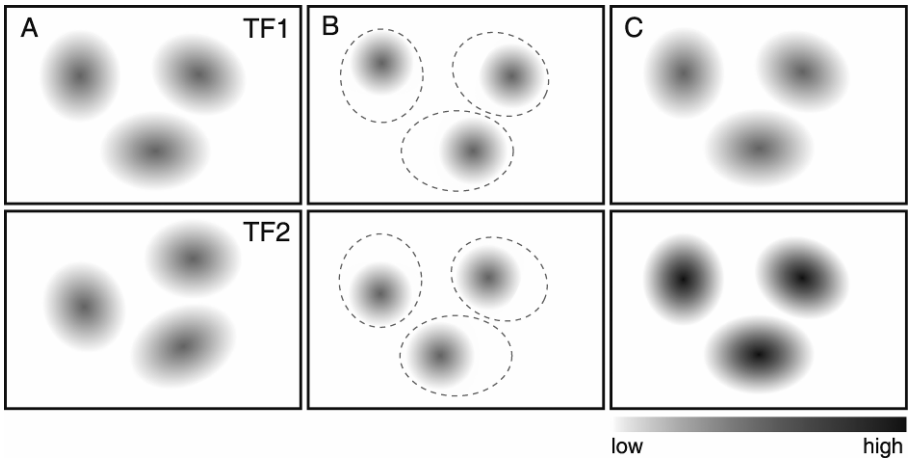

Figure 4-1. Three predictions concerning the relationship between temporal frequency and orientation preference domains. Orientation domains are shown as gray toned areas with increasing signal strength indicated by darker gray tones. TF1 and TF2 refer to two different temporal frequencies. A. If orientation tuning depends on temporal frequency tuning, the prediction is that orientation domains shift with different temporal frequencies as shown by the changes in domain positions from the top to the bottom panel. B. If orientation tuning does not depend on temporal frequency tuning, but groups of cells with different temporal frequency preferences cluster together, the prediction is that orientation domains would remain in the same positions (dashed lines), but that the area of strongest response within each domain would shift with change in temporal frequency of the stimuli. Again compare the top to the bottom panel. C. If orientation tuning of the cells does not depend on temporal frequency tuning and cells with different temporal frequency preferences are distributed uniformly across cortex, the prediction is that the only change would be a change in the strength of response with changing temporal frequency of the stimuli. In this example the three orientation domains shown are more responsive in the bottom panel (one temporal frequency) than in the top panel (another temporal frequency). From Khaytin et al. (2007)

Surgery and perfusion

All experiments were conducted under general anesthesia and paralysis. In acute experiments, anesthesia was induced with 2-4% isoflurane in O_2. At the same time animals were given intramuscular injections of dexamethasone (1 mg/kg), glycopyrrolate (Robinul 0.015 mg/kg) and ceftiofur sodium (Naxcel 2.2 mg/kg), and two venous catheters were inserted. Animals were intubated and mounted in a stereotaxic apparatus. Prior to induction of neuromuscular blockade (NMB), animals were connected to temperature, ECG and expired CO_2 probes, and baseline readings were taken. All optical imaging experiments were conducted under propofol /nitrous oxide anesthesia and NMB. Once all preparatory steps were undertaken, animals were switched from isoflurane to propofol and allowed at least fifteen minutes to remain in a stable plane of anesthesia before NMB, which was induced with an injection of 0.7-1.0 mg/kg of vencuronium bromide. Animals were respired with a ventilator delivering a 3:1 mixture of NO_2 and O_2 at a sufficient rate to maintain expired CO_2 at 4%.

During the surgery, anesthesia was maintained using propofol, delivered at ~10 mg/kg/h. During the experiment, the amount of propofol delivered was reduced to 4-7 mg/kg/h. NMB was maintained with vencuronium bromide (0.6 mg/kg/h) in a 5.0% dextrose lactated Ringers solution. An opening ~10mm in diameter was made over V1 centered at 8mm from the posterior pole and 9mm from the midline. The dura was removed and replaced with an artificial dura (Tecoflex®), as described by Sakas et al. (1990). The opening was covered with 1% agarose in saline, and sealed with a glass cover-slip. In chronic experiments, all procedures were carried out under sterile conditions. The first session in these experiments was reserved for the craniotomy of the

area above V1 and Tecoflex placement, and was conducted under isoflurane in O_2 anesthesia (1-3%) without paralysis. No imaging data were collected during this first surgical session. In the chronic experiments, at the end of each imaging session, animals were weaned from the ventilator after infusion of paralytic was stopped and were watched carefully until they were capable of eating and drinking on their own. These animals also were given the analgesic, buprenorphine (Buprenex 0.01 mg/kg), and the antibiotic, ceftiofur sodium (2.2 mg/kg), postoperatively.

Pupils were dilated with 2% cyclopentolate (Cyclogyl) and/or 1% atropine drops, and contact lenses with sufficient power and 3-mm pupils were used to make the retina conjugate with the viewing distance to the monitor of 28.5 cm. Retinal landmarks including the optic disks and *area centralii* were plotted using back reflection from the tapetum prior to the start of each experiment.

Histology and Alignment

Before each imaging session, a series of color images of the brain were taken using a handheld digital camera. These images, along with reference images taken with the optical imaging camera, later were used to aid in aligning the histological sections with the optical images. At the termination of each experiment, the animal was euthanized with an overdose of sodium pentobarbital (Nembutal, 50mg/kg) and perfused through the heart, first with a saline rinse containing 0.05% sodium nitrite, and then with a fixative solution containing 2% paraformaldehyde in 0.1M phosphate buffer. The brain was removed and flattened using the following procedure. First, the occipital cortex was cut from the rest of the brain in a coronal plane. Next, the medial wall (invisible to the

camera) was trimmed so that the cut was parallel to the surface of the imaged area of V1. It is noteworthy that over the course of the experiment the imaged surface of V1 becomes relatively flat under the combination of the cover glass and the gel-like layer of 1% agarose in saline. Finally, the V1 piece was placed on a slide in a Petri dish in 0.1M phosphate buffer, or buffer plus fixative with 30% sucrose added. The cover of the Petri dish was placed over the piece of brain and weighted with small weights (~100g). This process does not cause much distortion. These "flattened" pieces were frozen and cut tangentially with the surface vasculature preserved in the first 100 μm-150 μm section. The remaining tissue was sectioned at 52 μm.

Sections were stained for cytochrome oxidase (CO) according to methods described previously (Boyd and Matsubara, 1996). During cutting, a pin was used to make 3-4 holes at the periphery of the tissue piece. These holes were used as additional aids in section alignment.

All sections were photographed using a Nikon microscope with a 0.5X objective lens and digital camera. The first section contained visible surface blood vessels. Those vessels were found and marked (see Figure 4-2A and B). Similarly, reference images, taken during optical imaging, showed surface blood vessels visible to the camera. These also were marked (Figure 4-2D and E). Using these blood vessel marks, the first section was aligned to the reference image (Figure 4-2C). Since reference images and data images were taken from exactly the same camera position, simple alignment of the data images to the reference images ensured a near perfect alignment of the data images with the histological landmarks (such as the vertical meridian shown in Figure 4-2F). The

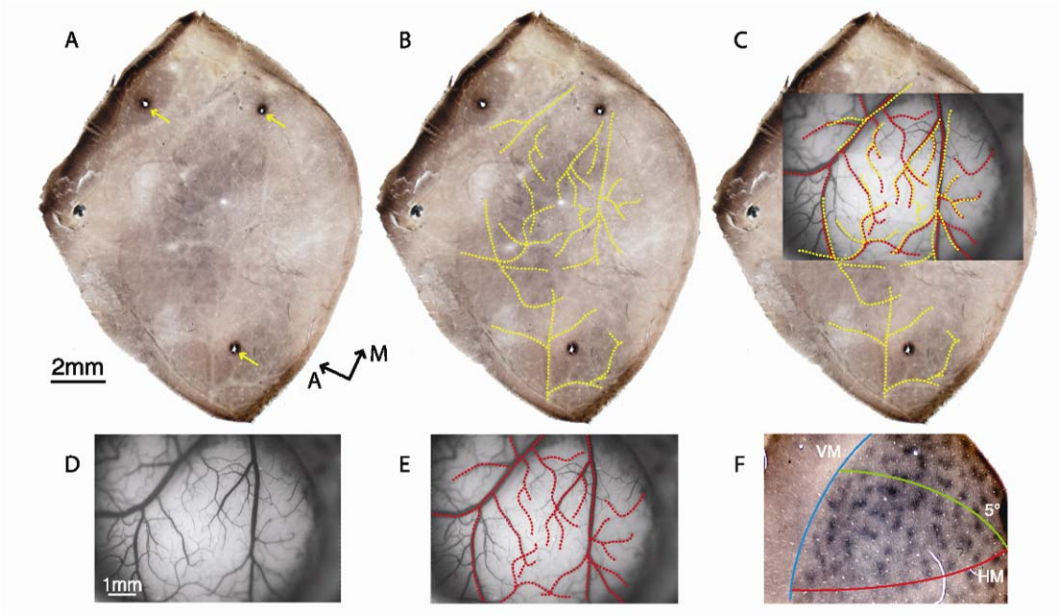

Figure 4-2. Histological alignment and activation from one case (06-07). A. A photomicrograph of the first CO stained histological section was taken and blood vessels identified. During cutting a pin was used to make holes perpendicular to the surface for further alignment of the sections (three yellow arrows). A, anterior, M, medial. B. Major blood vessels were identified and outlined (yellow dotted lines). In cases where there was difficulty assigning a particular vessel branch to a specific larger vessel, a digital color photo taken during experiment was consulted, however, all blood vessels used to align histology with imaging data were outlined on the first section. C. Using blood vessels identified in A and E, a low power reference image (D) was aligned to the first section shown in A. All alignment is done with only rotation and proportional scaling. D. A reference image was always taken by the imaging camera just before start of the data acquisition (see Methods). Because the camera was not moved, this reference image aligned to the data images. E. Blood vessels were identified in the reference image (red dotted lines). These blood vessel outlines were for alignment of imaging data to histology in C. F. Cytochrome oxidase stained section of cortex, showing major retinotopic landmarks obtained using retinotopically limited stimuli. Red line indicates horizontal meridian, identified by running retinotopically limited stimuli. The blue line indicates the vertical meridian, identified by both imaging and confirmed using histology since CO blobs are limited to V1 as, shown in Figure 13. Green line indicates 5º eccentricity, identified by running retinotopically limited stimuli. See text for details. From Khaytin et al. (2007)

remaining histological sections were aligned to the first section using the pin holes and tangential blood vessels. The only transformations used in this alignment procedure were rotations and proportional scaling, both applied only to the histological frames and not to any reference images or data image frames.

Optical imaging

All data were gathered using the Optical Imager 2001 (Optical Imaging Inc., Mountainside, NJ) using methods similar to those described in previous publications (Bosking et al., 1997; Xu et al., 2004b; 2005; 2007). In brief, the setup consisted of a differential amplifier, a CCD camera with tandem lens macroscope (Ratzlaff and Grinvald, 1991), two PC computers, and a constant light source with interchangeable filters. The interface to the system was provided through the first PC running the Optical Imaging software. The second PC was used for stimulus presentation with custom code written in MATLAB (Mathworks, Natck, MA) to drive a stimulus generator (Cambridge Research Systems, Rochester, UK). Stimuli were displayed on a 21-inch video monitor (Sony FD Trinitron, model GDM-F400, Sony, Tokyo, Japan) in 120 Hz non-interlaced mode and at a mean luminance of 30 cd/m^2. The monitor screen maximally subtended approximately 54˚ x 74˚ of visual stimulation at a distance of 28.5 cm. The macroscope consisted of two front-to-front tandem Nikon lenses: 50 mm/50 mm or 50 mm/135 mm. The image was focused just below the cortical surface and the diaphragm was closed by one or two f-stops. The light source was filtered at either 540 or 611 nm, with the former used to acquire a reference image of the surface vasculature and the latter used to collect functional data.

Several types of visual stimuli were used. To confirm the placement of the opening, a full field 100% contrast grating (0.5 c/deg fundamental spatial frequency) was presented at 4 orientations and moved back and forth at 2 Hz. To determine the location of central vision in V1, topographically restricted grating stimuli were presented at two orientations in small circular windows (2-5˚ in diameter), narrow rectangular windows (2˚ wide) or rings of various widths placed at different locations in the visual field (see Xu et al., 2005 for details). These stimuli allowed us to determine the retinotopic organization and extent of the imaged brain area as shown in Figure 2F.

To study temporal frequency tuning, full screen square wave gratings of 0.5 c/deg fundamental spatial frequency at 4 different orientations and 20% duty cycle were used. These stimuli were selected because, in our previous studies (Xu et al., 2005; Xu et al., 2007), this combination of stimulus attributes proved to be very effective in activating bush baby V1.. To examine temporal frequency preference maps, 4 frequencies were used: 1, 2, 5 or 10 Hz. These temporal frequencies were chosen based on our previous electrophysiological experiments in V1 of bush baby (Bonds et al., 1987; DeBruyn et al., 1993). Each experiment consisted of 16 conditions; 4 orientations and 4 temporal frequencies. In one animal, we also imaged at higher temporal frequencies (15 and 20 Hz) since V1 in this animal seemed to respond well above 10 Hz. In one additional animal, we used sine-wave grating stimuli at the same temporal frequencies, 0.5 c/deg spatial frequency and 50% contrast. These stimuli were used to examine whether the higher harmonic spatial frequencies inherent in our square wave gratings could have influenced the results. All stimulus sequences consisted of the following: 5 sec of uniform gray screen of mean luminance followed by 8 sec of a drifting grating, followed

by 12 or 17 sec of the same uniform gray screen. Each orientation and temporal frequency was pseudo-randomly repeated 10 to 30 times.

The Optical Imaging System stores data in proprietary data files. Before each block of stimuli, consisting of a single repetition of each type of stimulus, the camera records a single reference image for four seconds. This reference image is then automatically subtracted from all consequent frames and the residual amplified. Both the reference frame (frame zero) and amplification parameters are stored in a file header. During stimulus presentation, the camera collects 30 frames per second, and these 30 frames are automatically summed into a single data frame. Therefore, each stimulus condition of 25-30 sec produces 25-30 differential data frames.

Analysis

Reconstructed raw data (referred to here as raw data) were obtained by reversing the steps done by the Optical Imaging algorithm described above (Optical Imaging, personal communication). All quantitative analyses were performed on reconstructed raw data. To add certainty to our conclusions we performed a number of quantitative comparisons. Since some of these are new to the optical imaging literature, we have provided more details in the relevant subsections of the results.

The first step in our analysis was the conversion of raw frames into baseline normalized frames as described in Siegel et al. (2003). In brief, each reconstructed raw file consisted of a zero reference frame and 25-30 data frames, with frames 6-14 corresponding to the grating presentation and frames 1-5 corresponding to presentation of an equiluminant gray screen. The zero reference images from all trials were averaged,

their means and standard deviations were determined, and all pixels that had values higher than the mean plus half a standard deviation were selected as a region of interest (ROI). Frames 6-14 of each trial and condition were averaged and divided by the average of the first five frames, producing baseline normalized images. The means and standard deviations of the pixels within the ROI from the baseline normalized images were determined, producing a mean – standard deviation pair value for each frame. An automatic rejection procedure was used which removed all the frames whose means were more than two standard deviations away from the population's average mean, or whose standard deviations were more than three inter-quartile intervals away from the population's median standard deviation (Siegel et al., 2003). The remaining baseline normalized frames were averaged separately for each condition, producing 16 baseline normalized images, one for each orientation and temporal frequency. Before doing any quantitative analysis for each data set, a binary mask was created, in which bone and large blood vessels that show up in the baseline normalized images were marked as zero.

The next step involved obtaining the single condition images (Figure 4-4). Non-uniform bias due to cortical curvature (direct-coupled (DC) shifts) was removed by convolving each image with a Gaussian kernel with sigma of 1.0 mm and subtracting the result from the original image (Bosking et al., 1997; Xu et al., 2004a).

We employed multiple qualitative and quantitative methods to test our hypotheses. The details of these methods are included with the relevant results presented below. The main distinction between our different hypotheses concerned the position of the activation areas relative to each other when different combinations of temporal frequencies and orientations were presented (See Figure 4-1). Therefore, we needed to

show whether individual activation domains at single orientations and different temporal frequencies moved in relation to each other as temporal frequencies were changed and, if so, to determine the nature of that movement. We accomplished that by cross-correlating sample regions from single condition images, determining the precise positions of each individual activation domain in all conditions, comparing their respective positions, and performing similarity analysis across conditions (see below). Finally, we quantified the strength of the response at different temporal frequencies using a curve fitting technique.

To determine the signal strength for each pixel at each temporal frequency, we linearly fit the data, consisting of single condition images without low-pass filtering, to the following equation:

$$R_{I,J,\upsilon}(\theta) = a_{I,J,\nu} \times \sin(\theta) + b_{I,J,\upsilon} \times \cos(\theta) + c_{I,J,\upsilon} \qquad \text{(Equation 4-1)}$$

where $R_{I,J,\nu}(\theta)$ is the reflectance of (*I,J*) pixel for temporal frequency ,υ (four conditions), as a function of orientation θ (four orientations). Each temporal frequency and pixel was analyzed independently. For a given pixel the preferred angle is:

$$\Phi_{I,J,\upsilon} = \arctan(a_{I,J,\upsilon} / b_{I,J,\upsilon}) \qquad \text{(Equation 4-2),}$$

with appropriate quadrant correction and the pixel's maximum response at a given temporal frequency is:

$$M_{I,J,\upsilon} = \sqrt{a_{I,J,\upsilon}^2 + b_{I,J,\upsilon}^2} \qquad \text{(Equation 4-3).}$$

This analysis produced preferred orientation and magnitude of response maps for each temporal frequency (Figure 4-3). Preferred orientation map pixels were divided into eight groups with the mean strength in each group obtained from maps of the magnitudes of response (Figures 4-12 and 4-14). To simplify comparisons between cases, the average of the strongest response across all four temporal frequencies was set to unity. To determine if the differences in response magnitude were significant, a two-way ANOVA with a subsequent Tukey Honestly Significant Difference (HSD) test was run in Matlab on all mean response values.

We also were interested in whether there was a difference in temporal frequency preference in CO blob as opposed to interblob regions of V1. To map the appropriate regions of interest, we low-pass filtered images taken of the histological sections with a 50 μm filter averaging kernel and subtracted the background obtained with a 500 μm filter averaging kernel. The resulting images were then thresholded into three roughly equal groups according to pixel brightness (Figure 4-13). The darkest third of the pixels were assigned to CO blobs and the brightest third to interblobs (Boyd and Casagrande, 1999; Xu et al., 2005). Visual inspection was used to confirm that all of the regions of the cortex that were imaged were assigned to the correct compartment. We aligned these maps with activity maps as described above, which allowed us to repeat the strength calculations segmented by pixels within CO blob regions or interblob regions.

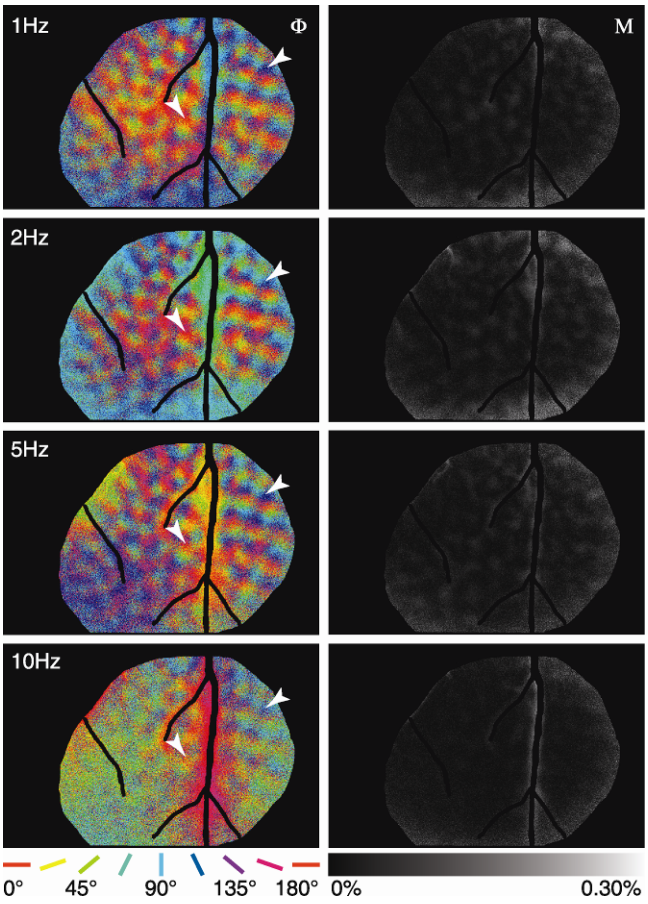

Figure 4-3. Pixel-wise linear fit. Preferred orientation maps (Φ) at four temporal frequencies (left column). Magnitude maps (M) (right column). Colors refer to the preferred orientations and the gray scale to the response magnitude relative to baseline as determined by linear fit. White arrowheads in the left column show that at different temporal frequencies, orientation preference at a given location does not change. See Methods for details (Case 06-07lo) From Khaytin et al. (2007)

Results

We first describe our findings using spatially restricted stimuli to define retinotopic regions in V1. Next, we demonstrate the overall organization of temporal frequency selectivity. Our results support the third hypothesis (fig 4-1C). Unlike spatial frequencies, temporal frequencies are not clustered in modules. Instead, all temporal frequencies are represented at each spatial location with no obvious shifts in preferences across the parts of V1 representing the central 10-15˚ of visual space. We then show that global measures of temporal frequency preference measured using optical imaging match closely with measures reported for single cells in V1 (DeBruyn et al., 1993). Finally, we describe results comparing the distribution of temporal frequencies across CO compartments. These results do not support previous results suggesting that there is a difference in optimal temporal frequency selectivity between CO blob and interblob regions.

Mapping V1 and aligning images

All of our reported results were collected from area V1 within the representation of the central 15˚ of visual space confirmed using visuotopically restricted stimuli and histology (see Methods). Figure 4-2F shows the representation of the horizontal and vertical meridians (HM and VM lines) based on cortical activation produced by using 2˚ rectangular windows presented either on the horizontal or vertical meridians. Note that the intersection of these lines defines the center of gaze or the *area centralis* representation. For this case, approximately 8-10˚ of visual space was within view of the camera on the dorsal surface of V1. In the other 6 cases, slightly different openings were

made but all allowed us to image the representation of approximately the central 10-15˚ of visual space. In all reported cases we had robust responses to optimal full field gratings. Two different lens arrangements were used in our experiments; the 50/50 mm lens combination provided an 87 pixels/mm (11.5 μm) level of resolution, while the 50/135 mm lens combination produced a 235 pixels/mm (4.26 μm) level of resolution (Figures 4-2F and Figure 4-13D). At both resolutions, we saw very strong activation of cortex with clearly defined orientation domains. It is important also to keep in mind, however, that optical imaging can only sample the supragranular layers of cortex and is not able to sample the functional organization of cortex much below ~ 500 μm of cortex, corresponding to the supragranular layers (Bonhoeffer and Grinvald, 1993). Therefore, when interpreting our data, as well as any optical imaging data, it is important to keep in mind that the structure of the functional maps could differ in the lower layers

Linear fitting of the orientation data

Baseline normalized single condition response data were organized into single temporal frequency groups and fitted using Equation 4-1. Resultant orientation preference images (Figure 4-3 left column) were similar at all tested temporal frequencies with the only difference being that there was less activation for all orientations at 10 Hz than at lower temporal frequencies (Figure 4-3 right column). This can be appreciated visually by examination of common activation points (arrows). The same general pattern, in which activation domains at different temporal frequencies and same orientation appeared to be in the same place, was evident in single condition images at both low and high power (Figure 4-4).

Responses at different temporal frequencies

Figure 4-4 shows activation patterns seen in V1 in three different cases in response to moving gratings shown at 4 different temporal frequencies (1, 2, 5 and 10 Hz). These images are single condition maps baseline normalized by the first five gray (blank screen) frames. Since all of the images in this Figure were normalized to the same range, the strength of response was roughly proportional to the contrast seen, with darker regions showing stronger responses and lighter areas - weak or no response. Animals showed some individual variability in the degree of sensitivity to higher temporal frequency stimulation.

For example in Figure 4-4, case 06-07hi all four temporal frequencies produced activation up to 10 Hz (far right panel). In case 05-05 (Figure 4-4), the response at 10 Hz was weaker making it virtually impossible to distinguish areas of activation from surrounding non-responding regions. Still, quantification of individual pixels suggested that activation was above background. In all cases the strongest responses were seen at the lower temporal frequencies (1 and 2 Hz) with a peak at 2 Hz. Careful examination of the different maps of activation at different frequencies suggested qualitatively that they overlapped with little variation. Small differences in the appearance of individual activation domains were only visible at the edges of the craniotomy and along the course of medium sized blood vessels. These blood vessels also tended to have an inconsistent appearance across conditions (blood vessels generally do change appearance at the same time as cortical tissue around them and are affected more than cortical tissue by minor changes in physiology). Therefore, our main result was that there were no major changes

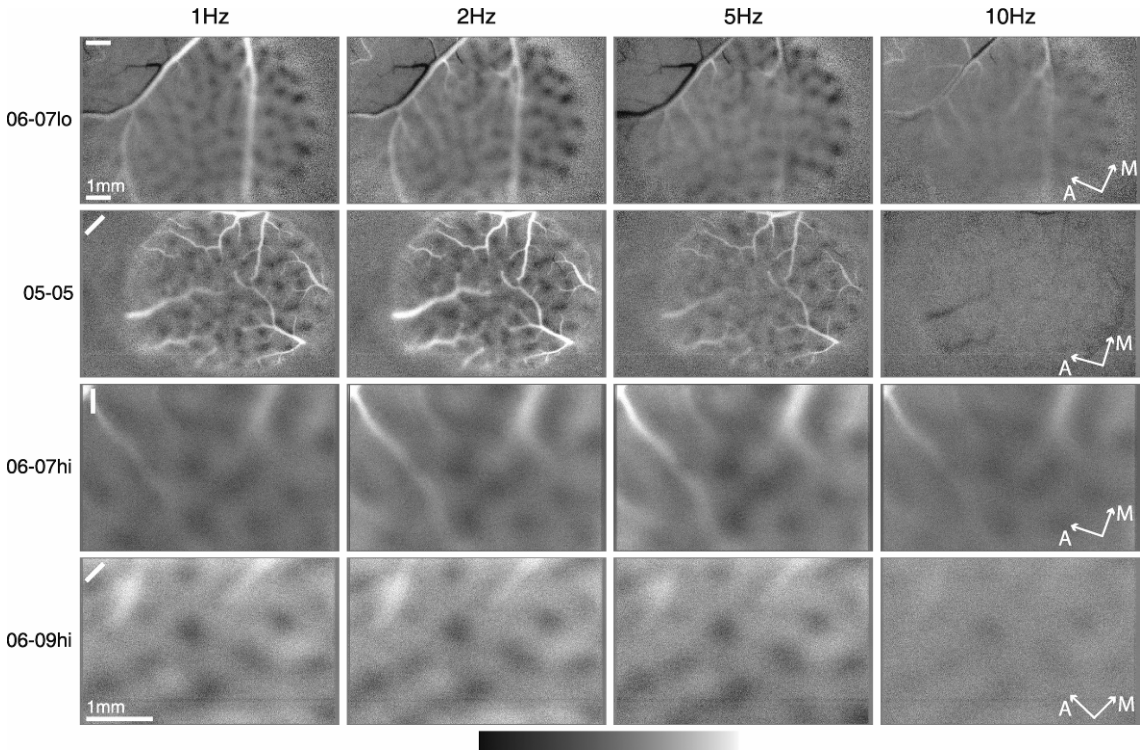

Figure 4-4. Single condition activation patterns. All images are single condition images normalized to the first five (blank) frames as described in Methods. Each column represents responses at the indicated temporal frequency. Each row shows the response to the indicated orientation (upper left corner of each image) in a separate case, case number indicated to the left. These images show reduction in the strength of the response with increases in temporal frequency of the stimuli. Darker areas represent stronger responses. The first two rows are low magnification (lo) and last two rows are high magnification (hi) images. The grayscale bar indicates range of response relative to baseline as follows: 06-07lo (-0.34 to 0.42%), 05-05 (-0.17 to 0.38%), 06-07hi (-0.22 to 0.12%) and 06-09hi (-0.09 to 0.12%). Cases (05-05, 06-07, and 06-09). A, anterior; M, medial. From Khaytin et al. (2007)

in the geometric structure of the single condition maps across temporal frequencies, such as changes in domain size or number. This is an important qualitative observation in light of our predictions (see Figure 4-1).

Structure of single condition maps at different temporal frequencies

To test whether regions of imaged cortex preferring the same temporal frequency were clustered, we used single condition images at different temporal frequencies. Figures 4-5 and 4-6 compare the relationship of single condition orientation domains at different temporal frequencies. Initially, we chose two representative regions of interest (ROIs) in the single conditions maps, free of blood vessels and centrally located, smoothed these ROIs using a 2x2 pixel (23x23 μm) kernel, and determined their similarities using cross correlations. The contrast in these images was increased to make signal comparisons easier. The sample ROIs at both magnifications were compared visually and quantitatively. Both Figures show that the shape, position, and size of the activation regions (darker areas) are similar at all four temporal frequencies.

At low magnification (Figure 4-5A-C), we found that regions of interest indicated by letters in Figure 5 at 1 Hz (Figure 4-5B and C) were well correlated with the same regions at 2, 5 and 10 Hz with correlation coefficients of 0.72 (0.83), 0.69 (0.72) and 0.57 (0.60) (numbers in parenthesis represent correlation coefficients for region B), respectively. To distinguish from a random organization the ROIs taken at 1 Hz temporal frequency were rotated 180 degrees. When this was done, correlation coefficients dropped to 0.02 (0.53), 0.08 (0.40), and 0.04 (0.44), respectively, for these same regions. The same analysis was repeated on images collected at high magnification (Figure 4-6A-

C). Once again we obtained high correlation coefficients of 0.82 (0.59), 0.86 (0.70), and 0.85 (0.71). For comparison, the "random" 180° rotated images at 1 Hz yielded correlation coefficients of 0.28 (0.17), 0.48 (-0.19), and 0.39 (-0.15). The high correlations between images at different temporal frequencies are not consistent with either the first or second predictions described in the Introduction (Figure 4-1). Analysis of data from all of the other cases showed the same result.

As a second approach to the question of stability of patches with varying temporal frequency of the stimuli, outlines of orientation domains were generated. The outlines of these orientation domains were compared as follows (Figures 4-5 and 4-6 D-H). First, to reduce the high spatial frequency noise, each image was convolved with a 57 μm averaging kernel. Next in Adobe Photoshop (Adobe Systems Inc., San Jose, CA), a binary threshold function was employed so that only the ~30% darkest pixels were selected in each image. The 30% cut-off was selected for consistency with our previous studies (2004a; Xu et al., 2005), and to provide a conservative estimate of the areas of activation. Finally, obvious noise artifacts and regions containing blood vessels were excluded. The resulting images were aligned in a stack to determine if any spatial shifts of orientation domains occurred that correlated with different temporal frequencies.

The patch locations, representing activation domains at different temporal frequencies, overlapped (Figure 4-5D-H and 4-6D-H, low and high magnification). These results again reinforced the point that the overall structure of single condition temporal frequency preference maps does not change with temporal frequency of the stimuli. In fact, Figures 5H and 6H demonstrate that the majority of domains at different temporal frequencies were aligned almost perfectly with each other; nevertheless, there were

always slight variations. At low magnification (Figure 4-5H) there were a few slightly misaligned domains or even an occasional non-matched domain, which likely resulted from increased noise at those locales since there was no consistency in the pattern. There also were a few misaligned domains at higher magnification (Figure 4-6H). Additionally, at high magnification, we saw changes in sizes of activation domains at different temporal frequencies but most of these domains overlapped completely which does not support hypothesis two (Figure 4-1), which predicts that activation domains at different temporal frequencies never overlap completely. In Figure 4-6H, the majority of domains totally overlap and, in fact, the10 Hz domains are often located completely inside activation domains produced by lower preferred temporal frequencies. The most likely conclusion from this result is that the size differences seen were the result of an "iceberg" effect, produced by decreasing signal at non-preferred frequencies; therefore, the data so far are consistent with the idea that different temporal frequencies are not represented as separate domains in V1. Additional quantification using a center-of-gravity computation is provided below, which supports this preliminary conclusion.

Structure of differential maps at different temporal frequencies using sine-wave gratings

In all of our experiments, we used drifting square wave gratings as stimuli. Given that square wave gratings contain a fundamental spatial frequency and the higher harmonics, we thought it important to test our conclusions using sine wave gratings presented at two orientations and all 4 temporal frequencies. The results are shown in Figure 4-7, with the only difference being that the images used in this analysis were differential images, obtained by dividing baseline normalized images from the 0° grating

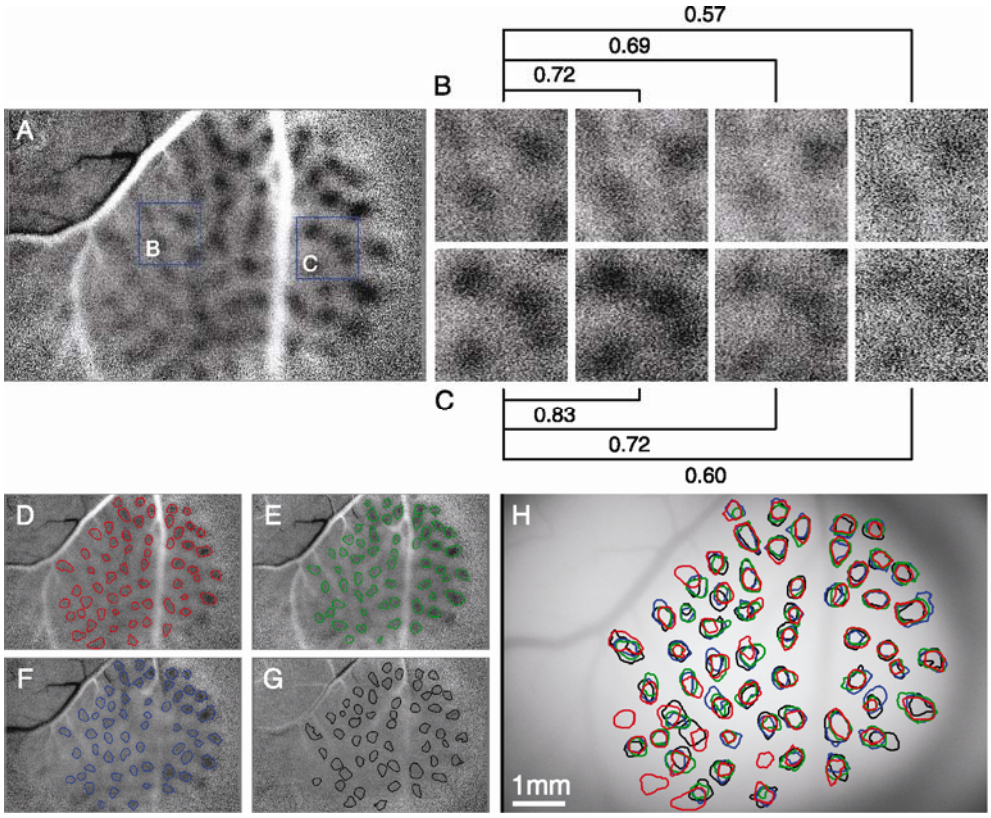

Figure 4-5. Analysis of low magnification single condition maps at different temporal frequencies (case 06-07). Panel A shows the same region as is shown in Figure 4 at higher contrast. Within panel A two regions of interests (ROIs) designated B and C were selected. These are shown enlarged in the four panel sets designated B and C to the right. In B and C activation (dark patches) at four temporal frequencies (1, 2, 5 and 10 Hz left to right) are shown for these ROIs. The connecting lines and numbers above the images are correlations for the corresponding images (see text for detailed description). D-G show the outlines of each area of activation in the entire imaged area shown in A at the four temporal frequencies D: 1 Hz, E: 2 Hz, F: 5 Hz, G – 10 Hz. H. The outlines in the same colors as shown in D-G superimposed on the reference image. See text for details. From Khaytin et al. (2007)

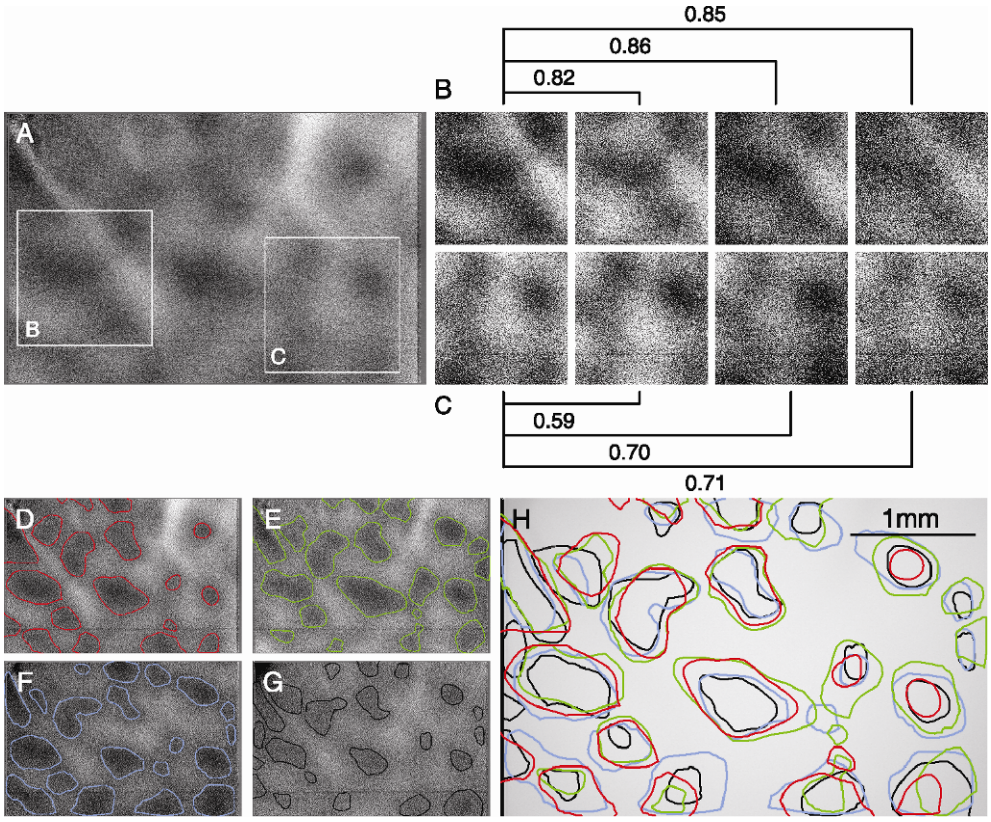

Figure 4-6. Analysis of high magnification single condition maps at different temporal frequencies (case 06-07). Same analysis as was preformed for Figure 5 was done on a high magnification images. All conventions are as in Figure 4-5 From Khaytin et al. (2007)

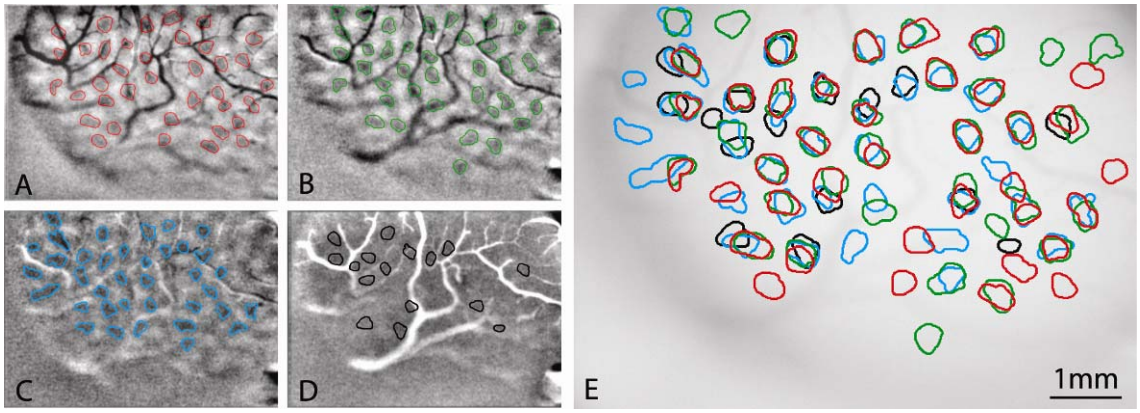

Figure 4-7. Differential images at different temporal frequencies acquired using sine wave gratings. A-D are responses at four temporal frequencies. A – 1Hz, B – 2Hz, C – 5Hz, D – 10Hz. Contrast was enhanced by clipping to 2SD. E. The outlines of activation domains in the same colors as shown in A-D superimposed on the reference image. See text for details. From Khaytin et al. (2007)

presentations by similar images from the 90° grating presentations. The images shown in Figure 7A-D were clipped at two standard deviations from the mean pixel value in the image. The domains activated by different temporal frequencies were outlined as described for Figures 4-5 and 4-6 (see Methods for details). The most significant difference between the responses to square and sine wave grating stimuli was a decrease in overall activation, as was expected from the decreased contrast in our sine-wave stimuli (see Methods and Xu et al., 2007). Additionally, blood vessel artifacts become more pronounced in the differential image. These two factors contribute to the differences in number and location of the domains. Nevertheless, the results, shown in Figure 4-7E, demonstrate that even with a single spatial frequency different temporal frequencies activated the same locations in cortex. At 10 Hz, due to very low response magnitude, the thresholding process yielded fewer activation domains, but the observed domains still were qualitatively aligned with domains activated at lower temporal frequencies.

Quantification of center of mass locations

Our results so far have been inconsistent with our first hypothesis (Figure 4-1A) which states that orientation and temporal frequency preference are interdependent. Next, we examined whether temporal frequency preference is mapped into domains similar to those found for spatial frequency (Xu et al., 2007). A commercially available image quantification software package (Image Processing Tool kit v.5 Reindeer Graphics, Asheville, NC) was used to determine the location of centers of mass of the activation domains shown in Figures 4-5 and 4-6 D-H. The computed nearest neighbor

distances between the centers of mass across different temporal frequencies are shown in Figures 4-8A and 4-8B. On average a single activation domain had the equivalent diameter, that is the diameter of a circle of the same total area, 298±64 μm (SD, N = 770). The nearest neighbor distance of the activation domains at one temporal frequency was 544±112 μm (SD, N=770). The nearest neighbor distance of the centers of activation at different temporal frequencies was 53±74 μm (SD, N=201) (median = 32 μm and interquartile range (range from 25th to 75th percentile) = 40 μm) (Figure 4-8C). These results support hypothesis 3 which predicts that the distance between the centers of mass should be close to zero, indicating extensive overlap.

Invariance of orientation domains with respect to temporal frequency changes

In order to quantify the shifts in the activation domains with different temporal frequencies in a manner independent of the centroid analysis, two further tests were employed. First, each image at a single temporal frequency was thresholded at 30% darkest pixels and obvious artifacts removed, as described above. Then, each image was processed separately to identify and label each of the domains as contiguous thresholded regions. Each of these domains was placed into a separate image. Thus, each image at a single temporal frequency provided 20-60 images. Cross-correlations were then computed between domains at each temporal frequency in the original set (0 mm displacement) and again after randomly shifting domains from 50 to 1000 μm from their original location in 50 μm steps (Figure 4-9A).

Second, the same analysis was run on data in which activation domains were outlined automatically as follows. The Z-normalized single condition images were

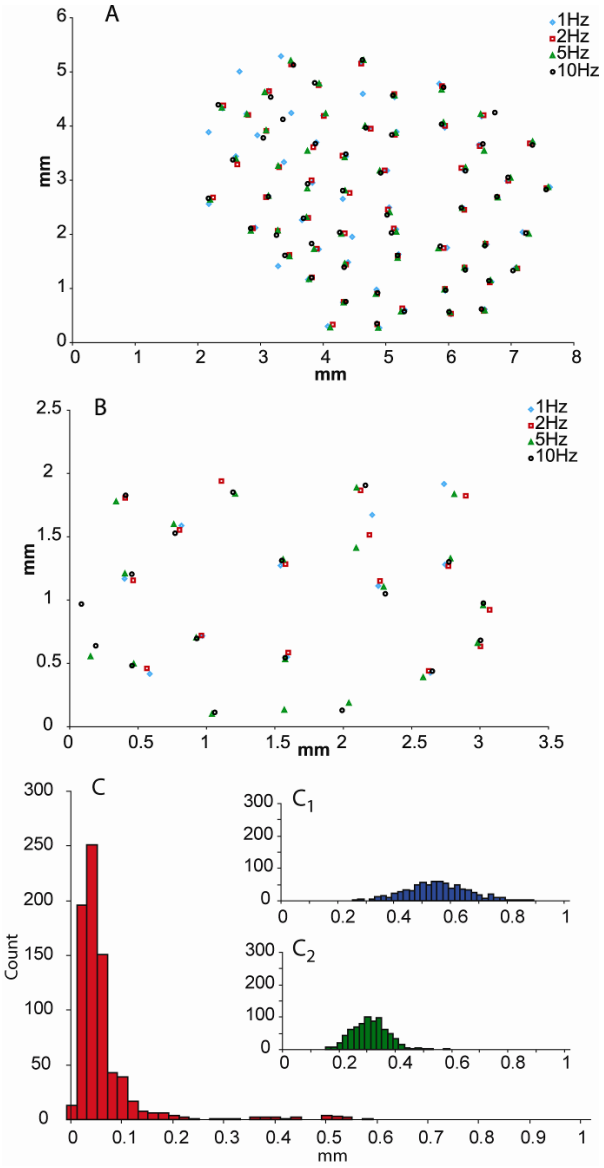

Figure 4-8. Locations of centers of mass of domains identified in Figures 4-5 and 4-6. A and B are locations of centers of mass of the activation domains outlined in Figures 5 and 6, respectively. Centers of mass are shown in real topographic coordinates. Colors and shapes represent centers of mass at four temporal frequencies 1Hz – blue, 2Hz – red, 5Hz – green, and 10Hz – black. C Distribution of the nearest neighbor distances of centers of mass of activation domains at same orientation and different temporal frequencies, as in panel A. Inset C1 depicts the distribution of nearest neighbor distances of centers of mass at the single temporal frequency and orientation. Inset C2 depicts distribution of equivalent diameters of activation domains. From Khaytin et al. (2007)

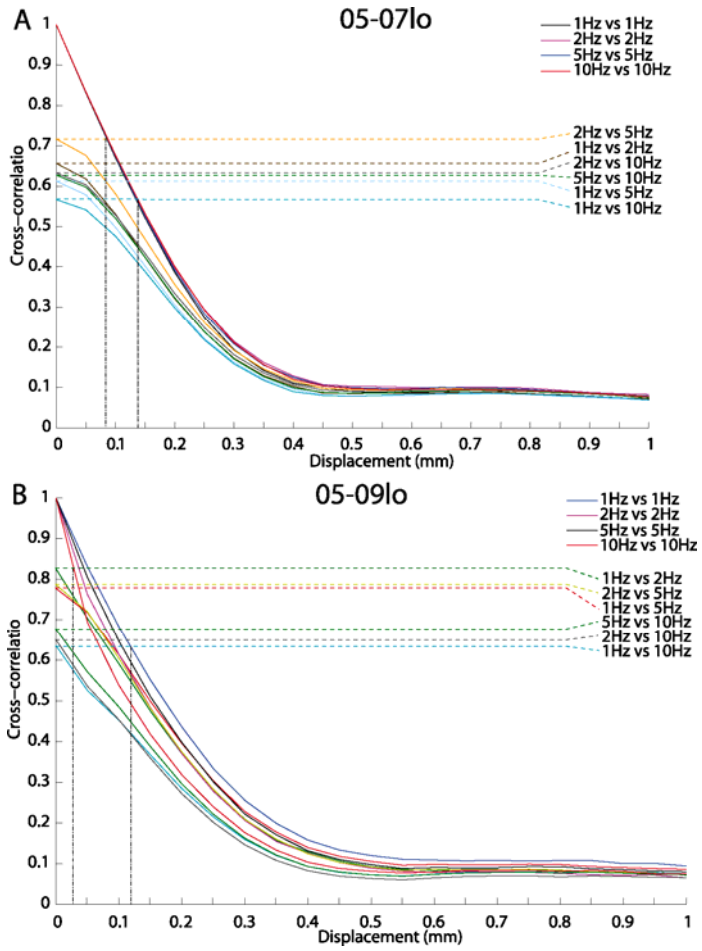

Figure 4-9. Cross-correlation coefficient as a function of independent random shift of activation domains. A and B are graphs of correlation coefficients obtained by running cross-correlations between images corresponding to responses to different temporal frequencies at the same orientation, with and without random independent shifts of individual domains. A. Graph of coefficient change in a case, in which activation domains were obtained by thresholding single condition images at the 30% darkest pixels. B. Similar to A, except domains in individual images were obtained by automatic thesholding of z-normalized images. The color legend indicates the temporal frequencies of the images that were correlated. Only domains in the image corresponding to the second temporal frequency were independently shifted by the indicated distance. The horizontal dotted lines indicate correlation levels of the images corresponding to different temporal frequencies without shift. Two vertical dotted lines indicate the equivalent random shift of the domains that would produce the same level of correlation as is seen between images of activation domains at different temporal frequencies. From Khaytin et al. (2007)

thresholded at a 0.4-0.5 standard deviation level (Figure 4-12) The cross-correlations between activation domains at different temporal frequencies were then computed with and without randomly shifting the locations of these activation domains (Figure 4-9B).

The cross-correlations between domains at different temporal frequencies at a fixed orientation were in the range of 0.57-0.82 (Figure 4-9). The results of the analysis on the manual and automatically thresholded data were similar (Figure 4-9). To achieve the level of correlation observed between the images at different temporal frequencies, domains in the original data can be randomly moved by no more than 25-140 μm. This is less than one half of the equivalent diameter of an activation domain (298±64 μm as calculated above). For comparison, cross-correlations between images of activation produced by different orientations lie in the range of -0.06 to 0.31 (data not shown). Taken together with the above analyses, these additional comparisons indicate that domain locations are reproducible across temporal frequencies within 25-140 μm. This finding supports our third hypothesis (Figure 4-1), which predicts that activation domains must have extensive overlap at different temporal frequencies.

Automatic classification of z-normalized images

As a third test of domain stability across temporal frequencies we used a hierarchical tree clustering analysis (Duda et al., 2001). This analysis was done on the z-normalized images using an automated classification algorithm. This analysis, without any *a priori* assumptions, determines the similarity of two or more images. In this analysis each image becomes a point in N*M dimensional space, where N and M are the dimensions of an individual image in pixels, and distances between those data points is

calculated, using a furthest neighbor algorithm. These distances were used to cluster the images into a hierarchical tree (dendrogram) (Duda et al., 2001), in which the lowest branches are singleton clusters of the original data and the length of the connecting branches indicates the closeness of the linked images. The more similar the images are, the closer they will be on a hierarchical tree.

This analysis reliably showed that the sixteen conditions can be consistently and reliably classified into four orientation groups (Figure 4-10 is an example). In other words, in this N*M dimensional space, images of responses to stimuli at different temporal frequencies at a given orientation are much closer to each other than are images of responses to the stimuli at different orientations at a given temporal frequency. This is further support that the domain location is independent of temporal frequency.

Absence of visible temporal frequency preference domains

Previous analyses demonstrated little support for the first or second hypothesis in Figure 4-1, however, there still could exist a possibility that temporal frequency preference is organized into domains similar to orientation and spatial frequency preference domains in bush babies (Xu et al., 2005; 2007), and that they could not be identified due to the strength of the orientation data. To eliminate the possibility of missing temporal frequency preference domains located within orientation preference domains, we averaged our sixteen baseline normalized single condition images either along the orientation dimension or along the temporal frequency dimension, thus producing eight images in which either the influence of orientation or of temporal frequency was removed (four images that had temporal frequency averaged out, and four

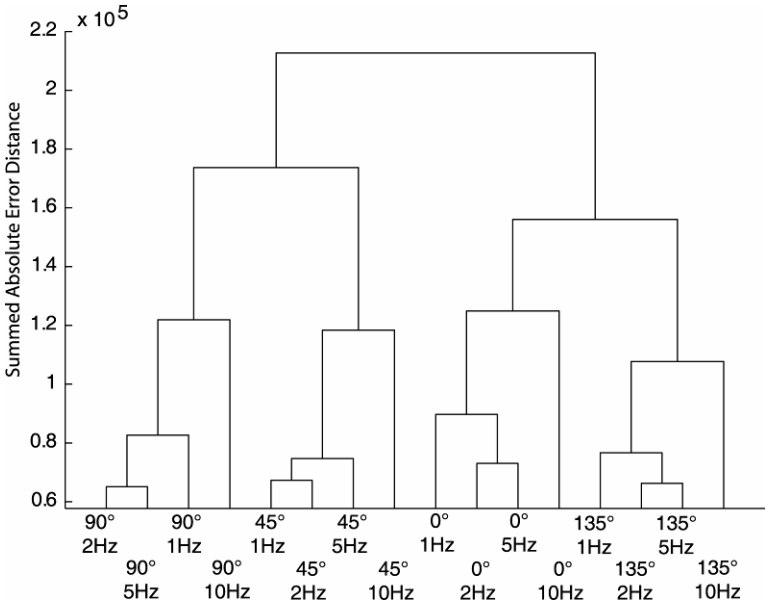

Figure 4-10. Dendrogram showing similarity between sixteen z-normalized conditions. This dendrogram was obtained by determining the distance between pairs of images using summed-absolute-error (SAE) distance metrics (see Methods and text for details). The lowest branches represent individual images. The length of linking branches indicates similarity between linked images. The Y-axis is the SAE-distance. From Khaytin et al. (2007)

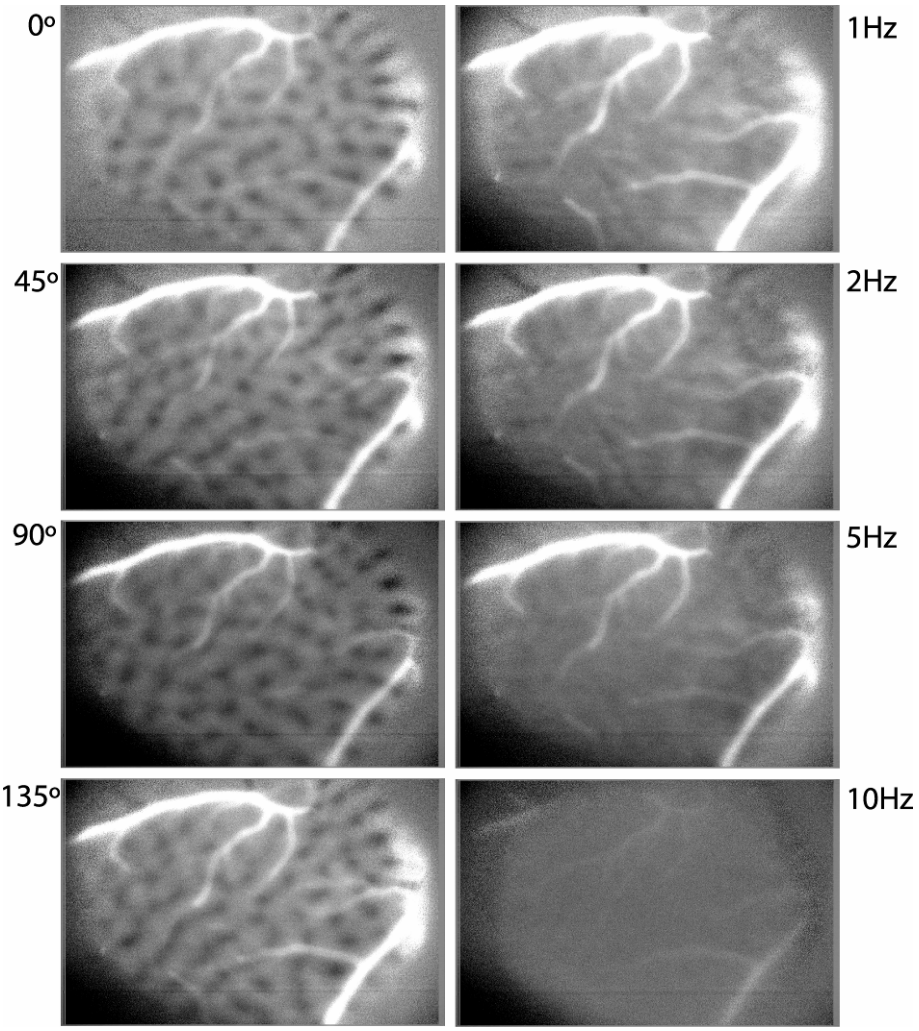

Figure 4-11. Orientation and temporal frequency preference images. In an attempt to isolate pure orientation and pure temporal frequency responses, 16 single condition images were averaged along temporal frequency or orientation dimension. Left column are responses to four orientations with temporal frequencies averaged out. Right column are responses to four temporal frequencies with orientations averaged out. From Khaytin et al. (2007)

images in which orientation was averaged out, Figure 4-11, left and right columns, respectively). There were very strong orientation domains in the absence of temporal frequency influence; there were no visible domains in the absence of orientation influence (to see how these averaged orientation preference domains align to the orientation domains in Figure 4-5 see Figure 4-15). This is an important finding since the same type of analysis clearly demonstrated the existence of spatial frequency domains in bush baby V1 (Xu et al., 2007). Therefore, we conclude that our data supports the third hypothesis (Figure 4-1), stating that temporal frequency preference is distributed uniformly across V1 cortex without any significant clustering.

Quantification of response strength at different temporal frequencies

The next analysis was to quantify the relative strength of response at different temporal frequencies and orientations. To reduce noise, the responses at each pixel of baseline normalized images were fit to a sinusoid, separately for each temporal frequency (Figure 4-3). The regressions produced two sets of data, orientation preference at each pixel location (Figure 4-3 left column), and magnitude of maximal response at each pixel location (Figure 4-3 right column), for each temporal frequency. Both sets of data were used to determine overall responses at different temporal frequencies (see Methods). Our previous electrophysiological investigations showed that most neurons in bush baby V1 can still respond at 10 Hz, even though the optimal temporal frequency for most cells lies within 1-5 Hz (DeBruyn et al., 1993). All optical imaging cases showed similar results, three of which are shown in Figure 4-12. Imaging at both high and low magnification resulted in the same response profiles at different temporal frequencies. Optical activation

was highest at the 2 Hz temporal frequency. The 2 Hz value was then used for normalization of the other temporal frequencies in Figure 4-12.

Activation magnitudes at 1 and 5 Hz were similar to each other, but about 5-10% lower than that seen at 2 Hz (with $p < 0.01$ in all but one case (N=7)). In four of the cases, the activation level at 5 Hz was lower than at 1 Hz ($p < 0.01$), as in case 05-05 (0.97 ± 0.02 normalized response units (nr) at 1 Hz versus 0.90 ± 0.002nr at 5 Hz, mean ± SE) or case 06-09lo (0.93 ± 0.03nr versus 0.89 ± 0.01nr). As illustrated by comparing high and low magnification results for cases 06-07 and 06-09, however, it is not the absolute magnitude of response at 1 and 5 Hz that is most preserved; rather, it is their relative strength in relationship to the strongest response at 2 Hz. In all cases, responses at the lowest three temporal frequencies were on average 10-15% higher than at 10 Hz ($p < 0.01$). Even though the response strength at 10 Hz was the smallest, it was still possible to detect the orientation domains visually in single condition maps (Figures 4-4, 4-5, and 4-6). In fact, in one case, hints of orientation domains in the differential images were identified even at 20Hz.

CO domain dependence of temporal frequency tuning

The relationship between the CO defined compartments and temporal frequency selectivity also was examined. Figure 4-13 depicts a thresholded image of V1. In these images cortex was segmented into three zones based on CO staining intensity: CO blobs (black), CO-blob borders (grey) and CO light interblobs (white). All three compartments were made to have approximately equal numbers of pixels. These images were superimposed on our optical maps of activation. Using a Monte-Carlo approach, 500

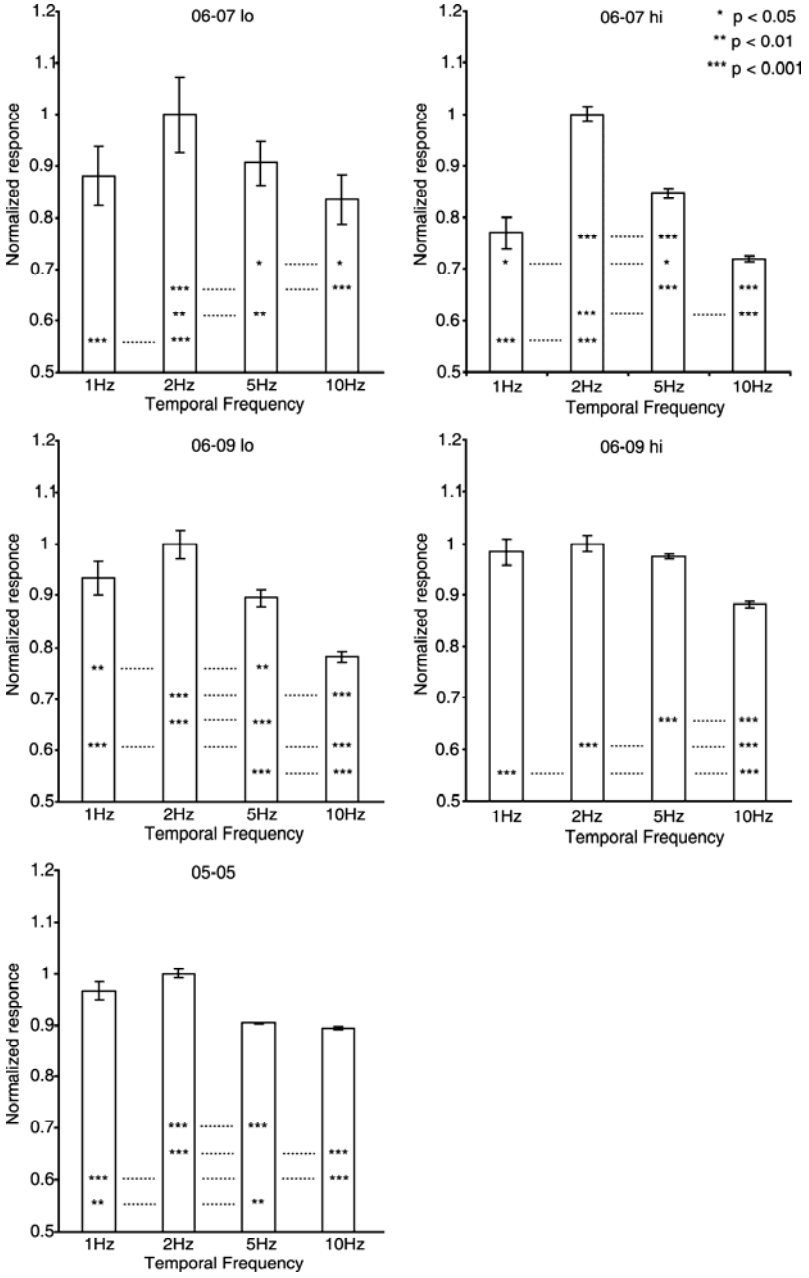

Figure 4-12. Response strengths at different temporal frequencies. Five representative examples are shown, with case numbers above the graphs. The strongest response in each case was at 2Hz. All other values were normalized to this value, taken as 1.0. Bars indicate the standard error around the mean. Results of post hoc Tukey HSD pairwise tests are shown on the graphs with stars (* $p < 0.05$, ** $p < 0.01$, *** $p < 0.001$) indicating level of significance. Each pairwise test is shown within an aligned row of asterisks connected by a dotted line. Only combinations that were significantly different are indicated. See text for details. From Khaytin et al. (2007)

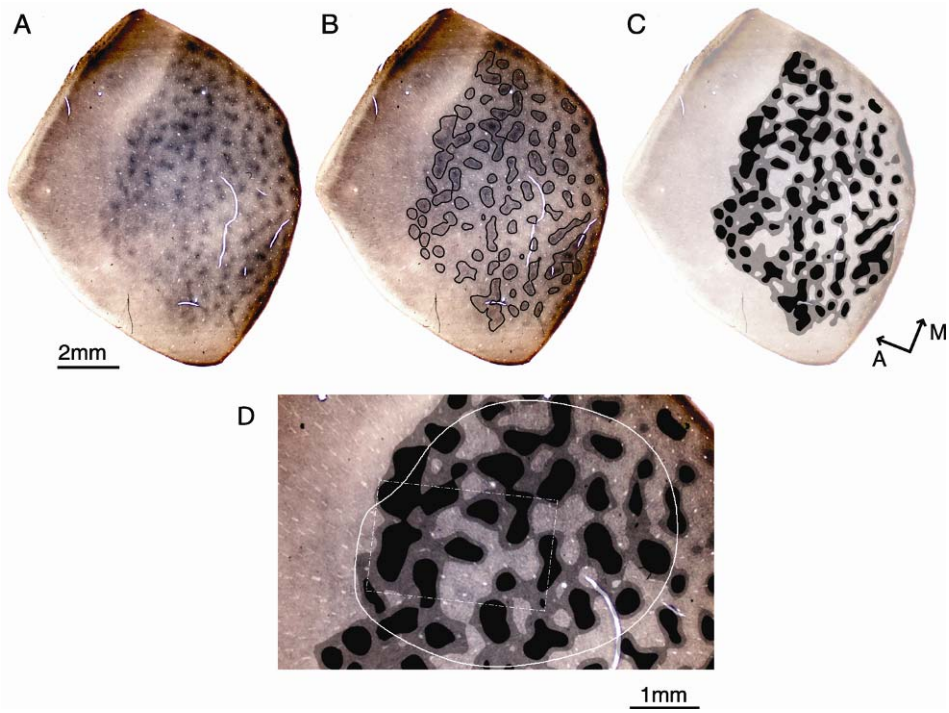

Figure 4-13. Example of thresholding method to separate CO compartments in V1 (case 06-07). A. CO stained tangential section. B Outlines of CO-blob domains. C All three subdomains, black – CO-blobs, gray – border regions, and white – interblobs. Only CO blob and interblob regions were compared for temporal frequency preference content. See also text. A, anterior: M, medial. D Area in C within view of our camera at low power (white outline). White rectangular outline is the area of the frame imaged by the camera at high power. From Khaytin et al. (2007)

pixels were selected randomly that belonged to either a blob or an interblob (repeated 50 times with replacement). Then using the magnitude of response maps (Figure 4-3 right column) the average strength of response in the respective compartments was determined. A modified Weibull function was fit to the response data. This allowed us to estimate the maximum temporal frequency preference in both compartments.

As can be seen from Figure 4-14, there was little difference in the preferred temporal frequency between blob vs. interblob compartments. Both areas have maximum responses at about 2 Hz (2.67±0.36 vs. 2.58±0.35(SD) Hz and 2.06±0.27 vs. 1.99±0.31 Hz for two cases presented). The t-test demonstrated that there is no significant difference ($p<0.22$ and $p<0.17$, respectively) in preferred temporal frequency between the two compartments.

Discussion

The primary goal of this study was to determine how temporal frequency selectivity is mapped in V1 of primates using bush babies as a model. We had three hypotheses for how temporal frequency selectivity could be organized. The first hypothesis was that orientation tuning depends on temporal frequency tuning and therefore orientation domains should shift with different temporal frequencies. The second hypothesis was that orientation domains do not depend on temporal frequency tuning but different temporal frequencies, like spatial frequencies, cluster into separate domains. This second hypothesis seemed most likely given that spatial frequency is organized this way in bush baby (Xu et al., 2007). Surprisingly, the data supported neither of these hypotheses. Instead, the data were most consistent with our third

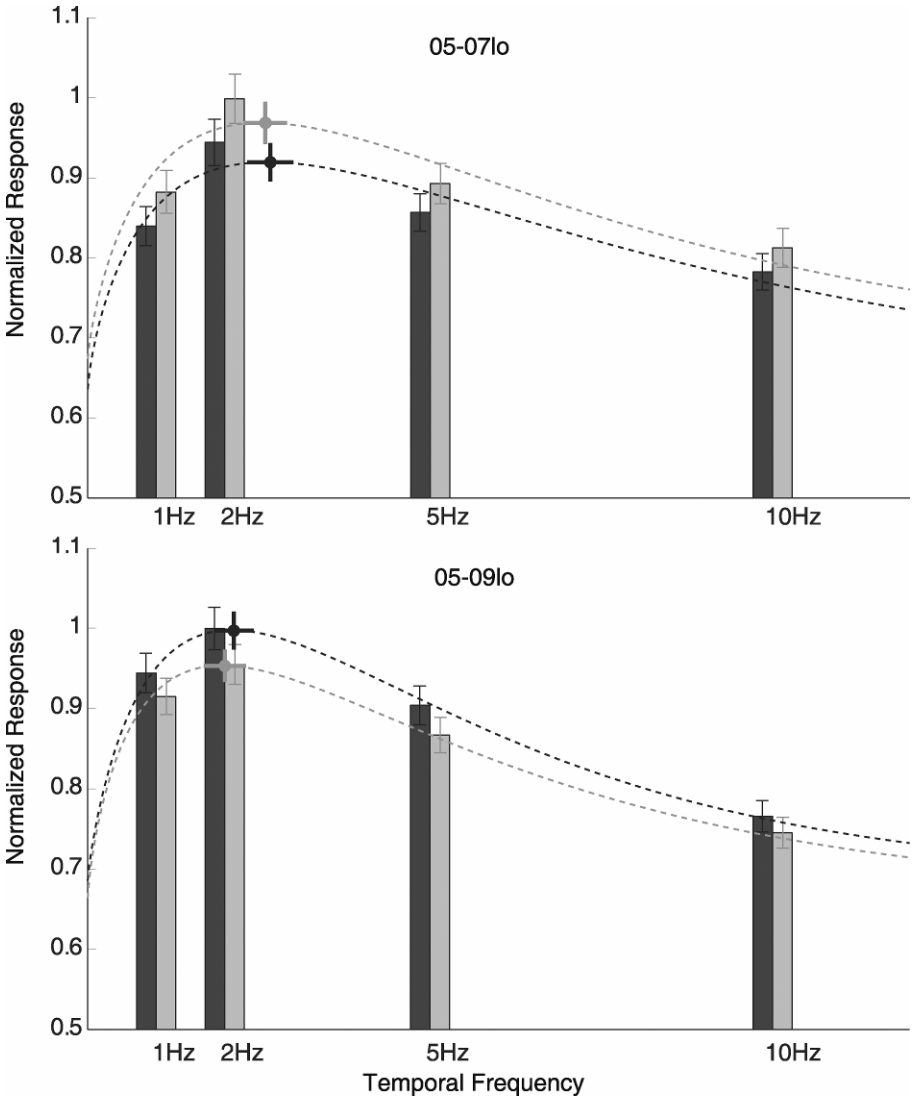

Figure 4-14. Response strength at different temporal frequencies in blob and interblob subdomains. Two representative examples are shown, with case numbers, above the graphs. The strength of the responses was normalized to the maximum average response for that case. Dotted lines indicate Weibull function fit to the data. A disk with horizontal and vertical bars indicates maximum estimated response at the preferred temporal frequency, with horizontal bar indicating one SD in preferred temporal frequency and vertical bar one SD in maximum estimated response. Black – CO blob compartment. Gray – CO interblob compartment. From Khaytin et al. (2007)

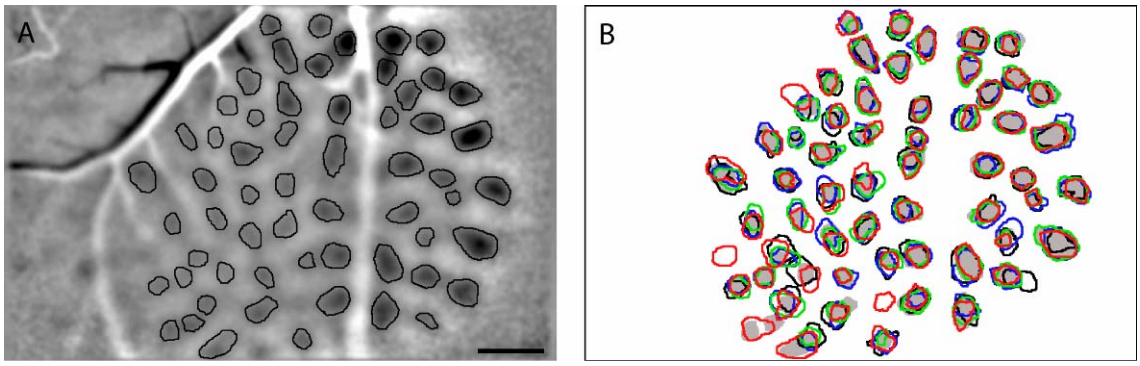

Figure 4-15. Comparison of activation domains different temporal frequencies to average orientation domains. A. Outlines of the orientation preference domains obtained by averaging activation images at one orientation and all temporal frequencies. B. Overlay of the outlines of activation domains from Figure 5H onto the outlines of average orientation preference domains. It shows that there is very strong match between two sets of data.

According to the second hypothesis the following criteria should be obtained: 1) the overall orientation preference domains must encompass all of the single temporal frequency preference activation domains at that orientation, 2) none of the single temporal frequency preference activation domains can be as large as an overall orientation domain, and 3) temporal frequency preference activation domains should not overlap completely. We found that activation domains at a single orientation and different temporal frequencies completely overlapped with some of the domains completely encompassed by the others. Moreover, the strongest activation domains completely covered the average orientation domains. This finding once again supported the third hypothesis, namely, that temporal frequencies do not organize into clusters. From Khaytin et al. (2007)

hypothesis, namely, that orientation does not depend on temporal frequency tuning and that sensitivities to different temporal frequencies do not cluster but are represented uniformly across V1. This result was particularly interesting given that other attribute maps of orientation, ocular dominance and spatial frequency in the bush baby are clearly organized into patch-like domains. Because this result was so surprising we used a range of independent quantitative methods to verify these findings. These methods, some of which have not been applied previously to optical imaging data, all suggest a lack of domains for temporal frequency selectivity and verify the existence of such domains for orientation.

These results suggest either that there is something unique about temporal frequency that requires that it be represented in this way or that only a certain number of variables can be represented as clusters and still achieve adequate coverage. Swindale (2004) has recently addressed some of these issues and pointed out that more binary (ocular dominance) or cyclic (orientation) variables can be organized into domains in V1 while still maintaining coverage than scalar variables such as spatial or temporal frequency. He argues that while five or more of binary or cyclic variables can be represented in such way, only 1 or 2 scalar variables can be represented without creating holes in the retinotopic map. Models of the type he describes would then support the third possibility, namely that two scalar variables cannot be adequately represented as clusters in bush baby V1.

In the following sections of the discussion, we first review how well the current optical imaging data in bush baby fit with previous physiological, behavioral and anatomical results in this species, then compare these results to data reported in other

species and consider the implications of these data for mapping of visual features in general. Finally, we discuss the relative stability of attribute maps when different combinations of stimulus properties are examined.

Mapping of visual features in bush baby

Bush babies are nocturnal primates that lack color vision. They have only a single cone type (Jacobs et al., 1996; Kawamura and Kubotera, 2004; Wikler and Rakic, 1990) which exists at highest density in the *area centralis* or fovea (Wikler and Rakic, 1990). Rods, which are also present in the *area centralis*, predominate in the rest of the retina. Like many nocturnal carnivores including cats and ferrets, bush babies have a well-developed tapetum, and their optimal spatial frequency sensitivity is lower than in macaque monkeys (DeBruyn et al., 1993). The temporal frequency band pass of the bush baby visual system is also low, with a critical flicker-fusion (CFF) frequency of 10-30 Hz (Ordy and Samorajski, 1968). This CFF value fits well with single unit and visual evoked potential (VEP) data showing that, as demonstrated here, the peak preferred temporal frequency in V1 is roughly 2 Hz, with a maximum cutoff temporal frequency of 20 Hz (Bonds et al., 1987; DeBruyn et al., 1993). Interestingly, we found that this high temporal frequency cutoff measured with optical imaging could vary from animal to animal, suggesting that some individual bush babies may have more cells representing the higher temporal frequencies than others. It would be interesting to know whether such variation correlated with individual differences in each animal's capacity to resolve gratings drifted at higher temporal frequencies.

Temporal frequency preference in bush baby is mapped uniformly, at least in the area of V1 representing the central 10-15° of visual space. As mentioned earlier this is clearly not the case for other feature maps examined in this primate. Spatial frequency, orientation preference and ocular dominance, mapped using optical imaging, appear to be organized in separate domains in bush baby V1 (Bonds et al., 1987; Xu et al., 2003; 2005; 2007). The only other stimulus feature examined that was not organized into domains in V1 was direction selectivity, even though directional domains were found in the middle temporal (MT) visual area in bush babies (Xu et al., 2004b). It is not clear why some feature maps in this primate show clustering and others do not, especially considering that there appears to be no precise relationships between V1 feature maps that do cluster (see Xu et al., 2005), and given that all features must ultimately be constrained by the necessity of providing adequate coverage across a continuous visual field map (see also below and Horton and Adams, 2005).

Functional maps in other species

To date, no other study that used optical imaging was specifically designed to map temporal frequency preference in V1 using drifting grating. Evidence exists that in cats high temporal frequency selectiviy measured with stimuli at low spatial frequency is represented separately from low temporal frequency selectivity measured with stimuli at high spatial frequency (Shoham et al., 1997), but other studies using optical imaging have not supported this claim (Baker and Issa, 2005; Everson et al., 1998; Issa et al., 2000). Studies using single unit recording add another dimension, but do not resolve the issue of how these stimulus features are mapped. For example, DeAngelis et al. (1993) found that despite a distribution of preferred spatial and temporal frequency preferences for

individual cells, in young cats (~8 weeks) there is no correlation between preferred spatial and temporal frequencies. As reported earlier by Baker (1990), DeAngelis et al. (1993) also found a negative correlation between spatial and temporal tuning in the adult cat. Neither study, however, examined the issue of whether there was any spatial clustering of stimulus properties in V1 in cats.

Complicating the question of how attributes are represented in V1 of other species is the fact that there appears to be no commonality between the variations seen or an obvious functional reason for them. Since Horton and Adams (2005) recently covered this subject in depth, we will mention only a few relevant points here.

Every mammalian species that has been studied shows a relatively organized map of visual field location in V1 (Chklovskii and Koulakov, 2004). There is general agreement that stimulus features that are important for the representation of objects useful for perception must somehow be represented in an iterated fashion across this continuous visual field map in order to avoid holes or gaps in the map (Swindale et al., 2000). The problem is that species appear to have solved the "coverage" problem in different ways even for the same stimulus attribute. Orientation tuning appears to be represented uniformly in all rodents and lagomorphs (e.g., rabbits), even those with well-developed relatively large V1 areas like squirrels (Van Hooser et al., 2005; Van Hooser et al., 2006). Orientation is represented in a clustered fashion (i.e. pinwheels) in primates and in both diurnal close relatives of primates, tree shrews and nocturnal distant relatives of primates, cats and ferrets (Blasdel, 1992; Bonhoeffer and Grinvald, 1991; Bosking et al., 2002; Rao et al., 1997). Similarly, some species segregate ocular input to V1 into layers (e.g., tree shrews), some segregate eye input into columns (e.g. bush babies) and some show little

evidence of either type of segregation (e.g. owl monkeys) (Casagrande and Kaas, 1994; Humphrey et al., 1977; Kaas et al., 1976; Xu et al., 2005; but see Rowe et al., 1978).

This conundrum is accentuated by our finding, reported here, that some features, such as temporal frequency selectivity in bush baby can be mapped uniformly in V1 while other features are clustered into domains. It may be that different species have come to different evolutionary solutions to the same problem, but even this explanation does not help to understand the functional significance of the enormous variation seen in some features such as the presence or absence of ocular dominance columns in the same species such as the squirrel monkey (Adams and Horton, 2003).

Are feature maps stable?

Still, such enormous variability in how different species map various visual features brings us back to the issues of how many feature maps there really are and how these features are related. As such, one important point which should be considered is the extent to which properties such as selectivity for temporal frequency, spatial frequency or orientation are hardwired in V1 or represent emergent properties that depend on the stimulus combination presented. In the current study, we examined whether there was an interaction between selectivity for orientation and temporal frequency using high contrast drifting gratings presented at either one fundamental spatial frequency plus its higher spatial frequency harmonics (square wave gratings) or a single spatial frequency (sine wave gratings). In either case the result was the same; no evidence was found for different domains devoted to different temporal frequencies.

In another study that examined this issue in ferrets using single unit recording and sinusoidal grating stimuli, orientation tuning also was found to be invariant to changes in temporal frequency (Moore et al., 2005). Yet in the same study the property of direction selectivity was found to be reduced and sometimes even reversed at non-preferred temporal frequencies (Moore et al., 2005), which suggests that these features are not hardwired but depend on stimulus conditions. In fact, Basole et al. (2003) used optical imaging in ferret V1 and showed that the same neural population can be activated by multiple combinations of orientated line segment texture patterns and dots depending on the axis of motion of these patterns and their speed. They proposed that, rather than reflecting the intersection of multiple hard wired maps, their results were better explained by considering V1 as a "single map of spatiotemporal energy". These conclusions also were supported by a subsequent modeling study (Mante and Carandini, 2005).
Since we did not use more complex stimuli of the sort they describe, we cannot address this issue for primates. Regardless, such dynamic maps still do not address the issue raised above concerning species differences seen in maps using the same grating stimuli. Future research will certainly require the use of richer stimulus sets more reminiscent of natural scenes for us to fully understand why stimulus attributes appear to be mapped in V1 in different ways when the same stimulus is used and how maps relate to each other under normal viewing conditions.

CHAPTER V

THE EFFECT OF REMOVING P OR M LGN INPUT ON FUNCTIONAL MAPS IN V1 OF BUSH BABY

Preface

After the experiments described in the previous chapter were completed, we proceeded to investigate the contribution of feedforward and feedback afferents to the functional maps in V1. This chapter describes the study designed to investigate the effect of blocking either the LGN P or M channel on orientation and spatial frequency preference maps in bush baby V1. We chose to concentrate on these two maps because both were shown to have distinct functional domains, making detection of the effects more straightforward, and because M and P channels show different selectivities for spatial frequency. We chose not to investigate the effect on the temporal frequency selectivity, described in the previous chapter, for the following three reasons: 1) Unexpectedly, we found that temporal frequency selectivity is distributed uniformly across bush baby V1, 2) The signal for pure temporal frequency is low, making it difficult to compare maps both before and after blockade, and 3) The differences in peak temporal frequency preferences between M and P LGN cells in bush baby are very small.

Introduction

The primate visual system is organized into at least two parallel streams of processing (see background Chapter 2); however the streams are not fully segregated at many levels and there is a significant amount of crosstalk between them. As in other

primates, in bush baby the initial segregation into streams occurs at the level of the retina. As described earlier, the two major classes of ganglion cells projecting to the LGN are midget and parasol which project to the P and M layers of the LGN, respectively (Yamada et al., 1998). The LGN, in turn, sends processed visual information to V1, where it arrives in different sublayers of layer 4. P cells send information to layer 4β, while M cells send afferents to 4α. Both send branches to layer 6 (Florence and Casagrande, 1987; see also Casagrande and Kaas, 1994 for rationale for laminar designations). Cells in layer 4α send their projections to layers 3C and both CO blob and interblob regions of layer 3B (Lachica et al., 1993). Cells in layer 4β project only to the CO interblobs in layer 3B in bush baby. Layer 3C (layer IVB of Brodmann) is thought to be the main source of input to the dorsal stream of processing in all primates including bush baby (see Boyd and Casagrande, 1999), while layers 3A and 3B are thought to be major contributors to the ventral stream (see Figure 5-1 and Casagrande and Ichida, 2002). Still, as can be appreciated from Figure 5-1, there is a significant amount of interconnection within V1. As a result, there is no direct correspondence between the M and P geniculate projections and the dorsal and ventral streams of processing. Instead, electrophysiological studies have shown (Allison et al., 2000; Nealey and Maunsell, 1994; Vidyasagar et al., 2002; for review see also Merigan and Maunsell, 1993) that the majority of the cells in V1 receive afferents from both pathways. Nealey and Maunsell (1994) showed, while recording from superficial layers in macaque V1, that removal of either major pathway with GABA blocking of either LGN P or M layers does not inactivate the majority of cells, but reduces their responses to a similar degree.

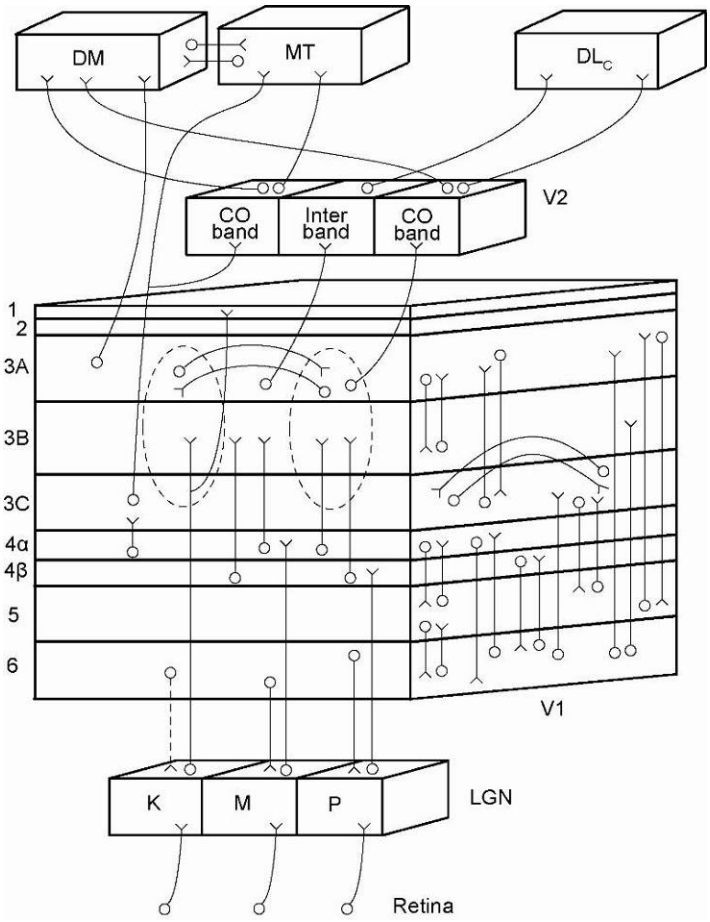

Figure 5-1. A schematic indicating some of the main intrinsic and extrinsic connections of V1 in primates as described in the text. No effort was made to define the strength of connections, or to indicate true axon collaterals or species-unique features. The major input to V1 is from the lateral geniculate nucleus (LGN) which arrives via three pathways, the koniocellular (K), magnocellular (M), and parvocellular (P) pathways. The retina also projects to other subcortical targets. Within V1, cell layers are heavily interconnected, not only by some of the axonal pathways shown but also via dendritic arbors (not shown). The main ipsilateral connections to extrastriate cortex exit from layers IIIA and IIIC. Within IIIA, the cells within cytochrome oxidase (CO)-rich blobs, indicated by dotted ovals, and CO-poor interblobs send information to different target cells within bands in V2. These three output pathways project into dorsal and ventral streams. Visual areas within each stream may represent functional clusters; however, visual areas within these streams are also heavily interconnected. Many of these areas also send feedback connections to VI (not shown). Areas are as follows: DLc, caudal dorsolateral (V4); DM, dorsomedial (V3a); MT (V5), middle temporal;
Modified from Casagrande and Kaas (1994) Fig. 22 with permission

Allison et al. (2000) observed that all recorded cells in bush baby V1 receive input from both P and M LGN layers based on blocking either the P or M layers individually with GABA.

On the other hand, multiple studies have demonstrated that the functional signatures of either pathway can be distinguished in the response properties of V1 neurons. Allison et al. (2000) observed not only continued responses of the cortical cells after LGN block, but also saw differential effects of the block. They demonstrated that the M pathway affects neuronal responses to lower contrast stimuli, while the P pathway affects neuronal responses to higher contrast stimuli. Similarly, Mazer et al. (2002) showed that the latency of the responses of V1 neurons increases in direct proportion to the spatial frequency of the stimulus. Frazor et al. (2004) not only showed that these cells respond at shorter latencies to stimuli at lower spatial frequencies, but also demonstrated that the spatial frequency preference of V1 neurons changes over the first 100 ms. Their findings were corroborated by Bredfeldt and Ringach (2002) in macaque monkey and also Chen et al. (2006) in bush baby. All of these observations support the original hypothesis by Hubel and Wiesel (1962) that the functional properties of V1 neurons evolve from the combined input from geniculate afferents.

The issue that is not covered by the previous research is to what degree the distribution of the functional preferences in V1 depends on the different LGN channels. If the original feedforward hypothesis is correct, removal of one of the LGN channels would result in very predictable changes in the structure of functional maps in V1. Removal of either the P layers or M layers should not substantially change the orientation tuning maps. On the other hand, removal of either channel should result in a shift in

spatial frequency preference to reflect the preference of the remaining channel. We investigated this question using optical imaging of bush baby V1.

Methods

Animals

Two bush babies (*Otolemur garnetti*) raised in our colony were used in these experiments. They were housed and handled according to approved protocols from the Institutional Animal Care and Use Committee (IACUC) at Vanderbilt University. Both animals underwent one surgical and two imaging procedures. During the initial surgical procedure, stereotaxic coordinates of the locations in LGN corresponding to central vision were determined. The first imaging session was used to determine the retinotopic extent of the exposed area of V1. The final session was used to collect the bulk of the data. A total of two hemispheres were imaged, one as part of the P layer blocking experiment and one as part of the M layer blocking experiment.

Surgery and perfusion

These experiments, in general, followed the same protocols that were described in the previous chapter. Here, only the procedures that were different will be described. During the first surgical session two craniotomies were performed. The V1 opening was 10 mm in diameter with posterior and lateral sides 1 mm away from the lambdoid and sagittal sutures. The opening over the LGN was 8 mm wide centered on stereotaxic coordinates of 8 mm lateral to the midline and 4 mm anterior to Horsley-Clark zero.

Visual evoked potential mapping of the LGN layers was done using 2-4 MΩ tungsten electrodes (FHC inc. Bowdoin, ME). The representation of the central visual field in LGN was usually found at about 9-10 mm depth from the surface. A more refined location corresponding to the center of the retinotopic location of the exposed V1 was found during the last imaging session using custom made injectrodes. The injectrodes were constructed by gluing an 85 μm diameter tungsten electrode (FHC) to the side of a glass pipette with 1 mm outer diameter and 0.5 mm inner diameter. The pipette was pulled and broken to achieve a 20 μm tip opening with a slight bevel. Ultraviolet (UV) curable glue (Loctite 3921, Loctite, Rocky Hills, CT) was used to attach the electrode to the pipette. This glue was chosen because it cures in ~10 sec when exposed to intense UV light, allowing precise positioning of the two elements. The tip of the electrode preceded the tip of the pipette by ~30-60 μm and was ~0-20 μm to one side (Figure 5-2). A styllette was used to draw up and eject the contents of the pipette. At the end of the last session animals were perfused as described earlier.

Muscimol injection

In order to inactivate a single layer of the LGN, muscimol, a $GABA_A$ agonist, was used. Muscimol was selected for blocking LGN layers because of its long action and because of its demonstrated effectiveness in visual system studies. Shaw and Cynader (1986) showed that there is a wide distribution of muscimol binding sites in LGN, with M layers showing especially dense binding. Huntsman et al. (1996) demonstrated that the LGN has the densest expression of GABA receptors of all thalamic nuclei. GABA has

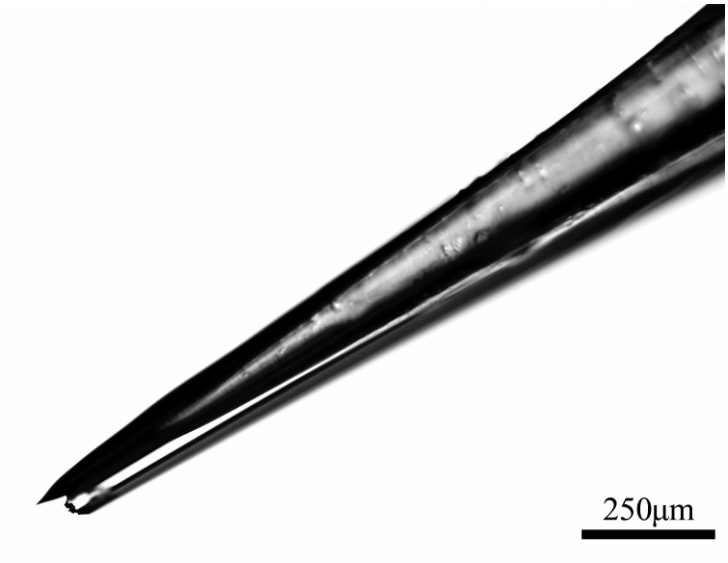

Figure 5-2. Photomicrograph of the tip if the injectrode, custom made in our lab. See text for the details of making this injectrode.

been used extensively for blocking studies in the visual system and, in particular, in electrophysiological studies of LGN blocking, but the effect of a GABA injection lasts much too short a time to be able to be used practically in optical imaging experiments. Additionally, Arikan et al. (2002) have done radiographic studies of the spread of muscimol in the central nervous system, and, therefore, we could estimate the optimal concentration and volume of muscimol needed to inactivate only one major geniculate layer.

After collecting the control imaging information, as described below, the injectrode was placed into the previously determined central vision representation in the LGN in the appropriate contralaterally innervated layer. It was then repositioned so that the receptive fields of the recorded multiunit activity were in the center of the corresponding retinotopic location in V1 from which imaging data was collected. After the appropriate location of the LGN was found, 200 nL of 50 mM muscimol in saline was pressure injected over a 5 min period with an additional 10 min of wait time before withdrawing the injectrode. To visualize the approximate spread of the muscimol in the nucleus, it was mixed with 5% 10,000 MW fluorescent dextran. In the M block experiment, to prevent leaking of the muscimol along the track while lowering the injectrode into position, 200 nL of thin silicone oil was drawn into the pipette after filling it with the muscimol/dextran mixture. In that experiment, silicone oil was pushed out of pipette over a 10 sec interval, before initiating a slow injection of muscimol.

Histology and alignment

In addition to the procedures described in previous chapters, the LGN was sectioned frozen, parasagitally into 50 μm sections. The sections were then photographed using fluorescent microscopy to visualize the spread of the muscimol. Sections were then Nissl-stained and photographed again to reveal the histological structure of the nucleus. Since the same sections were used both for the fluorescent photography and the Nissl staining, alignment of two photographs was done by matching the outlines of the brain sections in the two images (see Figure 5-4).

Optical imaging

The imaging was performed in the same way as described in the previous chapter and elsewhere (see Chapters 3 and 4) Data for the construction of orientation preference maps were obtained using square wave gratings at 4 orientations, 0.5 c/deg fundamental spatial frequency, 2 Hz fundamental temporal frequency, 100% contrast and 50% duty cycle. Data for the construction of spatial frequency preference maps were collected using sine wave gratings at 4 orientations, 4 spatial frequencies (0.2, 0.5, 0.9 and 1.6 c/deg), 2 Hz temporal frequency, and 50% contrast. The same stimuli were used before and after blocking one geniculate layer. Since all data were collected monocularly with the ipsilateral eye covered, it was only necessary to block one layer of each set of M and P layers. Each orientation condition was presented 20-30 times. Each spatial frequency condition was presented 40-70 times. Figure 5-3 depicts a schematic representation of the experiment.

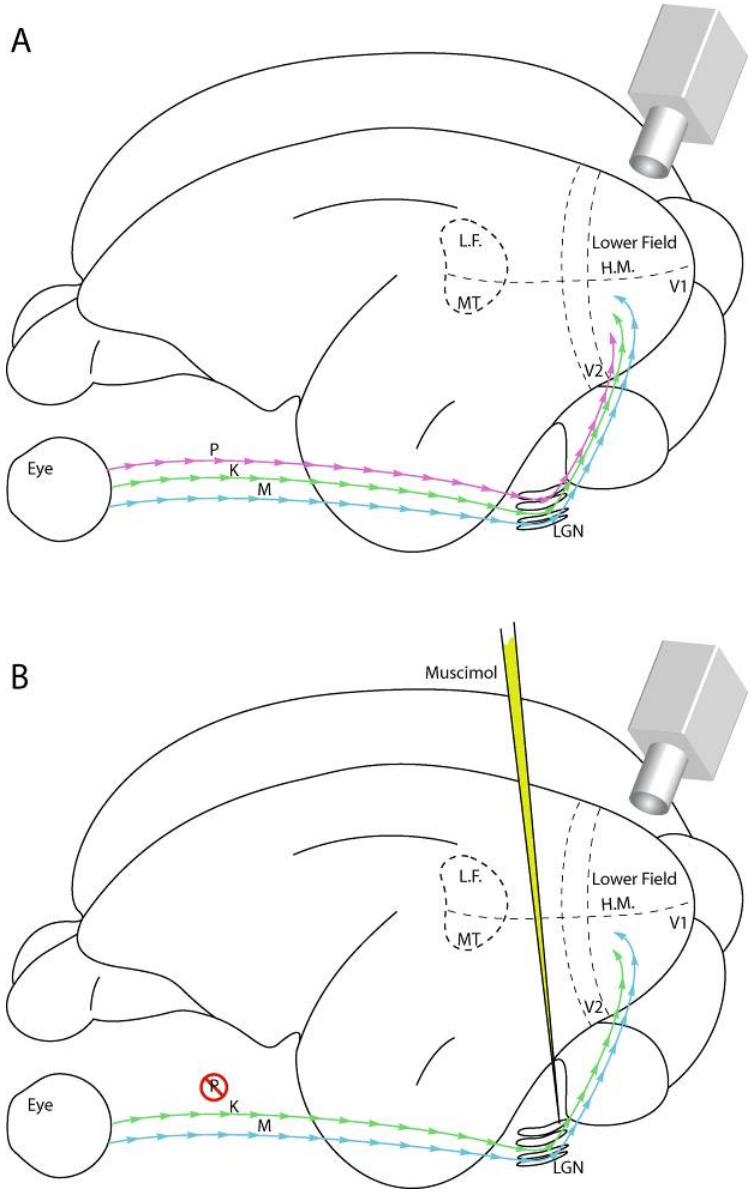

Figure 5-3. Schematic diagram of the LGN layer blocking experiment. Optical imaging data was obtained before blocking (A) and after blocking (B). The location of the LGN was determined during the original surgical procedure, and fine tuned during the blocking experiment. (see text for details). HM - horizontal meridian. LF -

Analysis

Several important differences from the analysis methods described before need to be mentioned here. To ensure that the mapping data could reliably be compared before and after the block, the camera position and angle were carefully recorded before the LGN injection and then repositioned to match the initial location. To further increase the match, reference images obtained before and after the block were aligned in Photoshop and the exact number of pixels necessary to eliminate any mismatch was noted. For the purpose of matching, all the data images that were constructed in the analysis were shifted by the noted number of pixels to align them perfectly.

The major difference used here in the analysis compared to the analysis described earlier was the construction of winner-takes-all (WTA) spatial frequency tuning maps. This analysis was performed using all 16 single conditions obtained by averaging single condition images across all trials. In this analysis, the maximum response of each pixel was noted across all conditions and then the spatial frequency at which this maximum response occurred was determined and assigned to that pixel. The procedure was repeated for all pixels in the image creating one control WTA spatial frequency map and one after blocking.

Results

Effect of blocking the P channel

The imaged area of V1 extended from 5-15 degrees eccentricity mainly in the lower visual field. The LGN the injection was made within a zone that overlapped the

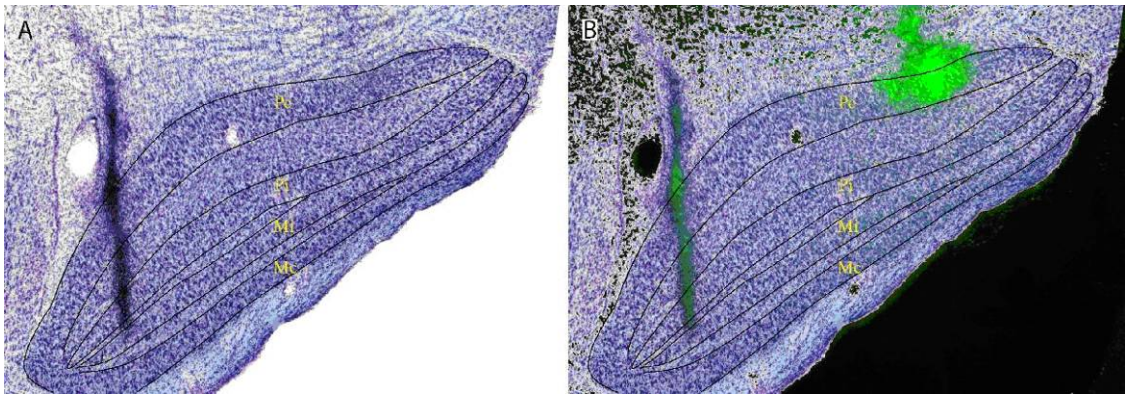

Figure 5-4. Bush baby LGN. A. Nissl stained parasaggital section of bush baby LGN. Anterior is to toward the left and dorsal toward the top of the figure. Pc and Pi are contralateral and ipsilateral parvocellular (P) layers, respectively. Mc and Mi are contralateral and ipsilateral magnocellular (M) layers. Notice that both contralateral layers are located at the top and bottom of the LGN, separated by a wide space of ipsilaterally innervated P and M layers and the koniocellular (K) layers. B. Same section as in A with overlaid image of the same section showing fluorescence (false colored bright green) where muscimol mixed with fluorescent dextran was injected. See text for details.

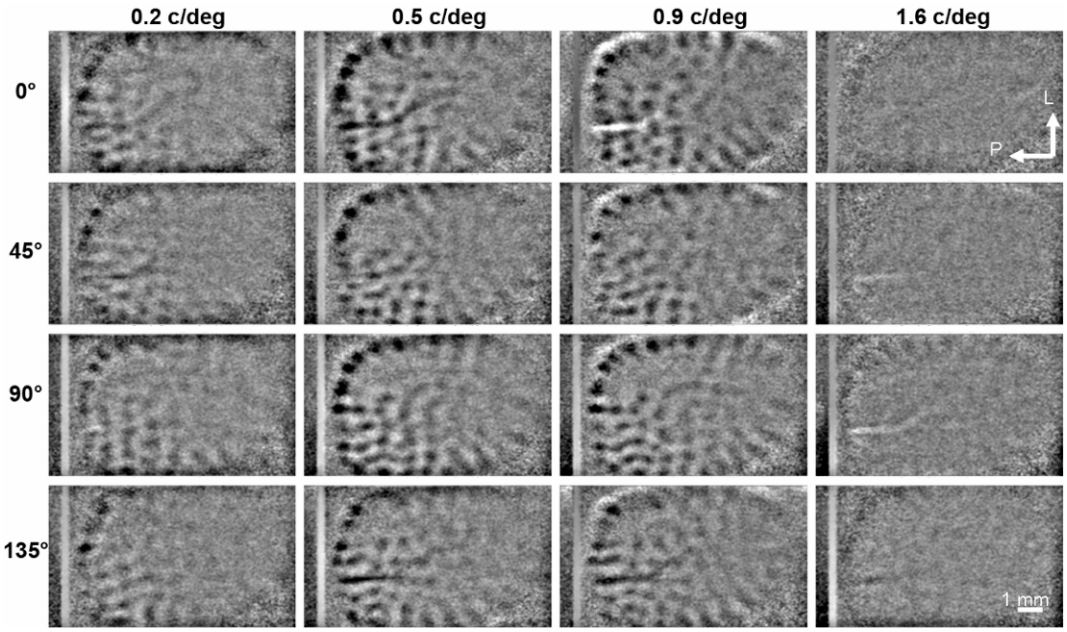

Figure 5-5. Responses of bush baby V1 to stimuli at four orientations and four spatial frequencies before block. These single condition baseline normalized images demonstrate patterns of activation to the indicated stimuli. Darker patches are zones of V1 which preferred the given stimulus. Note the dramatic decrease in activity at the highest spatial frequency. P - posterior. L - lateral.

imaged area at about 7 degrees eccentricity in the lower field. Figure 5-4A shows the lamination pattern of the bush baby LGN and Figure 5-4B depicts the injection site in the contralateral P layer. As can be seen, the injection was restricted to the contralateral P layer (green fluorescent patch at the top right of the image). There is minor leakage up the injectrode track, but it is confined to the white matter above LGN where there are no GABAa receptors and the axons are heavily myelinated. The size of the injection was approximately 400-500 μm in diameter, which we know from the previous experiments in our lab (Allison et al., 2000) to cover about 10-15 deg of visual space. Therefore, we are confident that the area which we were imaging was within the affected region. In order to reduce the possibility of contamination of results from regions of V1 that were not matched to the blocked LGN site we restricted our analysis to a small region centered on the eccentricity of the recordings in LGN. The track visible on the left side of the section corresponds to the initial penetration done with a tungsten electrode during our surgical procedure session to determine the location of the LGN in this animal. The fluorescence seen on this tract is an artifact of tissue scarring as no musimol was injected at this location.

Response to the moving sinusoidal grating

Figure 5-5 shows responses of V1 to the presentation of sinusoidal gratings at four orientations and four spatial frequencies. These are single condition images, as described in the previous chapter. They were normalized to the same scale and, therefore, relative contrast is directly proportional to the strength of activation. The dark regions are the areas that were most activated by the given combination of the orientation

and spatial frequency of the grating. There is a clear dependence of the strength of activation on the spatial frequency of the stimulus, with 0.5 and 0.9 c/deg being preferred frequencies and 1.6 being the least preferred frequency. Careful observation of the responses at a single orientation and different spatial frequencies also reveals that the activation domains are located at different positions confirming the spatial frequency map described earlier (Xu et al., 2007).

Signal strength before and after block

Blocking the P pathway resulted in a decrease in V1 activity as would be predicted from our single unit data (Allison et al., 2000 and Figure 5-6A). Both before and after images are normalized to the same range, so that the contrast is proportional to the actual optical activity in the cortex. Activity is clearly lower following the P block at the two depicted spatial frequencies. Activity also decreased at the 0.2 c/deg spatial frequencies (not shown), and was no longer apparent after blocking at 1.6 c/deg. The response strength was quantified the same way as it was done in the temporal frequency study (see Chapter 4), that is, the data were fit to a sinusoid on a pixelwise basis and the amplitude of the curve was taken as the response strength. The response for the control condition was defined as unity. Figure 5-6B shows quantitatively that the overall response of V1 decreased when input from the P layers was removed. There was a decrease at all frequencies.

Orientation preference with and without P layer input

Because the overall signal strength was lower after blocking the P channel, we also had to be concerned about the lower signal to noise ratio in our interpretation. As described by Polimeni et al. (2005 see also Chapter 3), vectorial values are more sensitive to signal to noise changes which can result in artifactual movement of pinwheel centers and incorrect conclusions about domain positions. Therefore, the locations of single condition activation domains were compared instead. The influence of spatial frequency was removed by averaging across the spatial frequencies for each orientation of the stimulus. As can be seen from Figure 5-7, the location of the orientation activation domains remained the same after the P input was blocked. The minor misalignments of the domains can be accounted for by a decrease in the signal to noise ratio in the after-block condition. The figure depicts the result of the block at one orientation; however, the same result was obtained at all orientations, supporting the idea that the orientation map did not undergo changes due to P block.

Spatial frequency preference with and without P layer input

The same could not be said about the spatial frequency preference map. The same analysis when applied to the spatial frequency activation domains, obtained by averaging out orientation, revealed dramatic changes in the areal distribution of the activity (Figure 5-8). Even qualitative observations of the amount of cortex activated by a single spatial frequency before and after the block revealed changes. The activity shown in the figure was obtained at 0.9 c/deg. There is a clear decrease in the number of activation domains in the post-block condition (Figure 5-8). Moreover, the domains that

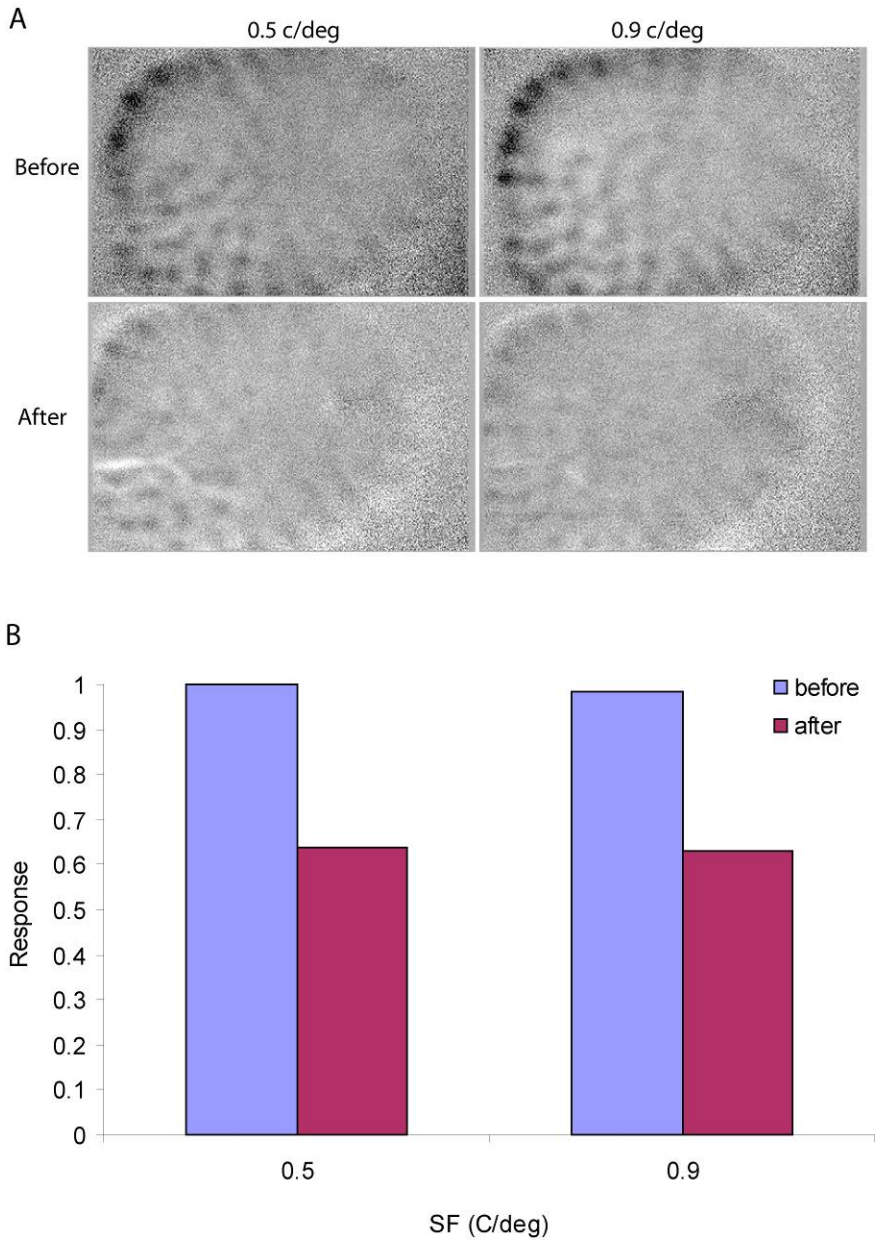

Figure 5-6. Effect of blocking the Pc layer of LGN. A. Single condition baseline normalized images of activation in response to horizontal moving grating at two spatial frequencies before and after the block. Dark patches are zones of activation. Contrast of the images is proportional to the response magnitude. There is clear decrease in activation after P channel block. B. Quantification of the response magnitude before and after P channel block. See text for quantification details.

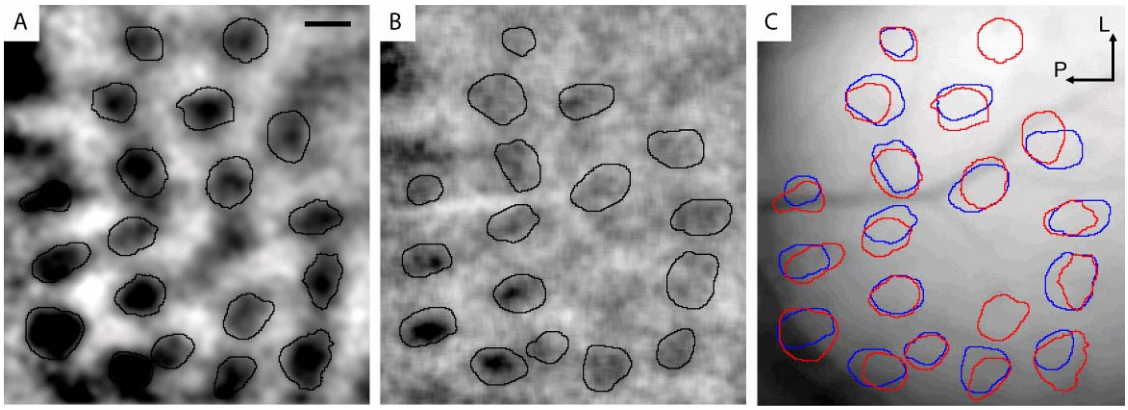

Figure 5-7. Example of orientation preference domains in V1 before and after P channel block. The images depict responses to horizontal grating with spatial frequency averaged out before (**A**) and after (**B**) the block. Contrast is enhanced to increase visibility. **C**. Overlay of the outlines of activation domains before and after the block on the reference image of the cortex. Red - before. Blue - after. P - posterior. L - lateral.

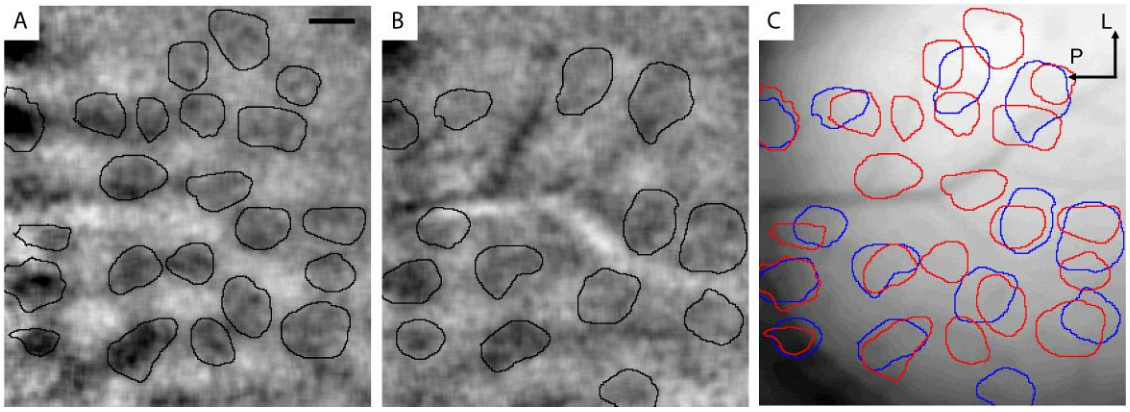

Figure 5-8. Example of spatial frequency preference domains in V1 before and after P channel block. The images depict responses to 0.9 c/deg grating with orientations averaged out before (A) and after (B) the block. Contrast is enhanced to increase visibility. C. Overlay of the outlines of activation domains before and after the block on the reference image of the cortex. Red - before. Blue - after. P - posterior. L - lateral.

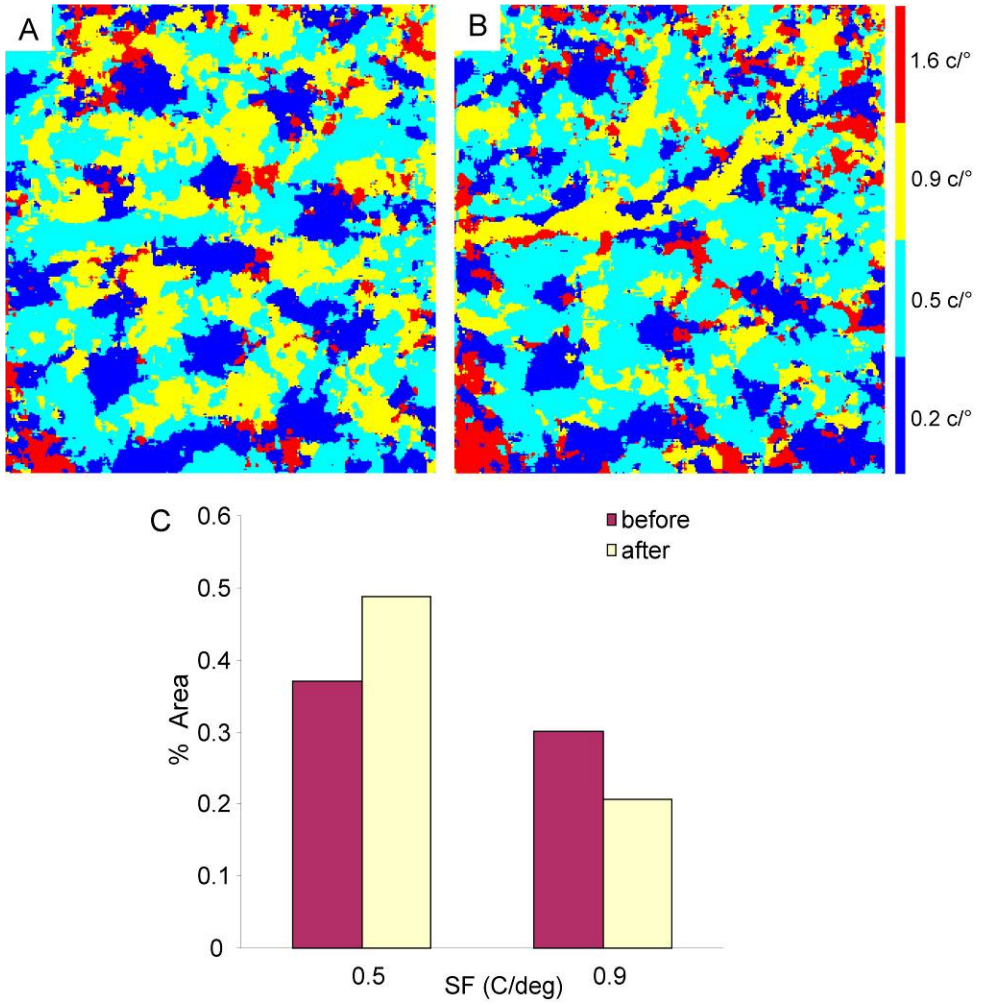

Figure 5-9. Spatial frequency (SF) preference in V1 before and after P channel block. A and B are winner-take-all maps of spatial frequency preference before and after the block, respectively. Color legend for SF is adjacent to B. See methods Chapter 5 for additional details. C. Quantification of the percent of total pixels responding to the gratings at 0.5 and 0.9 c/deg before and after the block obtained from the images in A and B.

remained active for the most part moved out of alignment with activation domains visible during the control condition. These qualitative observations suggested a shift in spatial frequency preference. In order to quantify this change, WTA maps were created (Figure 5-9). The spatial frequency preference map showed a patchy distribution of selectivity for different frequencies, as was demonstrated by Xu et al. (2007). The same could be said about the map after the P layer block. However, there was clear change in the amount of cortex that responded maximally at the lowest and highest spatial frequencies. Additionally, there was an obvious decrease in the number of 'hot' colored pixels, representing selectivity for the two higher spatial frequencies, with a proportional increase in the selectivity for the lower two frequencies. Figure 5-9C shows the number of pixels that responded maximally at 0.5 and 0.9 c/deg. Two observations can be made from this graph. First, as would be expected from the fact that 0.5 c/deg is the preferred spatial frequency of a majority of the cells in bush baby V1 (DeBruyn et al., 1993), the number of pixels showing maximal activity at that frequency before the block is higher than that at 0.9 c/deg. Second and more importantly, after the block the number of pixels showing maximal response at lower spatial frequencies became larger, while that for higher spatial frequencies became smaller. This finding is in agreement with results showing that both P and M channels contribute to the spatial frequency selectivity of V1 cells.

Effects of the M layer block on activity in V1

Figure 5-10 shows the LGN blocking site in the M layer in another bush baby. It demonstrates that the injection is confined to the M layers centered on the contralateral

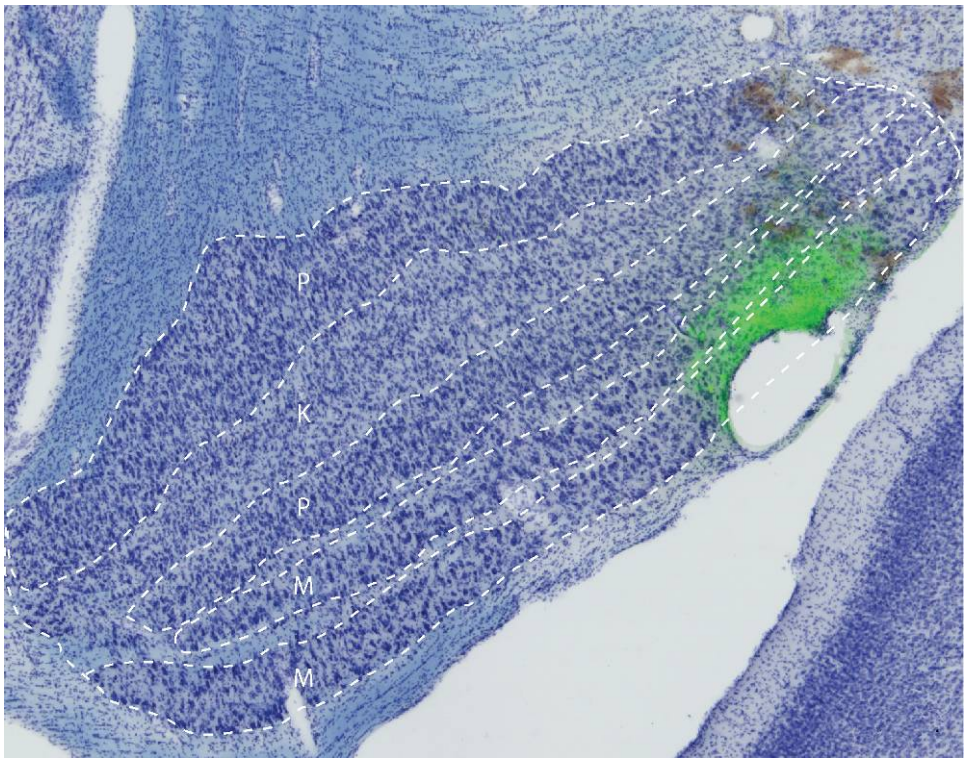

Figure 5-10. Image of bush baby LGN showing injection into the contralaterally innervated M layer. The bright staining is fluorescence indicating the extent of muscimol spread. The hole in the middle of the injection site is due to silicon oil which was used to seal the tip of the injectrode. Above the injection site it is possible to see the injectrode track. The injection was confined to the M layers.

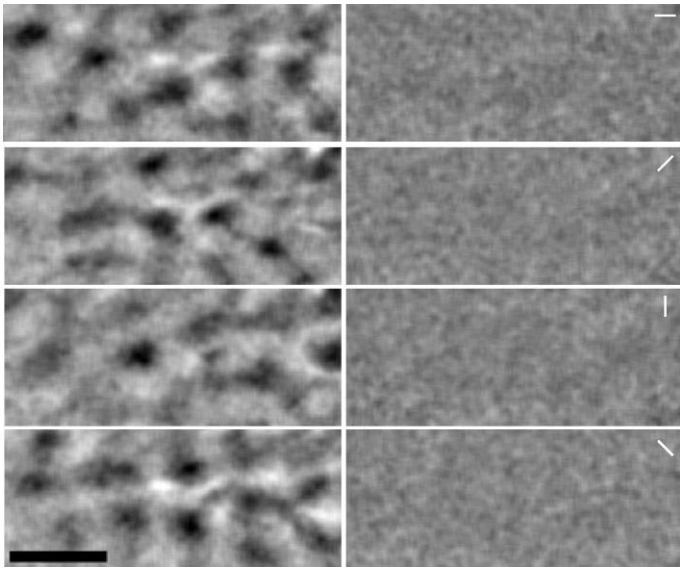

Figure 5-11. Orientation preference responses before and after M channel block. Single condition images in response to four orientations with spatial frequency averaged out are shown. Left column corresponds to before the block condition. Right column corresponds to after the block condition. Dark areas are the patches of V1 cortex responding to the grating at the preferred orientation, shown in the right column. Notice almost complete lack of activation after the block.

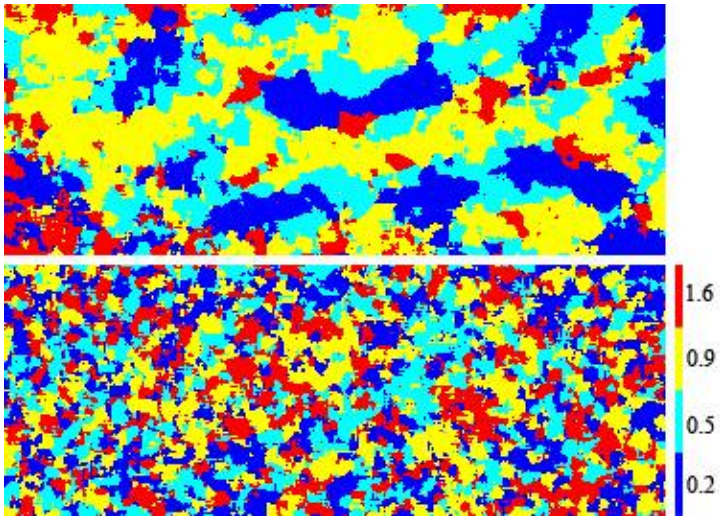

Figure 5-12. Winner-take-all (WTA) maps of spatial frequency preference before and after M channel block. Top image is map before the block. Bottom image is map after the block. The WTA map before the block exhibits patches of spatial frequency preference similar to ones seen in Figure 5-9A. After the block WTA map exhibits a random distribution of spatial frequency patches due to very low activation. Other conventions as in Figure 5-9

M layer. The hole in the middle of the injection site is the artifact left by the silicone oil. Silicone oil is inert and was used to prevent leakage of muscimol into the dorsal part of the LGN as the injectrode passed through the LGN. It is likely that this drop of oil simply displaced the tissue. The injection site spread across both M layers but did not invade the P layer.

Figure 5-11 compares the overall strength of activation before and after the block. The control images clearly demonstrate the presence of activation domains similar to those shown in Figure 5-5. Activation was sufficiently strong to allow us to create both orientation and spatial frequency preference maps (not shown), both of which were similar to the maps obtained previously. Unexpectedly, the activation after the block was almost not detectable. Clearly, inactivation of M layers had a much greater effect on the activity in V1 than inactivation of P layers; however, it is hard to make definitive conclusions based on a single case. Possible reasons for and implications of such a dramatic decrease in activity are considered below.

After M block we were unable to construct maps of either orientation or spatial frequency. Both revealed a noisy salt-and-pepper distribution of the domains activated by a particular stimulus. Figure 5-12 shows WTA maps of spatial frequency preference before and after the inactivation of the M layers. There are clear spatial frequency selective domains in the before-block condition, but a very random distribution of such domains in the post-block condition. Initial observation of the spatial frequency map after the inactivation suggests that more pixels are responding to the higher spatial frequencies. When the number of pixels responding to each spatial frequency was evaluated, however, it was found that ~25% of pixels were responding to each frequency.

Therefore, we had to conclude that the distribution of preferences in the WTA map was random.

Discussion

The goal of this study was to determine what role either of the LGN channels plays in the formation of the functional maps in bush baby V1. Previous electrophysiological studies showed that the majority of cells in V1 receive input from both major geniculate channels, and removal of one channel shifts selectivities of individual cells towards those of the remaining channel (Allison et al., 2000). Based on the latter results, it was expected that inactivating either the M or P pathway would result in no significant alteration of the orientation preference map but would cause changes in the spatial frequency selectivity map to reflect mean differences in selectivity of individual neurons in these two pathways.

Our results for the most part supported these expectations. The P blocking data are in full agreement with the hypothesis stated earlier. However, the M blocking results were unexpected. In the following sections of the discussion, we will first consider how well our results fit the classical Hubel and Wiesel (1962) model. Then we will consider the possible reasons for not supporting the hypothesis in the case of the M block. We will conclude with a discussion of the functional significance of these results.

The classical model

In the original model, Hubel and Wiesel (1962) argued that the functional properties of V1 neurons are based on the combined input from many LGN cells although they did not specifically address the issue of whether either the M or P LGN channel played a special role. They proposed that orientation selectivity, one of the most striking emergent properties of V1 neurons, is constructed by having a row of geniculate neurons of the same polarity (ON or OFF- center), aligned along a certain oriented line in visual space, providing an input to a single cortical neuron. Hubel and Wiesel (1962) termed such V1 neurons "simple" cells. They used the term "complex" cells to refer to neurons that built their receptive fields from the receptive fields of simple cells. The classical model assumed that the spatial frequency selectivity of both classes of V1 cells arises from the size and spatial arrangement of the excitatory centers of the receptive fields of either ON or OFF LGN cells.

This model, however, did not address the issue of how inputs of at least two different classes of LGN cells contribute to the formation of the receptive field properties of cortical neurons. As was described in the introduction, it is clear that the receptive field properties of cortical neurons are not stationary. Spatial frequency preference of individual neurons shifts in time. Moreover, stimuli at lower spatial frequencies elicit faster responses in the cortex (Chen et al., 2006; Frazor et al., 2004). Some efforts were therefore made to modify the classical model to account for the added complexity of the responses. Frazor et al. (2004) proposed a simple extension of the classical model that would account for spatial frequency and latency dynamics. They showed that by simply aligning receptive fields of projecting M and P neurons along the orientation preference

of the receiving neuron, it is possible to have that cell retain its orientation selectivity while dynamically changing spatial frequency preference. This model, therefore, relies exclusively on feedforward inputs from LGN for the creation of the functional properties of V1 neurons.

Support of the modified classical model

The P inactivation data presented in this study supports the modified classical model. The feedforward model predicts that the strength of the response of V1 neurons must depend on the amount of geniculate input it receives. Inhibiting a single LGN channel, therefore, must result in reduction of the cortical activity. Both P and M channel blocks in our study resulted in drops in cortical activation. The modified model predicts that, since M and P inputs arrive with different latencies, the spatial frequency selectivity must shift from an earlier M dominated lower frequency preference to P dominated higher frequencies. The P channel blocking study described here also agreed on the effect of block on spatial frequency selectivity although it could not address the temporal shift specifically due to the poor temporal resolution of optical imaging. As predicted, the overall preference of the neuronal populations in V1 shifted toward the selectivity of the remaining LGN channel. However, the M channel block did not yield enough data to see if the same held true in that case. We consider the reasons for this below.

Concerning orientation preference, most single cell recordings did not find dynamic shifts in orientation preference (Allison et al., 2000; Malpeli, 1983; Nealey and Maunsell, 1994; but see Ringach et al., 1997), as would be predicted by the purely feedforward model. The same appears to hold true on the population level. Using

voltage sensitive dyes, Grinvald and colleagues (Slovin et al., 2002) showed with at least ~10 ms resolution that orientation preference of the whole population of neurons in V1 of behaving macaque did not change significantly over the 350 ms of observation. Accordingly, we did not expect to see changes in orientation preference after inactivation of one geniculate channel. Results from our P block supported this idea but the results of our M block did not.

Mystery of the M block effects

As mentioned earlier, the most dramatic result of the M channel inactivation was a significant decrease in cortical activity detected by optical imaging. As a result, the signal to noise ratio dropped. One possible explanation, as was mentioned in the methods, is that there are some differences in the density of GABA receptors in LGN. At least in macaques, M layers stain significantly more densely for this receptor than do P layers (Hendry and Miller, 1996). It is possible, therefore, that the same amount of muscimol would produce a much more significant depression of the M layers than the P layers (assuming bush baby LGN is similar to macaque), resulting in much larger reduction in the response strength in V1 (Alitto and Usrey, 2008). It would be interesting to see if a simultaneous block of V1, and either channel in LGN, would result in equal reduction in synaptic activity in the corresponding subdivisions of layer 4.

Additionally Lachica et al. (1992; 1993) showed that while in macaques both layers 4α and 4β project into CO blob and interblob regions of layer 3, in bush babies interblobs receive input only from the upper tier of layer 4 which gets input from the M layers. As a result, the activity in layer 3 of bush baby may be more dependent on

contributions from the M channel than was seen in studies of macaque monkeys. Nevertheless, this explanation is hard to reconcile with all previous blocking studies which found that the majority of V1 neurons in macaque and bush baby continue to respond after blocking either channel (Nealey and Maunsell, 1994; Allison et al., 2000).

Role of the LGN inputs in function of V1

Our results agree with previous electrophysiological findings in bush baby that most V1 neurons receive inputs from both LGN channels (Allison et al., 2000). However, the unexpectedly significant changes in the V1 maps after the M block, either because of a dramatic reduction in overall activation or because there were also underlying changes in functional responses of the V1 population, indicate that the final functional properties of the V1 neurons may depend on more than just a linear summation of two inputs with a temporal offset.

What might account for our findings? Why would Allison et al. (2000) be able to show activation of bush baby V1 cells from either the M or P pathway while we showed little to no activation after a block of the M pathway in the same species? There are several possible interpretations. First, it could be that when small areas of the LGN are blocked the impact is different than when more extensive zones are blocked. In the former case the recorded cells might be activated well enough by neighboring cells in V1. This does not, of course, explain the big difference in results we see between the M and P blocks. The latter could be explained by a stronger anatomical dependence in the nocturnal bush baby on the M pathway than on the P pathway (see earlier). It is noteworthy that even in the Allison et al. (2000) study the impact on contrast response

was greater following the M than the P blocks. Additionally, Allison et al. (2000) only sampled from V1 cells that could be driven by the remaining LGN pathway. There may have been many V1 cells that were silenced that would not have been sampled with the electrode in that study..

It also is noteworthy that in studies with macaque monkeys ibotenic acid lesions of the P and M pathways had unexpected effects. As in bush babies, macaque M cells are more contrast sensitive than P LGN cells (see Purpura et al., 1988). Therefore, one would predict, behaviorally, that M LGN layer lesions in macaques would result in a loss of contrast sensitivity. Unexpectedly, the exact opposite result was obtained, namely, the monkeys' contrast sensitivity dropped dramatically after P layer lesions (Merigan et al., 1991a; 1991b; Schiller et al., 1990). No change was seen after M layer lesions (Merigan et al., 1991a; 1991b; Schiller et al., 1990). Why was there this mismatch between LGN cell behavior and the results of these LGN layer lesions on the contrast sensitivity of these macaque monkeys? One possible explanation is that since in central V1 of macaque there is almost a 50 times higher density of P afferents than M afferents per mm^2 (Schein and de Monasterio, 1987) and the ibotenic acid lesions were very large, the V1 activity was reduced to such degree, overall, that M cells could not longer provide an adequate drive.

Returning to our experiments, this sort of logic would suggest that V1 cells require some minimum level of baseline activity for either pathway to demonstrate its impact. In nocturnal primates the M pathway may have more of an impact than in diurnal primates where the P pathway may dominate. Regardless, if this is true one test of this idea might be to artificially raise the baseline activity in V1 pharmacologically and then

measure the maps following M layer block in bush babies or P block in macaque monkeys.

Another possibility is that the effects we saw relate more to processes happening in and beyond V1. Multiple studies have demonstrated single cell and population properties in V1, which cannot depend solely on feedforward input from LGN. For instance, Kenet et al. (2003) showed using voltage sensitive dyes that orientation preference domains can be seen in cat area 18 even without presenting any stimuli. Also, as was mentioned before, the post V1 processing of visual information can be roughly subdivided into dorsal and ventral streams. Both have very heavy feedback projections to V1 (Bullier et al., 2001), and can potentially have a significant impact on the processing and signal strength in V1. Multiple studies have implicated a combination of internal long range connections and feedback as a source of surround suppression in extraclassical receptive fields. For instance, Grinvald et al. (1994) were able to demonstrate suppression of the responses to small "center stimuli" when near "surround stimuli" were presented at the same time using voltage sensitive dye imaging in macaque V1. Similarly, multiple electrophysiological blocking studies of extrastriate areas (Galuske et al., 2002; Hupe et al., 1998; Hupe et al., 2001; Payne et al., 1996; Vanduffel et al., 1997) demonstrated that removal of the feedback reduces activation in V1. Therefore, these additional factors may have contributed to the results we saw.

This idea, that activity in V1 is dependent on both feedforward, as well as, lateral and feedback connections, once again may help us understand why the removal of the M pathway resulted in more dramatic changes in V1 activation. It is important to stress that M and P pathways do not impact the dorsal and ventral pathways in the same way. For

example, Maunsell and colleagues (Ferrera et al., 1994; Maunsell et al., 1990) demonstrated that removal of the P pathway does not result in a dramatic reduction in activity in either the dorsal pathway (area MT) or the ventral pathway (area V4). In contrast, similar manipulation of the M pathway virtually silenced area MT in macaque. This finding suggests that blocking LGN M layers not only reduced feedforward activation from LGN, but, by virtue of reducing feedback from MT, also could have reduced VI activity even more. Of course, for this hypothesis to be true, it is important to show that activity in MT of bush babies undergoes a similar reduction as has been demonstrated in macaques after M channel block or at least V1 which provides its main input.

In summary, we attempted to verify the classical Hubel and Wiesel model of the emergence of functional properties in V1 neurons using optical imaging of intrinsic signals while manipulating M and P channel inputs. Our P channel inactivation study was in full agreement with the model; however, removal of M channel led to an unexpectedly large reduction of activation. We propose that this effect may be related to functional connectivity of M layers specific for bush babies and/or it could be related to the effect of the M channel block on extrastriate areas with consequent reduction of feedback. The latter hypothesis, of course, assumes that reduction in feedback input has a significant enough effect in V1 to be detectable by optical imaging on a population level. We tested this hypothesis in Chapter 7.

CHAPTER VI

THE ORGANIZATION OF THE MIDDLE TEMPORAL (MT) AREA IN OWL MONKEYS

Some parts of this chapter were published (Xu X, Collins EC, Khaytin I, Kaas JH, Casagrande VA. 2006. Unequal representation of cardinal vs. oblique orientations in the middle temporal visual area. PNAS 103:17490-17495) and some parts are still in preparation. Since I am a third author on the published manuscript, I will provide my own description of this study here. The study in preparation will be presented in full.

Preface

The previous chapter focused on the effects of blocking each of the two major feedforward pathways from LGN to V1, namely, the M and P channels. As mentioned earlier, the unexpected result was that blocking the M pathway reduced the activity in V1 dramatically. One of several proposed mechanisms that might account for such a dramatic change is that blocking the M pathway would actually block both the feedforward M geniculate input to V1, while also reducing the feedback from MT onto the same neurons. According to that proposal, feedback from MT could contribute significantly to the activity in V1. Because MT also receives input from V1, when the M pathway is blocked, M channel activity in V1, needed for MT, is also reduced, in turn, resulting in a decrease in MT activation. This could then reduce the impact of feedback, resulting in an even greater decrease in V1 activity. Blocking the P channel may not result in a similar effect since the upstream ventral pathway areas appear to remain quite

active after blocking either the M or P channel, at least in macaque monkeys (Ferrera et al., 1994). In preparation to test the interactions between V1 and MT more directly, we needed to scrutinize the details of the organization of MT. As mentioned earlier (Background) there has been controversy concerning details of the retinotopic organization of area MT. Therefore, to examine interactions between retinotopically limited regions of both areas, we needed a more complete understanding of the organization of area MT. Below we present the results of retinotopic mapping in area MT. An interesting additional result that emerged from this effort was our finding that the map in area MT is anisotropic. I have reported some of these results previously in abstract form (Khaytin et al., 2007 and in preparation); some results also have been published (Xu et al., 2006).

Part 1: Background

Connections of MT

Area MT was first identified at about the same time by two different groups in owl monkey (Allman and Kaas, 1971) and macaque (Dubner and Zeki, 1971). MT is a myelin rich area with complete visuotopic representation of the opposite hemifield lying at the posterior end of superior temporal sulcus (Allman et al., 1973; Van Essen et al., 1981). MT receives rich projections from and projects to multiple visual areas (Felleman and Van Essen, 1991; Krubitzer and Kaas, 1990; Lin et al., 1982; Maunsell and Van Essen, 1983; Wall et al., 1982; Weller et al., 1984; Weller and Kaas, 1983). MT receives its major afferents from layer 3C of V1 (Boyd and Casagrande, 1999; Shipp and Zeki,

1989). The other large input from V1 originates from the large Meynert cells in layer VI in macaque and owl monkey (Boyd and Casagrande, 1999; Nassi et al., 2006; Shipp and Zeki, 1989) and bottom of layer 5 in bush baby (Boyd and Casagrande, 1999). It is important to note that layer 3C is not uniform and contains at least two anatomically distinct groups of cells that project to MT (but see Elston and Rosa, 1997). The spiny stellate cells receive mostly M channel projections indirectly from layer 4α and provide the dominant direct input to MT (Shipp and Zeki, 1989; Yabuta et al., 2001). The other cells that send indirect input to MT are pyramidal cells. These pyramidal cells receive inputs from both layers 4α and 4β, and therefore, are influenced by both M and P LGN channels (Yabuta et al., 2001). These pyramidal cells also project to other areas including areas V3 and the thick stripes of V2 (Burkhalter and Van Essen, 1986; Levitt et al., 1994b; Rockland, 1992), both of which send efferents to MT (DeYoe and Van Essen, 1988; Felleman and Van Essen, 1991; Zeki and Shipp, 1988). Additionally, MT projecting cells in layer 3C are not distributed uniformly. They tend to be clustered underneath CO blobs in bush baby, less clustered in owl monkey and least clustered in macaque (Boyd and Casagrande, 1999). Recently Nassi et al. (2006) suggested that Meynert cells also serve as a relay to MT for both P and M geniculate inputs. Additionally, several subcortical structures have connections to MT. The K pathway seems to have direct input into MT bypassing V1 (Sincich et al., 2004; Stepniewska et al., 1999). Pulvinar also has a very rich set of connections to MT (Kaas and Lyon, 2007). It was suggested that pulvinar serves as a relay of inputs to MT from superior colliculus (Rodman et al., 1990) but finding histological evidence of this indirect connection proved to be somewhat problematic (Stepniewska et al., 1999). The functional significance of

such rich direct and indirect innervations from cortical and subcortical sources is at the center of an ongoing controversy over whether area MT can be active without input from V1 (Collins et al., 2003; Kaas and Krubitzer, 1992; but see Rodman et al., 1990; Rosa et al., 2000). This issue is re-investigated in Chapter 7.

Functional properties of MT

The functional organization of MT has been studied in several species and was found to have both similarities and differences across species. Some of the details of this organization were reviewed earlier. Relevant to this chapter is the fact that there have been some controversies concerning the retinotopic organization of MT. Both Gattas and Gross (1981) and van Essen et al. (1981) reported that there were 'considerable irregularities' in receptive field centers along an electrode penetration in macaque MT, but neither group estimated how much of this irregularity was attributable to scatter. Albright and Desimone (1987) investigated retinotopy in macaques and found that globally and locally receptive fields had different extents of retinotopy. They found, however, that even though the receptive field sizes in MT were significantly larger than in V1, both have scatter of receptive field locations equal to about 1/3 of the diameter of the mapped receptive field at that eccentricity. The issue of the retinotopic organization of MT is considered in more detail below.

Area MT has several defining functional characteristics which were reviewed above. Relevant to our studies described here, however, is an interesting observation made by Felleman and Kaas (1984) in owl monkey MT. These authors report finding groups of cells with low, middle and high velocity selectivity. This finding may indicate

that owl monkeys have both maps of spatial and temporal frequency preference in area MT, and, therefore, silencing MT could have a differential impact on the properties of cells in V1, an issue we address in Chapter 7.

Orientation and direction selectivity were also studied using optical imaging. Malonek et al. (1994) found that owl monkey MT has a well-defined orientation preference map with features similar to those in V1, such as linear zones of slow orientation preference change and pinwheels around which preference changed rapidly. They found that depending on the type of stimulus they used, they saw different direction preference maps with often overlapping regions of opposite direction selectivity. In contrast to this result, in bush babies direction selectivity determined with moving gratings and random dots produced very similar direction selectivity maps regardless of the stimuli; domains of opposed directions were always located within each orientation domain (Xu et al., 2005). Both studies, however, agreed that there are approximately twice as many direction selective domains as there are orientation selective domains, with coaxial direction and orientation preference domains overlapping.

Part 2: The Middle Temporal (MT) Visual Area: What rules apply to its retinotopic organization?

Introduction

The rationale for this portion of my thesis was to determine the details of the retinotopic organization of area MT in relationship to V1 in order to be able to precisely test their interactions as described in chapter 7. As described earlier we know area MT receives major input from V1 and that both V1 and MT have maps of visual space. In

V1, however, it is well known that much more tissue is devoted to the representation of central vision than peripheral vision (Gattass et al., 1987; Schein and de Monasterio, 1987; Wassle et al., 1989; Rosa et al., 1997; Silveira et al., 1989; Tootell et al., 1988e). Within the LGN input to V1, however, magnification factors vary with cell type such that the M layers show less of an over-representation of central vision than the P layers (Connolly and Van Essen, 1984; Malpeli and Baker, 1975; Malpeli et al., 1996) in keeping with the differences in the distributions of these cells classes in the retina (Wassle et al., 1989; 1990). In V1 the magnification factor appears to reflect the organization of the P layers more closely than the M layers (Schein and de Monasterio, 1987). Here we asked whether the opposite might be true of area MT, given that MT is known to depend heavily on input from LGN M cells (Nealey and Maunsell, 1994 and see earlier discussion).

Methods

Animals

Three owl monkeys (*Aotus trivirgatus*) were used in these experiments. Animals were housed and handled according to approved protocols from the Institutional Animal Care and Use Committee (IACUC) at Vanderbilt University. All procedures were done acutely and each animal had one hemisphere imaged.

Surgery and histology

Procedures were similar to those described in more detail earlier (Xu et al., 2004a; 2005; 2006) and are only briefly described here. Initial surgery was done under isofluorane/O_2 anesthetic (2-4%). For imaging the animals were subsequently switched to an infusion of propofol (~10 mg/kg/hr) and sufenta (2-4 μg/kg/hr) plus lactated ringers with 5% dextrose as a nutrient mixture. The animals also were given a neuromuscular block (vencuronium bromide 0.6 mg/kg/h) and respired with a 75/25 % mixture of NO_2/O_2. CO_2. ECG, heart rate and temperature were monitored continuously and maintained within the normal range.

Contact lenses with 3-mm artificial pupils with sufficient power were used to make the retina conjugate with the viewing distance to the monitor of 28.5 cm. Retinal landmarks (*area centralis* and optic discs) were identified and marked on the monitor using a reversible ophthalmoscope technique.

At the end of each experiment, the animals were euthanized with an overdose of sodium pentobarbital (Nembutal, 100 mg/kg) and perfused through the heart with saline followed by an aldehyde fixative in buffer. The brain was removed, and the piece of the cortex containing the imaged area was dissected free from the remainder of the brain and placed overnight in a 30% sucrose fixative solution under a lightly weighted Petri dish cover. No unfolding or further dissection of the tissue was done. The weights simply maintained the tissue surface flat in a plane parallel to the original cover glass used during optical imaging so each tissue section could be cut in a plane appropriate to later alignment with the imaged surface. Both MT and V1 were sectioned tangentially with the first section cut at 150 μm to preserve surface blood vessels and the remainder of the

piece cut at 50 μm. Two to three pinholes were made at the periphery of the tissue to aid in later alignment. Alternate sections were stained for either cytochrome oxidase (CO) (Boyd and Matsubara, 1996) or myelin (Gallyas, 1979). All the sections were digitally photographed through a Nikon 0.5X objective. Sections were aligned to each other using tangential blood vessels and pinholes and images of blood vessels taken during the experiment. The location of MT was confirmed by dense CO and myelin staining around the superior temporal sulcus (STS).

Imaging

The data were collected using the Optical Imager 2001 (Optical Imaging Inc., Mountainside, NJ) using methods similar to those described in previous publications (Bosking et al., 1997; Xu et al., 2004a; Xu et al., 2005; Xu et al., 2007). In brief, the brain was illuminated using either 610 nm or 540 nm light, with latter used only to collect the reference image and the former to collect the data. The camera recorded at 30 frames per second and averaged each of the 30 frames into one data frame. Each stimulus presentation lasted 22 seconds, therefore, producing 22 data frames per presentation. The stimuli were presented using a 21-inch video monitor (Sony FD Trinitron, model GDM-F400, Sony, Tokyo, Japan) in 120 Hz non-interlaced mode and at a mean luminance of 30 cd/m^2. The monitor screen maximally subtended approximately 54˚ x 74˚ of visual stimulation angle at a distance of 28.5 cm. All stimuli consisted of square wave gratings (0.5 c/deg fundamental spatial frequency, 3 Hz temporal frequency, 20% duty cycle, either 0 or 90 degrees orientation) confined either to the full screen, or to an aperture. The apertures used were rectangular bars at or parallel to the horizontal or vertical

meridians, circles and rings of various diameters centered on *area centralis.* Retinotopy was mapped using bars and rings and data used to calculate the cortical magnification (CMF) was collected using circles. Each stimulus consisted of 2 sec of gray screen at a luminance equal to the average luminance of the grating, followed by 8 sec of grating presentation and finally 12 sec of the gray screen (blank condition). All the activation data were stored in proprietary Optical Imager 2001 files and processed offline.

Analysis

All frames corresponding to the one stimulus condition were averaged together using WinMix (Optical Imaging, Inc., Mountainside, NJ) or custom made Matlab (MatWorks, Inc.) programs. Differential images were obtained by division of the averaged images of activation resulting from the presentation of orthogonal stimuli. These resultant differential images were smoothed using a 45 μm averaging kernel, and low frequency noise was removed by convolving images with a 700 μm averaging kernel and subtracting the resultant image from the original. These differential images were thresholded at the 15% brightest and darkest pixels, and artifacts, such as blood vessels, were removed. Finally, the 'rubber band' outline of the activation zone, in which outer edges of the single orientation activation domains were connected by a line, was created. An Image Processing Toolkit (Reindeergraphics, Ashville, NC) was used to determine the exact size of the activation zones. To find the relative increase in the activation zone size, the activation zone from the smaller stimulus was subtracted from the activation zone produced by the larger stimulus. Similarly, the relative increase in the size of the stimuli was determined by subtracting the stimulus areas of the smaller stimuli from areas

of the larger stimuli. The resultant relative increase in activation zones was then divided by relative increase in the size of the stimulus, the square root of which produces the linear cortical magnification factor (CMF). We fitted the resultant data to a power function using the Microsoft Excel (Microsoft Corp, Redmond, WA) trend fitting function.

Results

Retinotopic organization of Owl Monkey area MT

Our first goal was to see if an orderly increase in the stimulus size would result in an orderly increase in the activation area in MT. We were able to produce reliable activation with stimuli as small as 0.5 and as large as 20 degrees in radius presented in the opposite hemifield. As can be seen from Figure 6-1, increasing the size of the stimulus resulted in orderly increase in the area of activation within MT. For instance in the case shown in Figure 6-1, a semi-circle of 1.0 degree radius activated approximately 1.87 mm^2 of cortex, while a semicircle 2.5 degrees activated 3.89 mm^2 of cortex. As expected from prior anatomical data, the areas of activation were confined within approximately an oval cortical zone at the tip of the STS. The activation domains produced by the smaller stimuli were completely confined within activation domains produced by larger stimuli. For instance, careful inspection of the activation provided by the 2.5 and 5 degree radius semicircles in Figure 6-1 reveals that all of the activation domains present for the smaller stimulus are present following stimulation with the larger stimulus, however, domains at the edge of the smaller zone of activation are activated

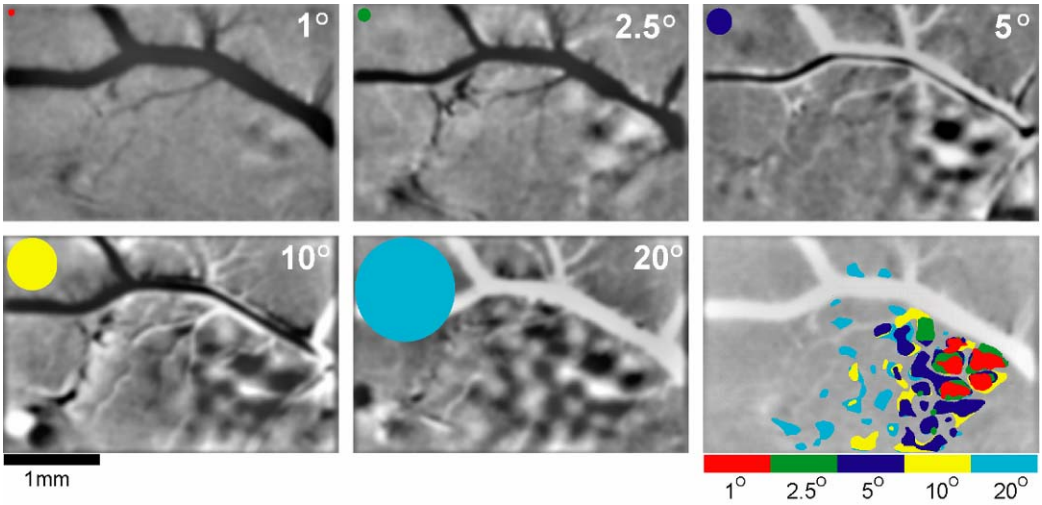

Figure 6-1. Activation of MT by 0/90 degree gratings inside a circular window centered on the *area centralis*. Stimulus radius is shown in the upper right corner of each image. The relative size of individual stimuli is indicated by circles in the upper left corner. Bottom right image is a summary image, demonstrating the relative size of activation produced by indicated stimuli.

only partially by the smaller stimulus and completely by the larger one. This is understandable given that the cells on the edge of the zone of activation would only have part of their receptive fields within the stimulus area. The same figure also demonstrates another important feature of the activation pattern, that a larger amount of cortical tissue is dedicated to processing more central vs. more peripheral locations in the visual field. As the size of the stimulus was increased (i.e., moving the edge of the whole stimulus into the visual periphery), the relative increase in the cortical activation territory became smaller. For instance, the change in the cortical activation area produced by going from a 1.0 to a 2.5 degree radius semicircle was 2.02 mm^2, but going twice that distance (2.5 to 5 degree radius) into the visual periphery resulted in only a 2.76 mm^2 increase in total activation area. Both of these findings, namely, a larger activation area for larger stimuli and a smaller relative change in activation area with larger stimuli, are consistent with the global retinotopic organization observed in owl monkey MT. In order to quantify this relation and test if this retinotopy was smooth, we next constructed a cortical magnification factor curve based on comparisons of the activation patterns produced by 4-6 circular stimuli.

Cortical Magnification factor (CMF) calculations

In order to quantitatively determine cortical magnification factor, we calculated the relative increase in the size of the activation zone vs. the relative increase in the size of the stimulus. Also, as described above qualitatively, it was clear that more cortical tissue was devoted to representing central as opposed to peripheral parts of the visual field. These qualitative observations were confirmed when we fitted a power function to

the millimeters of activation per degree of stimulus vs. eccentricity as shown in Figure 6-2. We found that the power function that fitted our data best was $M_{MT} = 0.664*E^{-0.663}$, where M_{MT} is the cortical magnification factor, and E is the eccentricity. As can be seen from this figure all 3 animals were well fit by the curve with low scatter (r = 0.93)

Comparison with other primates

We next compared the CMF curve of owl monkey MT to similar curves generated in other primates. As can be seen in Figure 6-3, the owl monkey CMF curve is similar to that of other primates. There is a very strong emphasis on the central vision representation, as demonstrated by a much steeper curve close to the fovea or *area centralis* respresentation. Also, as in other primates, the CMF curve flattens out beyond 8-10 degrees eccentricity. The CMFs of different primates, however, are not identical. The MT curves of bush babies and owl monkeys are obviously much shallower than those of cebus and macaque monkeys. Interpretation of these differences, however, requires that we have data on the relative sizes of MT in these different species which we consider in the next section.

Relationship between V1 and MT

It is reasonable to assume that the absolute amount of cortex that a given visual area dedicates to processing of portions of visual space relates to the size of that area. For instance, if a given area is twice as large as the same area in a different animal, it is reasonable to assume that twice as many mm^2 would be dedicated to processing of the

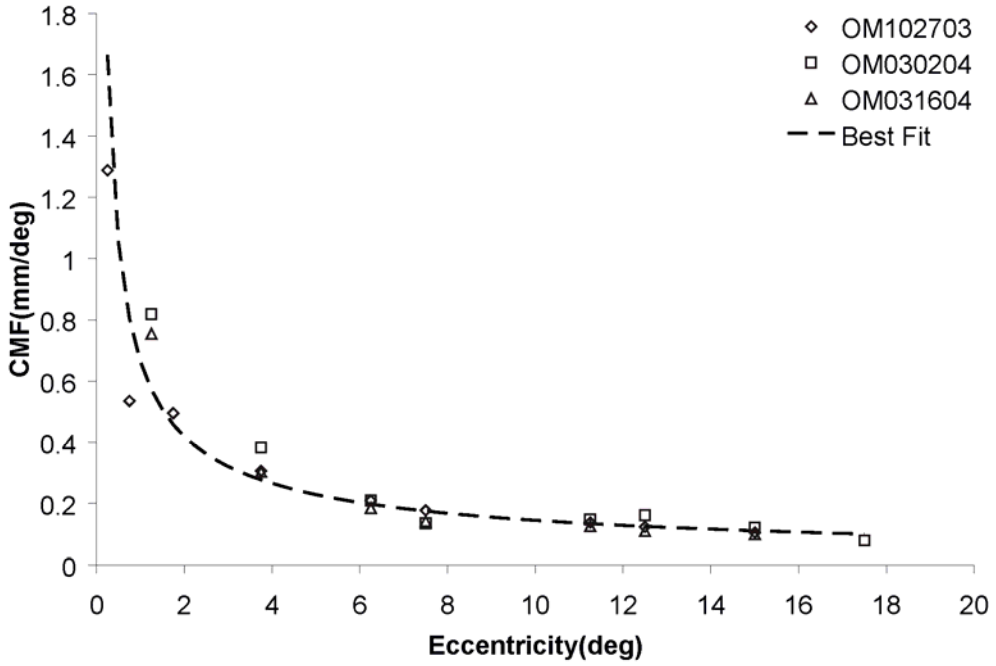

Figure 6-2. Cortical magnification factor curve in owl monkey MT. Cortical magnification data points were obtained as described in Methods from imaging data, such as shown in Figure 6-1. Data for three owl monkeys is shown. Best fit curve was obtained by fitting exponential curve across all data points from all three animals as described in Methods.

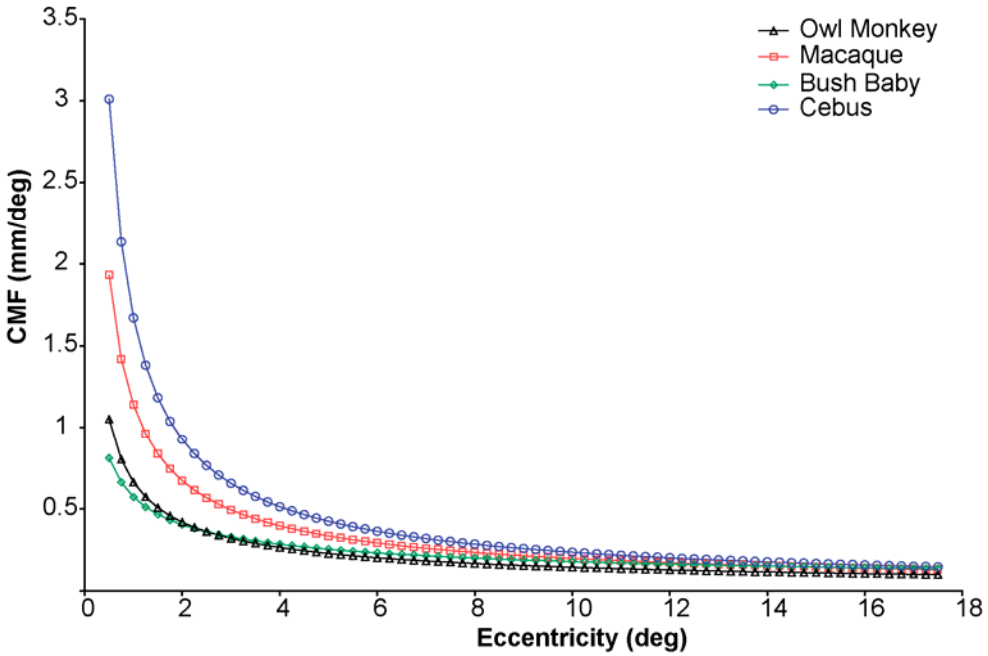

Figure 6-3. Plot of CMF curves for four primate species. Data for species other then owl monkey was obtained from the literature: bush baby (Xu et al., 2005), macaque (Albright and Desimone, 1987), cebus (Fiorani, Jr. et al., 1989). The curves show that for owl monkeys and bush babies CMF curves are very similar and shallower than for cebus or macaque.

same amount of visual space. Previously it was found that across primates area MT is approximately 9% the size of area of V1 (Pessoa et al., 1992). As can be seen from Table 6-1, the CMFs in V1 of macaque and cebus monkeys are very similar, followed by that of owl monkey and bush baby with shallower curves. This distribution of CMFs' is very similar to that of V1 areas in these primates. As mentioned, however, CMF curves in MT of bush babies and owl monkeys are very similar, while the surface areas of the MT in these two species are quite different. Therefore, we did not see direct proportionality between CMF in V1, CMF in MT and their respective area extents. In spite of these results, there still could be some relationship between the CMFs in V1 and MT. In macaque, Malpeli and Baker (1975) found that the magnification factor in V1 was proportional to the magnification factor in LGN to the power of 1.35, and LGN provides the main drive for V1 cells. We asked if the same power relationship obtains between V1 and MT. Indeed, we found that the magnification factor in V1 was proportional to the cortical magnification factor of MT to the power of 1-1.5. The significance of these findings is considered below.

Table 6-1. Summary data of cortical magnification factors and surface areas in V1 and MT across four pimates.

	Macaca	**Cebus**	**Owl Monkey**	**Bush Baby**
CMF in V1	$10.1*(E+0.82)^{-1.14}$	$7.72*E^{-0.94}$	$3.76*E^{-0.969}$	$2.36*(E+0.73)^{-0.8}$
Area of V1	1080	1063	400	211
CMF in MT	$1.14*E^{-0.76}$	$1.67*E^{-0.85}$	$0.664*E^{-0.663}$	$0.573*E^{-0.504}$
Area of MT	82	70	37	~20
Exponents Ratio	1.50	1.11	1.46	1.59

E – eccentricity. Area is given in mm^2. Exponent ratio is obtained by dividing exponent in the CMF expression for V1 by exponent in the CMF expression of MT. Data for the table was obtained as follows: macaque areas (Pessoa et al. (1992) computed from (Gattass and Gross, 1981; Ungerleider and Desimone, 1986; Van Essen and Maunsell, 1980; Van Essen et al., 1984; Weller and Kaas, 1983), macaque CMF (Albright and Desimone, 1987; Van Essen et al., 1984), cebus areas (Pessoa et al. (1992) computed from (Fiorani, Jr. et al., 1989; Gattass et al., 1987), cebus CMF (Pessoa et al. (1992) computed from (Fiorani, Jr. et al., 1989; Gattass et al., 1987), owl monkey areas (Tootell et al., 1985), owl monkey CMF (our computation from Myerson et al., 1977 and present study), bush baby areas (our computation from Rosa et al., 1997 and personal communication with Kaas and Collins), bush baby CMF (Rosa et al., 1997; Xu et al., 2004b)

Discussion

Our optical imaging data support the existence of a global and local retinotopic organization for owl monkey area MT. The relative emphasis on central vision, however, is less than is seen in V1 of this species and less than is found in MT of diurnal simians that have been examined. Below we consider the significance of this finding in the context of cortical organization in general and visual maps, in particular.

What can account for the organization in area MT?

It is known that different extrastriate visual areas in primates represent visual space differently. For example, in area V4/DL in several primate species, the fovea shows a much more magnified representation than has been reported for other areas including area MT (Pinon et al., 1998). There is, however, evidence to suggest that both V4/DL and MT are dependent on input directly or indirectly from V1 as discussed above. This suggests that scaling of the visual field representation for the different inputs coming from V1 is not the same and must depend on the type of input that is transmitted. This may seem obvious but, in fact, the relationship between scaling of inputs and maps within an area are not as obvious as might be imagined.

Schein and de Monasterio (1987), based on the previous studies by Cowey and colleagues (Perry et al., 1984; Perry and Cowey, 1985; Rolls and Cowey, 1970), proposed a one to one relationship between the number of retinal ganglion cells and LGN cells in macaque. Unfortunately the detailed relationship of the number of M and P retinal ganglion cells projecting to individual M and P geniculate cells is still poorly understood. On the other hand, Stevens (2001) showed that across species the number of

the cortical V1 cells increases as power of 1.5 relative to the number of LGN cells present. Again, however, it is not even clear exactly how the number of V1 cells depends on number of M and P cells even for the precisely organized cortical input layers in V1. Regardless, Malpeli and Baker (1975) found that, in macaque, $M_{cortex} \sim M_{lgn}^{1.35}$ and $M_{lgn} \sim M_{retina}^{1.34}$, where M stands for magnification factor at a particular eccentricity. Myerson et al. (1977) found that in owl monkey $M_{cortex} \sim M_{retina}^{2.35}$. These data indicate that there must be very precise scaling laws that regulate proportionality between retinal, geniculate and V1 machinery dedicated to the processing of the visual space.

Scaling across parallel pathways

The above data, however, ignore one of the fundamental principles of visual system organization, namely, that the visual information leaving the retina is transmitted to LGN and cortex via functionally distinct major pathways, with P and M being the principle players in primates. Both electrophysiological and anatomical studies have shown that both M and P pathways contribute to the functional properties of V1 and early extrastriate areas, such as MT. For example as described earlier, inactivation of either the M or P pathway was found to have similar effects on the activity of single neurons in V1 of macaque monkeys (Malpeli et al., 1981; Nealey and Maunsell, 1994). The same was not the case with area MT (Maunsell et al., 1990), however, where removal of the M pathway silenced most cells in MT, whereas removal of the P pathway appeared to have little effect. These results support the idea that area MT is more dependent on indirect M pathway input than on total V1 input.

These results argue against the idea that there exists some overall scaling factor that can be applied across visual areas as suggested originally by Stevens (2001). Instead, scaling appears to relate more to functional specialization. In support of this notion, Connolly and Van Essen (1984) found that in macaque $M_P \sim M_M^{1.25}$. They also found that number of M LGN neurons varies between 1.4 and 2.8 % of the number of P LGN neurons depending on eccentricity. Therefore, the question remains do these subcortical differences translate into differences in magnification seen between cortical areas? Interestingly they seem to do so. Our data, combined with data from other labs (Table 6-1) demonstrated that $M_{V1} \sim M_{MT}^{1\text{-}1.5}$. This is an important finding in light of the data by Maunsell et al. (1990) and Connolly and Van Essen (1984). One possible explanation for the observed relationship between MT and V1 CMF is that the magnification in V1 is based on the combined input from both P and M pathways, but MT magnification is based on the dominant M pathway influence. One of the ways to test this hypothesis would be to compare CMF in V1 and MT across species and see if there is evidence that CMFs reflect species differences in the geniculate inputs. In fact, Yamada et al. (1998) showed that the dendritic field areas of P ganglion cells at different eccentricities were very similar for macaque and cebus, larger in owl monkeys and largest in bush babies. On the other hand, while M ganglion cell dendritic fields of macaques and cebus monkeys were still similar, those of owl monkeys and bush babies were much closer. We found that MT CMFs in owl monkeys and bush babies are very similar, while V1 CMFs are not. A prediction would be that the CMF in MT reflects the CMF in the M layers of both of these species; a prediction that could easily be tested.

Part 3: Unequal representation of visual space in area MT

This section presents relevant parts of the following published study:

Xu X, Collins EC, Khaytin I, Kaas JH, Casagrande VA. 2006. Unequal representation of cardinal vs. oblique orientations in the middle temporal visual area. PNAS 103 :17490-17495

Introduction

In the previous section we investigated the CMF in owl monkey MT. Results showed that the data fit smoothly to a single CMF curve. As will be described next, however, this CMF can show distortions in the representations of different parts of space and in the representation of different orientation domains within that space. Therefore, before blocking of MT could be undertaken, it was important to investigate the organization of area MT more closely.

The first type of anisotropy that had to be investigated before MT blocking experiments could be undertaken is anisotropy in the CMF. In macaque monkeys Van Essen et al. (1984) found that the iso-polar and iso-eccentricity CMF at the horizontal meridian were close to unity, but the iso-polar CMF became up to 3 times larger than the iso-eccentricity CMF as polarity approached the vertical meridian. Similarly, Xu et al. (2005) noted that the CMF in bush baby V1 was greater along the iso-azimuth than along the iso-elevation dimensions. Interestingly, even though several studies investigated retinotopy in both owl monkey and macaque MT, very little is known about whether MT also has analogous anisotropy in its representation of visual space as was shown in V1.

Another type of anisotropy that is seen in visual system involves representation of cardinal vs. oblique stimuli. Several psychophysical studies in humans demonstrated that subjects are better at discrimination of cardinally oriented stimuli (Appelle, 1972; Campbell and Kulikowski, 1966; Timney and Muir, 1976) and cardinally directed stimuli (Coletta et al., 1993; Gros et al., 1998; Matthews and Qian, 1999) than oblique ones. The same effect also was found psychophysically in experiments with animals (Bauer, Jr. et al., 1979; Vandenbussche and Orban, 1983). One of the proposed explanations for these psychophysical results was the idea that the amount of cortex processing cardinal and oblique stimuli was not the same. Some electrophysiological studies in monkeys found more cells responding to horizontal and vertical stimuli than to oblique stimuli (De Valois et al., 1982; Mansfield, 1974). Similar results were obtained using visually evoked potentials (Bonds, 1982; Mansfield and Ronner, 1978). Other studies, however, failed to find this difference (Finlay et al., 1976; Poggio and Fischer, 1977; Rose and Blakemore, 1974; Wilson and Sherman, 1976). Moreover, some studies (Berkley et al., 1975; Orban and Kennedy, 1981; Vandenbussche et al., 1986) indicated that this effect could be dependent on the eccentricity of the stimuli.

Additionally, some studies demonstrated that the inequality in responses may be due to unequal populations of neurons responding to cardinal and oblique stimuli outside of V1. For instance, Heeley and Buchanan-Smith (1992) demonstrated an 'oblique effect' in humans using moving plaids. This would place the origin beyond V1, since V1 cells do not respond to such stimuli (Movshon et al., 1985). Westheimer (2003) showed that several types of stimuli that would elicit only insignificant responses in V1 still produced a robust 'oblique effect' when humans were tested psychophysically. This

suggested to him that the oblique effect may originate in areas beyond V1. There is also some electrophysiological data to support such a view. Levitt et al. (1994a) saw an overrepresentation of cells preferring vertically oriented stimuli over those preferring horizontal or oblique orientations in macaque V2 (however, they did not find this overrepresentation to be statistically significant). Huang et al. (2006) found that in cats there is overrepresentation of cardinal orientation selective cells not only in are a 17 but also in area 21a and, in fact, area 21a showed a more prominent overrepresentation. Interestingly, there is no data concerning whether there is 'oblique effect' in primate MT. Therefore, the second goal of the following study was to determine if owl monkey MT demonstrates an 'oblique effect' measured using optical imaging.

Methods

Two owl monkeys in addition to the ones used in the previous study (Part 2) were used in these experiments. The surgery, imaging, perfusion and histology were done using same methods as described above. In order to quantify the differences in the representation of orientation preferences in MT, vector orientation preference maps were constructed (Blasdel, 1992), and numbers of pixels responding to stimuli of various orientations were counted. In order to assess whether there is a difference in the representation of horizontal vs. vertical stimuli in relationship to eccentricity, we also presented one of the animals with moving square wave gratings within circular apertures away from the *area centralis* along the horizontal meridian.

Results

Full field moving gratings at four orientations produced robust responses in owl monkey MT (Figure 6-4a-b). The orientation preference map produced from these responses (Figure 6-4c) exhibited features similar to the orientation preference maps in owl monkey V1, including pinwheels and linear zones of orientation preference as described earlier (Xu et al., 2004a). However, iso-orientation domains in MT were significantly larger than the domains in V1 (Xu et al., 2004a). The average domain size in MT was 0.136 +/- 0.075 (SD) mm^2 vs. 0.076 +/- 0.046 mm^2 in V1.

Comparison of the zones of MT processing stimuli at different orientations revealed that there was a significant difference in how much space was devoted to cardinal and oblique orientations (Figure 6-4d-g). Moreover, the difference was eccentricity dependent. Across all sampled animals, within the representation of the central 10 deg of visual space, cardinal stimuli activated 10.1 +/- 5.3% (SD) more of pixels than oblique stimuli. In the periphery (within 10 – 40 deg of visual representation), cardinal orientations were overrepresented by a much smaller factor, 3.6 +/- 2.8% (SD) of pixels. In order to see if the observed 'oblique effect' had its origin in V1, several previous animals, in which V1 was imaged (Xu et al., 2004a), were reanalyzed. It was found that, even though there was some inter-individual variability, on average, there was no difference in the representation of cardinal and oblique orientations in V1.

Surprisingly, we found that when the animal was presented with circular stimuli away from *area centralis* along horizontal meridian, the zones of activation were elongated along that meridian (Figure 6-5). The axis of the activation zone along

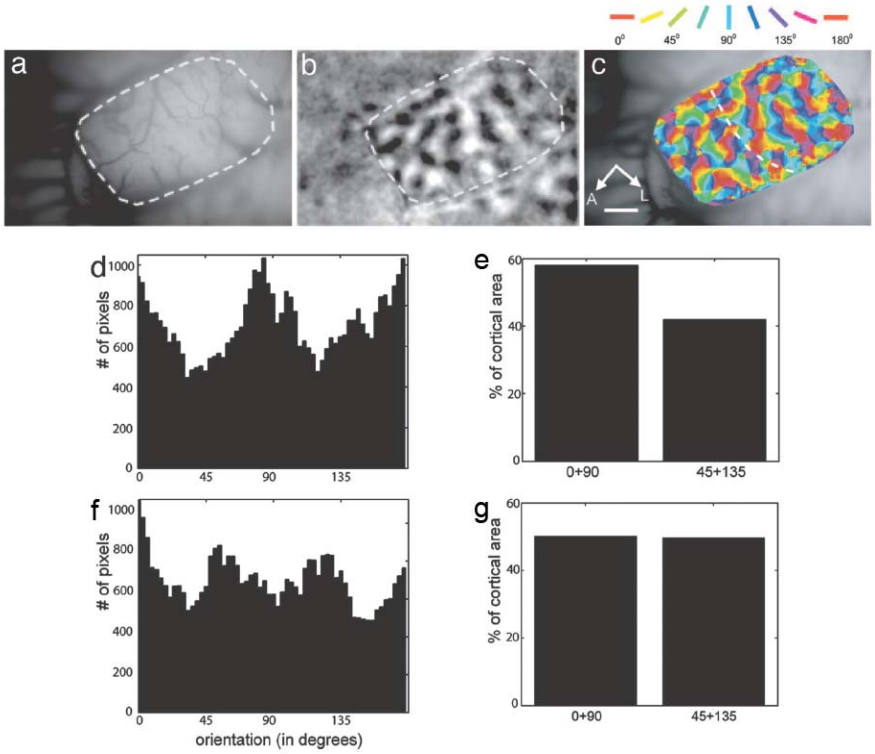

Figure 6-4. Unequal representation of cardinal and oblique orientations in owl monkey MT. A. Reference image of owl monkey MT obtained using optical imaging camera in the beginning of recording session. Dashed outline delineates the portion of MT that was used for analysis and responded strongly to full screen stimuli, (see Methods). B. Differential image of activation in MT. Dark and light patches are regions of MT that responded preferentially to vertical and horizontal gratings respectively. The region of MT that was analyzed is delineated with dashed line. C. Color-coded orientation preference map in the region of interest. The dashed line separates representation of central 10 deg of visual space (on the right) from peripheral (on the left). Scale bar is 1mm. A - anterior, L - lateral. D. Histogram showing distribution of pixels responding to different orientation in the central vision representation. E. Bar graph showing the percent of cortical area preferring cardinal and oblique orientations. It was obtained by binning data in D at 0, 90, 45, 135 ± 22.5 degrees. F. and G. Same type of data as D and E for the peripheral part of the region of interest. Modified from Xu et al. 2006 with permission.

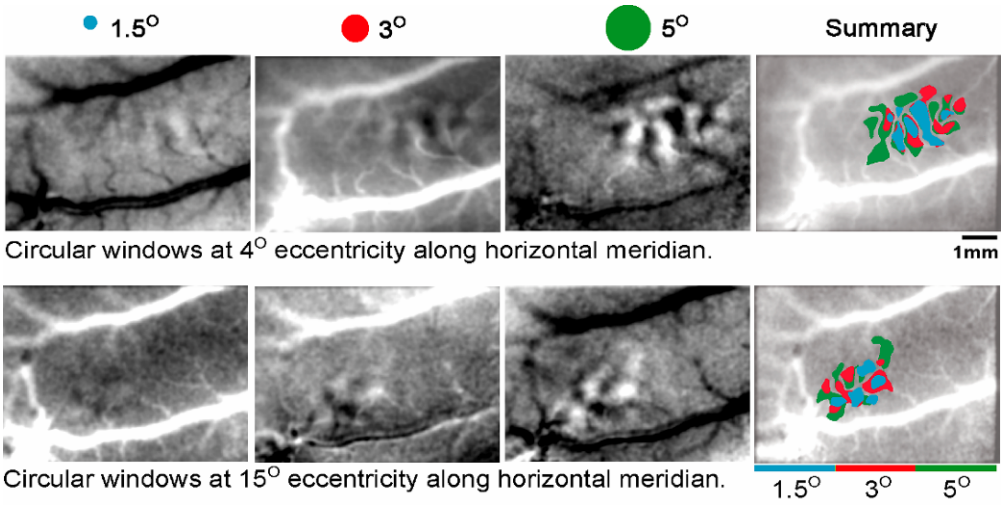

Figure 6-5. Point spread activation produced from circular stimulus patches of 1.5, 3, and 5 degrees in diameter at 4 degrees eccentricity (top row) and 15 degees eccentricity (bottom row) presented along the horizontal meridian. Activation demonstrates clear asymmetry with an aspect ratio of 1.5-1.9 to 1.0 of the horizontal to the vertical spread of activation.

horizontal meridian was 1.5 – 1.9 times longer than the orthogonal axis. This finding may indicate that unlike the anisotropy described in V1, in MT the iso-polar cortical magnification factor may be larger than iso-eccentric one.

Discussion

These findings, for the first time, demonstrated an 'oblique effect' in primate area MT. This was a very significant result, since it showed that in MT horizontal and vertical axes of orientation are overrepresented. This is also a significant result because it demonstrates that blocking MT might affect areas of V1 responsible for processing cardinal stimuli to greater extent than the areas responsible for processing oblique ones.

Interestingly this finding does not actually explain the better detectability of cardinal stimuli vs oblique stimuli as has been claimed in many psychophysical studies. As Purushothaman and Bradley (Purushothaman and Bradley, 2005) have demonstrated, the neurons that are most predictive of a monkey's psychophysical responses are the ones whose direction selectivity is ~ 67 deg away from the presented direction of motion of the stimulus. Their results, though contrary to the generally accepted notion of 'the more, the better', are actually rather logical. The neurons whose direction selectivities are aligned with the stimuli are responding near their peak. Therefore, small deviations from the preferred direction does not result in a significant change in firing (the rate of change in response near the peak is always almost zero). On the other hand, neurons with preferences away from the presented stimulus have their firing in the mid range of the tuning curve, which means that small changes in direction of the stimulus will elicit large changes in firing (the rate of change in the responses on the slopes of the tuning curve is

the greatest). This consideration indicates that while our findings may better explain *detectability* of cardinal stimuli, they are not sufficient to explain better *disciminability* of near cardinally oriented stimuli.

Current results would indicate that overrepresentation of cardinal orientations originates in MT or an area higher than V1, since reanalysis of previous V1 mapping cases did not find an 'oblique effect' in V1. This result may be due to the fact that in these cases it was necessary to average across 10-15 deg of central vision. In bush baby it was found that there is an 'oblique effect', but only in the representation of the central 3 deg of visual space (see also Xu et al., 2007; Bonds et al., 1987). It is also possible that there are real species differences between owl monkeys and bush babies in the origins of the 'oblique effect.'

Finally, we found that the circular stimuli along horizontal meridian are represented by a cortical area in MT that is elongated along horizontal meridian. This finding indicates that, at least along the horizontal meridian, the iso-polar CMF is greater than the iso-eccentricity CMF. Of course, to see if the same rule applies along the other polarities, it would be necessary to systematically vary the stimulus position not only along horizontal meridian, but also along other polarities. Albright (1989) found such a radial bias in macaque MT, so it is possible. Again, however, it is important to point out that such an anisotropy of CMF in MT is dramatically different than that seen in V1. As was mentioned in the Introduction, in V1 of both macaque and bush babies (Van Essen et al., 1981; Xu et al., 2005), the iso-eccentricity CMF was equal to or larger than the iso-polar one. Therefore, there exists an additional transformation of visuotopic representation that occurs between V1 and MT.

CHAPTER VII

EEFFECT S OF BLOCKING V1 AND MT: FUNCTIONAL TESTS OF FEEDFORWARD AND FEEDBACK PATHWAYS

Some parts of this chapter were published (Collins EC, Xu X, Khaytin I, Kaskan PM, Kaas JH, Casagrande VA. 2005. Optical imaging of visually evoked responses in the middle temporal area after deactivation of primary visual cortex in adult primates. PNAS 102 :5594-5599.), and some parts are still in preparation. Since I am not the first author of the published manuscript, I will provide my own description of these studies. The study of the effects of blocking MT on responses in V1 will be presented in full.

Preface

In the previous chapter we described the retinotopic organization of area MT. The results of this effort were an important prerequisite for the two studies described here. In this chapter we show results of blocking the interactions between V1 and MT by either blocking a portion of V1 (PART 1) or blocking a portion of MT (PART 1). We hypothesized based on the results of our LGN layer blocking experiments that in our primate species (owl monkeys and bush babies) there should be a very strong dependence of V1 on the M channel, and that, because the M channel has been suggested to play a special role in the formation of properties in MT, manipulating this channel would impact not only feedforward connections between V1 and MT, but also feedback connections from MT to V1. The latter is described in PART II of this chapter.

Part 1: Optical imaging of visually evoked responses in the middle temporal area after deactivation of primary visual cortex in adult primates

This section provides some of the results from the following published study:

Collins EC, Xu X, Khaytin I, Kaskan PM, Kaas JH, Casagrande VA. 2005. Optical imaging of visually evoked responses in the middle temporal area after deactivation of primary visual cortex in adult primates. PNAS 102 :5594-5599.

Introduction

Given the numerous inputs to area MT, described earlier, it is important to know whether any of the inputs dominates, providing the main driving input, as is the case for LGN input to V1. Surprisingly, determining the answer to this question was not straightforward. On the one hand, there were several studies suggesting that MT can remain active even in the absence of the V1 input. For example, Rodman et al. (1989) showed that either ablation or cooling of V1 in macaque monkeys did not remove activity from most of MT neurons, and these neurons, though having weaker activation, still had direction selectivity and binocular responses. These authors then demonstrated that concurrent inactivation of the superior colliculus silenced activity in MT. Rodman et al. (1990) suggested that visual activity in MT can be maintained in the absence of V1 due to connections from the superior colliculus either through pulvinar or through the LGN. Girard et al. (1992) found that reversible inactivation of V1 led to a reduction in activity in MT, but that the majority of neurons continued to be active. Moreover, they found that the direction selectivity of the majority of neurons either remained the same or changed

only slightly, although the tuning became broader. Interestingly, they found that section of corpus callosum reduced residual activity, suggesting involvement of activation from the opposite hemisphere. They also discovered that increases in anesthesia level abolished residual activity, suggesting involvement of some pathway that was more sensitive to anesthetic, perhaps the tectopulvinar pathway.

Unlike previous recordings in macaque, both short and long standing lesions of V1 in owl monkey led to the complete abolishment of responses in MT (Collins et al., 2003; Kaas and Krubitzer, 1992). These studies demonstrated that parts of MT that responded to the same retinotopic locations as ablated parts of V1 had no residual activity. Nevertheless, neurons at the border zones did show residual activity suggesting that some of the residual activity reported by others might have resulted from incomplete lesions of V1.

All the studies reported above, conducted on macaques and owl monkeys, were done using electrophysiological recording, therefore limiting the sampling to just a few neurons. Therefore, we decided to examine if removal of retinotopically limited parts of V1 could produce zones of inactivation in the corresponding areas of MT using optical imaging of the entire area MT. In this way we could examine the activity of populations of neurons both within regions connected to the inactivation zone and outside of this zone simultaneously.

Methods

One owl monkey and four bush babies were used for this study. Both hemispheres in the owl monkey were studied, along with five hemispheres of the bush

babies. Activity was recoded using our optical imaging setup (Optical imager 2001, Optical imaging Inc., New York, NY), described elsewhere (Xu et al., 2004a; 2005). Normal responses of V1 and MT were imaged before a small patch of V1 was inactivated using a piece of gelfoam soaked in muscimol (50 mM) and placed on the surface of the cortex. After the block repeated imaging was done to see the area of inactivation. Due to anatomical constraints only ~10-15 degrees of visual space representation are accessible to the camera on the surface of V1 of the owl monkey and ~15-20 degrees of visual space representation are exposed on the surface of bush baby V1. Most of the camera accessible V1 represents the lower visual field. Before blocking, V1 was mapped using retinotopically limited stimuli (Xu et al., 2004a; 2005) and efforts were made to limit the blocked area of V1 to the ~10 deg of cortex representing the lower visual field. Two types of stimuli were used. Initial recordings were done using full screen moving square wave gratings at the optimal spatial and temporal frequencies appropriate for each species and each visual area at four orientations (DeBruyn et al., 1993; O'Keefe et al., 1998; Xu et al., 2004b; 2006). After the block, in addition to the full screen stimuli, retinotopically limited stimuli were used. These stimuli consisted of moving square wave gratings confined to a circular aperture of 10 degree radius and centered on *area centralis.* Differential orientation preference maps were constructed (Blasdel, 1992) and compared before and after inactivation. At the end of these experiments animals were perfused and the imaged cortical areas were flattened (Xu et al., 2004a). The cortex pieces then were sectioned in the plane parallel to the surface and sections stained for myelin (MT) or cytochrome oxidase (V1), to confirm the proper placement of the camera.

Results

The myelin staining revealed an area of dense myelination at the tip of superior temporal sulcus (Figure 7-1a). Aligning the activation pattern resulting from the full screen stimulation revealed perfect overlap with the zone of activation and the zone of dense staining, confirming that the camera was collecting activity from area MT (Figure 7-1b). Differential images of activation in response to horizontal and vertical gratings revealed MT as a highly responsive area with a patchwork of orientation domains approximately 700-900 μm in diameter. The highly active zone that corresponds to the extent of the full screen stimulus is outlined in the Figure 7-1. It is interesting to note that even anterior to the outline, which corresponds to more peripheral MT locations (not within the area of screen stimulation), it is possible to see a weak activation pattern. This indicates that activity in MT can spread beyond the retinotopic zone corresponding to the stimulus on the screen. Figure 7-1e shows a differential image of the activation pattern after the block of a central patch of V1. As mentioned in the methods section above in this chapter, the inactivated area occupied a representation of roughly 10 degrees of central vision in the lower visual hemifield. There is a clear lack of activation domains in the area that corresponds to the blocked patch in V1 (compare activation in Figure 7-1d and 7-1e in the lower field indicated by a black arrow near the intersection of the horizontal and vertical meridian), indicating that without V1 input to the corresponding area of MT becomes inactive. Nevertheless, it is possible to see two activation domains along the horizontal meridian representation. The dramatic reduction in contrast indicates that those two domains are much less active and again points to possible spread

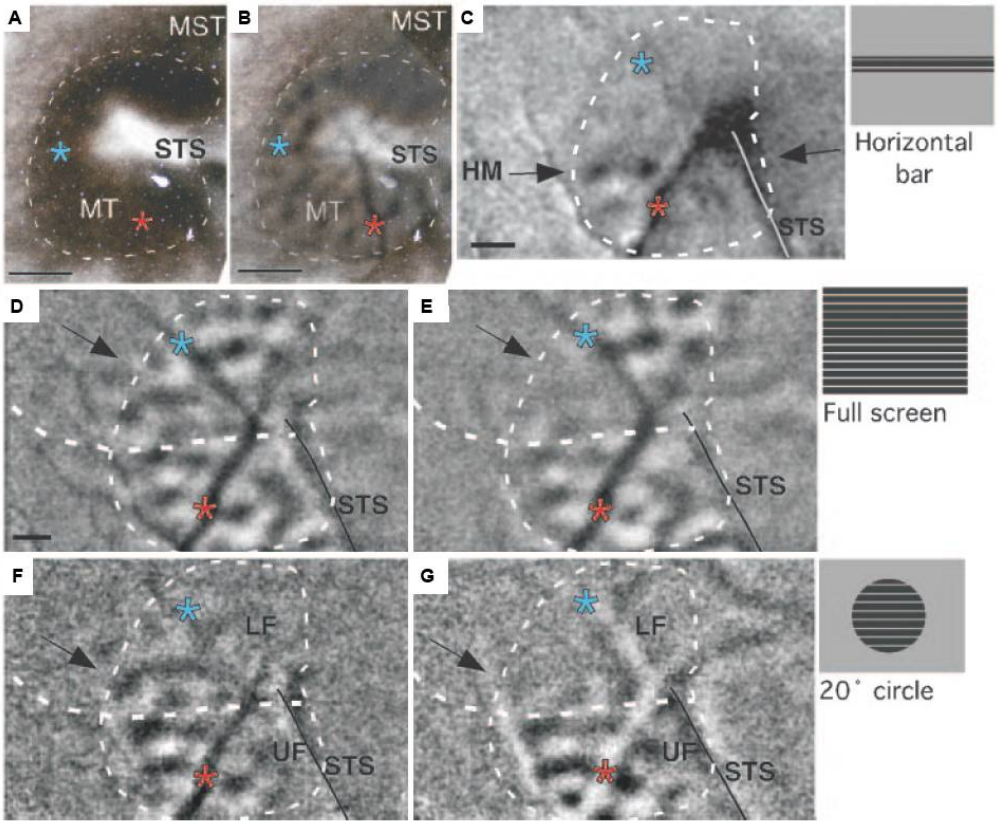

Figure 7-1. Effect of blocking part of V1 on the activity in MT. A. Section of owl monkey cortex stained for myelin. MT is a densely stained region at the tip of the superior temporal sulcus. STS - superior temporal sulcus. MST - middle superior temporal area. Two asterics mark locations of blood vessels (not shown) that were used in aligning the histological and imaging data. The dashed outline corresponds to the part of MT that was activated by our stimuli. B. Same histological section as A with 50% transparent image of optical imaging activity overlaid. C. Differential image of activation in response to moving grating confined within 3 deg high horizontal window centered on horizontal meridian (diagram of stimulus is adjacent to the panel). The activity along horizontal meridian is marked by two arrows (HM). Scale bar is 1 mm. D. Differential image of activation in response to full screen grating (diagram of stimulus is adjacent to the panel E). Arrow points to the part of MT that showed decrease in activation after V1 block. E. Same as D after the block. There is clear zone of decreased activation, marked by an arrow. F. Differential image of activation in response to 10 deg radius circular stimulus centered on *area centralis*. Comparison with D reveals strong activation in the central part of MT and no activation in more peripheral locations. LF - lower field. UF - upper field. Arrow points to the part of MT that showed decreased activity after V1 block. G. Same as F after block. Most of the lower field does not show any activity. Modified from Collins et al. 2005 with permission

of activation either from neighboring active parts of MT or from still active bordering parts of V1. When responses to retinotopically restricted stimuli are compared before and after the block (Figure 7-1f and g), it is possible to see very similar results to the ones obtained with full screen gratings. Figure 7-1g demonstrates that when there is no stimulation outside of the inactive zone in V1, activity in MT in the corresponding zone completely disappears, as can be seen by the complete lack of activation domains in the area representing the lower visual field. Similar results were obtained in the bush babies. The two most evident species differences were the much lower overall strength of activation in bush baby MT, even before the block, and a slower time course of inactivation.

Discussion

The two major findings of this study were the confirmation of results showing that: 1) in owl monkey activity in MT is highly dependent on the activity in V1, and 2) the activity in MT can spread beyond areas that are retinotopically matched to V1. These findings are consistent with previous studies in owl monkeys and marmosets (Collins et al., 2003; Kaas and Krubitzer, 1992), which demonstrated that cells within the region corresponding to the ablated part of V1 stop responding. The findings are also consistent with studies (Kaas and Krubitzer, 1992; Rosa et al., 1997) showing that cells corresponding to the border region of the lesion in V1 often continue to fire with new receptive fields shifted toward those of the cells in the intact portion of V1. This spread of activity could be based both on the horizontal connections within MT and on the inputs from V1, considering that receptive fields of MT neurons are much larger than

those of V1 neurons (Rosa et al., 1997) and that connections between areas are retinotopically precise (Angelucci et al., 2002b).

It is harder to reconcile these results with findings in macaque monkey cited in the introduction. The most likely reason for such a difference in dependence of MT on V1 inputs is a difference between species. As was mentioned above, both bush babies and owl monkeys have LGN and V1 organizations that are somewhat different from that found in macaques (see previous chapters). Additionally, as was mentioned by Girard et al. (1992), anesthesia may play a role in the extent to which MT can remain active during inactivation of V1. Girard et al. (1992) used halothane and saw a reduction in residual activation. The current study was done using propofol as an anesthetic. Several studies have concluded that propofol may cause a reduction in cerebral blood flow in the pulvinar (Byas-Smith et al., 2002; Ogawa et al., 2003); however, current work done in our laboratory indicates that it is possible to obtain stimulus dependent activity in the visual pulvinar under propofol anesthesia (unpublished results). Finally, it is possible that due to the decreased strength of response in the affected area of MT, optical imaging may not be sensitive enough to detect residual activity, and that the spread of activity that was observed is actually the residual activity equivalent to that reported in macaques.

Regardless, this study provides additional evidence that, in the species that are the subjects of this thesis, V1 provides the main driving input to MT. Therefore, blocking of the M LGN channel (see results in Chapter V) may have resulted not only in a decrease in V1 activity, but also in a decrease in MT activity. In the next section we test the degree to which feedback from MT to V1 influences the activity in V1 in these species.

Part 2: Effect of blocking middle temporal area in bush baby on activity in V1

Introduction

In all species examined, including owl monkeys and bush babies, MT back projections terminate in patchy zones in V1 (Kaskan and Kaas, 2007; Montero, 1980; Rosa et al., 1993; Shipp and Zeki, 1989; Ungerleider and Desimone, 1986; Van Essen et al., 1981; Weller et al., 1984). Several earlier studies (Maunsell and Van Essen, 1983; Rockland and Pandya, 1979; Shipp and Zeki, 1989; Ungerleider and Desimone, 1986) concluded that feedback connections from higher visual areas, including MT, are retinotopic, but more distributed than the corresponding feedforward connections from V1. Later, more detailed investigations of connections between MT and V1 brought into question these earlier findings (Angelucci et al., 2002b; 2002a; Shmuel et al., 2005). These studies showed that the feedback and feedforward connections are strictly retinotopic, i.e. the termination of the feedback projections is in visuotopic register with neurons that provide the feedforward inputs. Still, all studies have shown that because of the almost 10 times larger receptive fields in MT (for review see Rosa, 1997) individual cells in MT send projections that feedback to many V1 cells while individual V1 cells send their feedforward input to a very restricted set of MT cells.

Such divergence of feedback serves as a basis for one of the most convincing hypotheses concerning the function of MT back projections at a single cell level. This hypothesis proposes that the role of feedback is to modulate V1 cells through center/surround interactions (Angelucci and Bressloff, 2006). Before considering this proposal in detail it is important to spend a moment describing the concept of center and

surround organization in V1 cells. The minimal receptive field center of a typical V1 neuron is a visuotopic region in which the presentation of a moving grating or bar (or other appropriate stimulus) at the preferred orientation first increases the firing rate of the neuron above background (Barlow et al., 1967; Hubel and Wiesel, 1962). Increasing the size of the stimulus first increases the firing rate and then, as the size is further increased, begins to suppress the firing rate (DeAngelis et al., 1994; Levitt and Lund, 2002; Sceniak et al., 2001). The optimal size of the stimulus using high contrast (the high contrast summation receptive field) is smaller than using low contrast (the low contrast summation receptive field) gratings (Sceniak et al., 1999). The region outside the minimal receptive field is defined as the near surround, while the region outside the largest optimal receptive field is defined as the far surround.

With these descriptions in mind, it is possible to discuss the role of the feedback in establishing the center/surround interactions in V1. According to this hypotheses (Angelucci and Bressloff, 2006), feedback provides a means of summing activity over the low and high contrast optimal receptive field regions, while providing inhibition over the far surround region. This hypothesis is based on a variety of electrophysiological and anatomical data. Several studies have shown that removal of feedback reduces activation in the receptive field center of V1 neurons (Hupe et al., 1998; 2001; Mignard and Malpeli, 1991; Sandell and Schiller, 1982). On the other hand, Hupe et al. (1998) found that inactivation of MT results in decreased surround suppression and sometimes facilitation of responses to stimuli extending into the near surround especially for low salience stimuli. Similarly, anatomical data by Angelluci et al. (2002b) showed that the feedback projections cover an area large enough to participate in far surround

suppression. In sum, Angelucci and Bressloff (2006) proposed that feedback acts through a balance of strong facilitative and weak suppressive mechanisms. As the size of the stimulus increases at first facilitation outweighs inhibition resulting in the increased firing rate of V1 neurons. However, as the size of the stimulus continues to increase, the area over which inhibition sums becomes large enough to outweigh facilitation, thereby resulting in suppression of the response.

So, what predictions can be made based on this hypothesis about the population effect of MT feedback? The whole model is based on the balance of suppressive and facilitative effects of feedback on the single V1 neurons as the size of the stimulus is increased. What happens if the stimulus far exceeds the size of the receptive field, as happens with full screen moving grating stimuli, which can cover as much as 40 deg of visual space? We hypothesize that since the previous electrophysiological and anatomical data demonstrate that feedback acts through stronger facilitative mechanisms, removal of feedback should decrease the overall responses in V1. That is, the population response includes a product of both summed suppression and summed facilitation, and since both act over the same visuotopic area, under the control conditions facilitation should win. To test these hypotheses, we recorded population responses in bush baby V1 using in vivo optical imaging, before and after inactivating area MT.

Methods

The experiments described in this section were done on 3 of the bush babies used in the experiments described in chapter 4. Therefore, only the methods that are different from the ones used in that study will be described here.

During the original surgery, a second opening was made above MT, using coordinates from previous studies (Collins et al., 2005; Xu et al., 2006). Just as in V1, this opening was covered with a protective film of tecoflex. During the first survival optical imaging procedure, area MT was imaged using full screen square wave moving gratings of preferred spatial and temporal frequency (0.2 c/deg, 5 Hz) and two orientations. This session allowed us to verify the location of the central ~35 degrees of visual space representation in area MT. Differential maps of orientation preference domains were made and overlaid on the image of the surface vasculature, in order to guide placement of muscimol in subsequent blocking experiments. During these terminal experiments, control data were collected as described in Chapter 4. Afterwards, a muscimol (50 mM) filled micropipette was placed above MT and 3-4 injections of 500-1000 nL of muscimol were made into MT, covering the entire patch of MT that was activated by full screen stimuli. To visually verify the spread of the muscimol, it was mixed with fast green dye and additional injections were made if necessary to completely encompass previously activated area of MT. After 30 min., the same set of stimuli as before the block was run.

We analyzed the data in two ways. First, qualitatively results were compared by creating single condition images of activation at different orientations and temporal frequencies before and after block. Second, the strength of response was determined by

pixelwise fitting a sinusoid to the data at each temporal frequency and finding the average strength of response in V1 for each frequency before and after the block.

Results

Figure 7-2 shows patches of activation to horizontal moving gratings at four temporal frequencies before and after MT block. The darker patches in all images are the zones in V1 which preferred a given stimulus. We obtained good activation under all conditions before and after the block. Before the block, cortex responded better to lower temporal frequency stimuli, as can be seen from comparing contrast, which is proportional to the response, in Figure 7-2. After the block there was a general decrease in response across cortex (Figure 7-2), however, unexpectedly, the response at 10 Hz seemed to increase, as can be seen from the higher contrast in the last panel. In order, to study the changes in the response more closely, we collected the second set of data before and after the block using a higher magnification lens (not shown). Again we saw good responses before and after the block, however, changes in contrast between two conditions were even smaller.

Given the small signal strength inherent in optical imaging we next attempted to quantify these results. The quantification was performed using the same technique used to quantify responses at four temporal frequencies in Chapter 4. In brief, response magnitude at each temporal frequency before and after the block was found by averaging response amplitudes across the population, obtained by fitting sinusoids to each pixel's response at four orientations and that temporal frequency. Figure 7-3 depicts the result of this quantification. As can be seen from both panels, in general, blocking MT resulted in

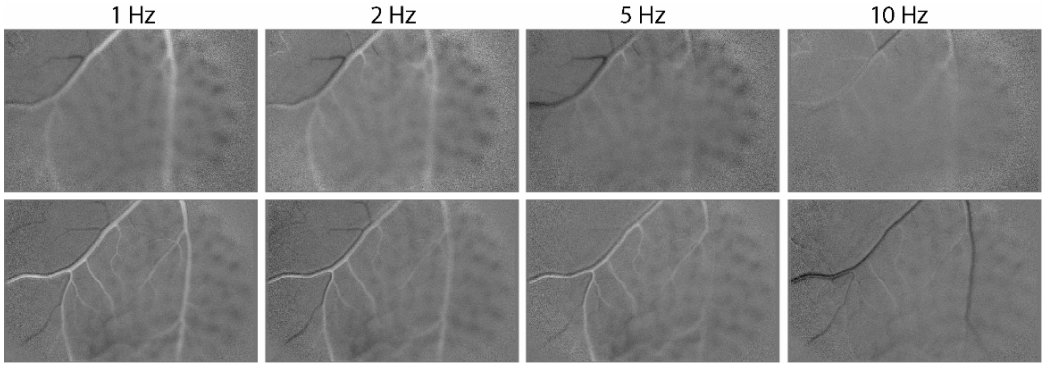

Figure 7-2. Effect of blocking retinotopically matching part of MT on activity in V1. Single condition baseline normalized images of activity before (upper row) and after (lower row) block of MT. The dark patches represent activity in V1 in response to horizontal full screen moving grating at four temporal frequencies indicated above the panels. The contrast in each image is proportional to the activity.

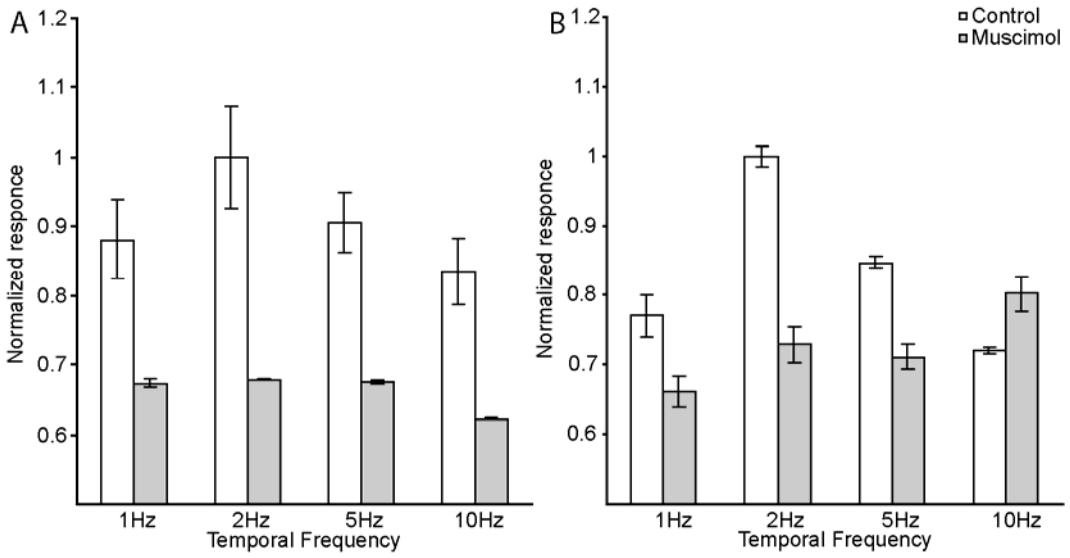

Figure 7-3. Quantification of the activation in owl monkey V1 before and after blocking MT. The magnitudes of the responses determined as described in the text using low (A) and high (B) magnification lens setups. Responses are normalized by the average response at 2 Hz before block. Control - before block condition, Muscimol - after block condition.

a reduced response seen at both low and high magnification. Also, the general tendency of the cortex to respond better to stimuli at lower temporal frequencies than at higher frequencies remained unchanged. Still, it is interesting to note that the response at 2 Hz underwent a proportionally larger decrease in activation than the neighboring less preferred frequencies. Two additional points are noteworthy. First, contrary to the qualitative results in the Figure 7-2, the quantification demonstrated a clear decrease in activation in response to the10 Hz stimulus. Second, surprisingly, quantification showed that, in the same animal the response at 10 Hz was actually higher after the block when imaged using a higher magnification lens. The possible reasons for these results are discussed next.

Discussion

The results of the MT blocking study, in general, supported the hypothesis that MT feedback enhances the activity of V1 on a population level. As was noted above, however, there were a couple inconsistencies in the data with the highest temporal frequency, 10 Hz. Surprisingly, using high contrast gratings and imaging at 10 Hz at low magnification results showed a reduction in activity post blocking. In contrast, the opposite result was found when the same experiment was repeated using higher magnification. What could cause this difference?

The first possibility relates to the timing of the two imaging sessions and the delayed action of muscimol. In the V1 blocking study in bush babies, described above, we observed that sometimes it took up to two hours for the muscimol to take full effect. Due to time constraints, in these studies, we initiated post block imaging within 30

minutes after the block. Therefore, the results could have been contaminated by the incomplete block of MT (in the case shown, post-block high magnification results were collected before switching back to low the magnification lens). More strenuous testing would be required to see if this is true.

The second possibility is that these inconsistencies may be a result of a change in baseline. As described in the background (Chapter 3), optical imaging is an indirect functional imaging technique. Das and Gilbert (1995; 1997) and Toth et al. (1996) showed that optical imaging is capable of recording subthreshold activation. Those authors demonstrated that the activation domains to restricted stimuli recorded with optical imaging are much larger than the patch of the cortex in which same stimuli produce spiking activity. This fact is usually considered an advantage of this technique. As the stimulus specific activity goes down, however, the changes in baseline activity begin to dominate the recorded signal. As a result, the inconsistent results that we obtained at 10 Hz might be a result of our inability to completely eliminate the baseline modulations. If true, averaging across larger numbers of repetitions could make our results more consistent.

Overall, however, the results demonstrated a very consistent decrease in activation across most temporal frequencies. This result is in good agreement with our hypothesis that blocking MT would decrease activity in V1. Equally important is that blocking MT did not seem to decrease activity proportionally but had its strongest impact at the preferred temporal frequency of V1 cells (see also Chapter 4). This finding may indicate greater involvement of MT feedback in setting up V1 stimulus preference by having larger suppressive effects at non-preferred frequencies. It would also be

interesting to conduct additional studies with a larger number of repetitions, to see if one could demonstrate a difference in the effect of blocking feedback also at different orientations and spatial frequencies.

CHAPTER VIII

CONCLUSIONS

The original questions posed by this thesis concerned the functional significance of individual feedforward channels and the impact of feedback on the organization of functional maps in V1. We proposed to answer these questions by blocking various pathways feeding into V1 and studying the effect of these manipulations on the relative responsiveness and the functional organization of different properties in V1. Here I summarize my main conclusions and outline some key questions that remain to be addressed.

Summary of results

The main investigative technique that we used was optical imaging. Therefore, it was important to verify its validity in studying the functional organization of cortex. Previous research in our lab has successfully utilized this technique for this purpose (Xu et al., 2004a; 2005; 2007); however, it was suggested that the filtering technique used by our lab and the Grinvald lab (Bonhoeffer and Grinvald, 1993; Xu et al., 2004a) can significantly alter the results (Polimeni et al., 2005). Using real data, we were able to demonstrate that optical imaging results are fairly resistant to noise. We showed that filtering with a low pass filter several pixels in diameter (35-60 um), we could remove most of the high frequency noise in the data without changing the structure of the functional maps. We also showed that the upper limit on the filter diameter is

comparable to the size of the functional domains present in the imaging data and, therefore, our post processing technique was both conservative and appropriate.

Nevertheless, this study combined with the inherent difficulties in measuring small optical signals required that we develop new tools. While studying temporal frequency preference in bush baby V1, we employed multiple analytical techniques, several of which were new to optical imaging. We implemented an automatic outlier removal algorithm that allowed us to remove contamination from our data caused by abrupt changes in animal physiology (Siegel et al., 2003). We developed a novel method of comparing the locations of functional domains within functional maps and used a non-parametric technique of comparing functional maps (Khaytin et al., 2007).

The development of these new tools allowed us to investigate the functional organization of temporal frequency selectivity in V1, a property that has not been studied systematically outside of single cells in any primate. We found that unlike some functional properties, such as orientation and spatial frequency preference, other properties like temporal frequency preference are distributed uniformly across cortex, without regions of low and high frequency selectivity. This result supported an idea put forth by Swindale et al. (Swindale et al., 2000; Swindale, 2004) that there may be a limit to how many scalar properties are mapped onto cortex without creating coverage non-uniformities.

Armed with a more complete understanding of functional organization of bush baby V1, we could investigate the significance of feedforward input from LGN. We developed a method of delivering 200-300 nL of blocking agent into precise locations in LGN that could simultaneously be recorded from and used this technique to selectively

remove either the M or P LGN pathway to V1 while studying orientation and spatial frequency preference in V1. Interestingly, the results of blocking were not similar for the two LGN pathways as originally predicted. P channel inactivation did not affect the orientation preference map in V1, but it resulted in a significant reorganization of spatial frequency preference, with the preference shifting from high toward low spatial frequencies perhaps due to the remaining M channel. In contrast, M channel inactivation resulted in a dramatic reduction in V1 activity. This finding reinforced the significance of a not very widely appreciated difference in thalamocortical connectivity in nocturnal and diurnal primates, namely, that V1 in nocturnal primates may be more heavily dependent on M input than P input. Additionally, this prompted a question of whether blocking the M pathway acted in a purely feedforward manner. We proposed that, in addition to direct effects on V1, the M pathway block set up a reiterative loop of activity reduction between V1 and MT. To be true, this proposal required us to show that MT is dependent on V1 for activity and that removing MT activity reduces activation in V1.

We tested MT dependence on V1 first by blocking retinotopically restricted patches of V1 and observing changes in activity in MT, as part of a collaborative effort. The results of this manipulation suggested that in owl monkeys and bush babies MT is completely dependent on V1 for its main drive. We then initiated investigations of the details of the retinotopic organization in area MT. These investigations demonstrated that MT has retinotopy at both the local and global scale. Moreover, comparison of the CMF in MT and V1 across four primates indicated that scaling across several cortical areas can carry a scaling signature of the main thalamic afferent supplying those areas, even indirectly. These investigations also demonstrated that there are significant anisotropies

in area MT. We saw that cardinal orientations are overrepresented, probably increasing the animal's ability to detect the cardinally oriented stimuli. We also noted that along the horizontal meridian the iso-polar magnification factor is larger than the one devoted to iso-eccentricity. Both of these findings should be taken into consideration when interpreting the MT blocking results.

As our final study, we tested the effect of blocking MT on the functional properties of V1. In support of our hypothesis that reduced activity in MT plays role in deactivation of V1 after M channel block, we found that removing MT activity reduced V1 responses. However, our quantification results were hindered by changes in baseline activation, something that we will need to investigate in future studies.

Future directions

The studies described in this thesis laid important groundwork for additional future studies concerning the functional significance of feedback and feedforward connections to V1. Below are listed several important questions that remain to be answered.

- Would the use of a more powerful ROC based technique allow us to segregate the changes in stimulus dependent activity and baseline activity after MT blocking?
- Would the balance of facilitation/inhibition in the feedback be reversed at lower contrasts, resulting in increased in activation of V1 after MT block?
- Are anisotropies in MT organization reflected in the pattern of feedback effects?

- What effect on MT functional organization does block of the M channel have in nocturnal compared to diurnal primates?
- Would application of more powerful analytic tools allow us to study the functional maps in V1 under the M block condition?

Reference List

Adams DL, Horton JC (2003) Capricious expression of cortical columns in the primate brain. *Nat Neurosci* 6: 113-114

Albright TD (1989) Centrifugal directional bias in the middle temporal visual area (MT) of the macaque. *Vis Neurosci* 2: 177-188

Albright TD, Desimone R (1987) Local precision of visuotopic organization in the middle temporal area (MT) of the macaque. *Experimental Brain Research* 65: 582-592

Alitto HJ, Usrey WM (2008) Origin and dynamics of extraclassical suppression in the lateral geniculate nucleus of the macaque monkey. *Neuron* 57: 135-146

Allison JD, Melzer P, Ding Y, Bonds AB, Casagrande VA (2000) Differential contributions of magnocellular and parvocellular pathways to the contrast response of neurons in bush baby primary visual cortex (V1). *Vis Neurosci* 17: 71-76

Allman JM, Kaas JH (1971) A representation of the visual field in the caudal third of the middle tempral gyrus of the owl monkey (Aotus trivirgatus). *Brain Res* 31: 85-105

Allman JM, Kaas JH, Lane RH (1973) The middle temporal visual area(MT)in the bushbaby, Galago senegalensis. *Brain Research* 57: 197-202

Angelucci A, Bressloff PC (2006) Contribution of feedforward, lateral and feedback connections to the classical receptive field center and extra-classical receptive field surround of primate V1 neurons. *Prog Brain Res* 154: 93-120

Angelucci A, Levitt JB, Lund JS (2002a) Anatomical origins of the classical receptive field and modulatory surround field of single neurons in macaque visual cortical area V1. *Prog Brain Res* 136: 373-388

Angelucci A, Levitt JB, Walton EJ, Hupe JM, Bullier J, Lund JS (2002b) Circuits for local and global signal integration in primary visual cortex. *J Neurosci* 22: 8633-8646

Appelle S (1972) Perception and discrimination as a function of stimulus orientation: the "oblique effect" in man and animals. *Psychol Bull* 78: 266-278

Arieli A, Grinvald A (2002) Optical imaging combined with targeted electrical recordings, microstimulation, or tracer injections. *J Neurosci Methods* 116: 15-28

Arikan R, Blake NM, Erinjeri JP, Woolsey TA, Giraud L, Highstein SM (2002) A method to measure the effective spread of focally injected muscimol into the central nervous system with electrophysiology and light microscopy. *J Neurosci Methods* 118: 51-57

Baker CL, Jr. (1990) Spatial- and temporal-frequency selectivity as a basis for velocity preference in cat striate cortex neurons. *Vis Neurosci* 4: 101-113

Baker TI, Issa NP (2005) Cortical maps of separable tuning properties predict population responses to complex visual stimuli. *J Neurophysiol* 94: 775-787

Barlow HB, Blakemore C, Pettigrew JD (1967) The neural mechanism of binocular depth discrimination. *J Physiol* 193: 327-342

Basole A, White LE, Fitzpatrick D (2003) Mapping multiple features in the population response of visual cortex. *Nature* 423: 986-990

Bauer JA, Jr., Owens DA, Thomas J, Held R (1979) Monkeys show an oblique effect. *Perception* 8: 247-253

Berardi N, Bisti S, Cattaneo A, Fiorentini A, Maffei L (1982) Correlation between the preferred orientation and spatial frequency of neurones in visual areas 17 and 18 of the cat. *J Physiol* 323: 603-618

Berkley MA, Kitterle F, Watkins DW (1975) Grating visibility as a function of orientation and retinal eccentricity. *Vision Res* 15: 239-244

Berman NE, Wilkes ME, Payne BR (1987) Organization of orientation and direction selectivity in areas 17 and 18 of cat cerebral cortex. *J Neurophysiol* 58: 676-699

Blasdel GG (1992) Orientation selectivity, preference, and continuity in monkey striate cortex. *J Neurosci* 12: 3139-3161

Blasdel GG, Salama G (1986) Voltage-sensitive dyes reveal a modular organization in monkey striate cortex. *Nature* 321: 579-585

Bonds AB (1982) An "oblique effect" in the visual evoked potential of the cat. *Exp Brain Res* 46: 151-154

Bonds AB, Casagrande VA, Norton TT, Debruyn EJ (1987) Visual resolution and sensitivity in a nocturnal primate (galago) measured with visual evoked potentials. *Vision Res* 27: 845-857

Bonhoeffer T, Grinvald A (1991) Iso-orientation domains in cat visual cortex are arranged in pinwheel-like patterns. *Nature* 353: 429-431

Bonhoeffer T, Grinvald A (1993) The layout of iso-orientation domains in area 18 of cat visual cortex: optical imaging reveals a pinwheel-like organization. *J Neurosci* 13: 4157-4180

Bonhoeffer T, Kim DS, Malonek D, Shoham D, Grinvald A (1995) Optical imaging of the layout of functional domains in area 17 and across the area 17/18 border in cat visual cortex. *Eur J Neurosci* 7: 1973-1988

Bosking WH, Crowley JC, Fitzpatrick D (2002) Spatial coding of position and orientation in primary visual cortex. *Nat Neurosci* 5: 874-882

Bosking WH, Zhang Y, Schofield B, Fitzpatrick D (1997) Orientation selectivity and the arrangement of horizontal connections in tree shrew striate cortex. *J Neurosci* 17: 2112-2127

Boyd JD, Casagrande VA (1999) Relationships between cytochrome oxidase (CO) blobs in primate primary visual cortex (V1) and the distribution of neurons projecting to the middle temporal area (MT). *J Comp Neurol* 409: 573-591

Boyd JD, Matsubara JA (1996) Laminar and columnar patterns of geniculocortical projections in the cat: relationship to cytochrome oxidase. *J Comp Neurol* 365: 659-682

Bredfeldt CE, Ringach DL (2002) Dynamics of spatial frequency tuning in macaque V1. *J Neurosci* 22: 1976-1984

Bullier J, Hupe JM, James AC, Girard P (2001) The role of feedback connections in shaping the responses of visual cortical neurons. *Prog Brain Res* 134: 193-204

Burkhalter A, Van Essen DC (1986) Processing of color, form and disparity information in visual areas VP and V2 of ventral extrastriate cortex in the macaque monkey. *J Neurosci* 6: 2327-2351

Byas-Smith M, Frolich MA, Votaw JR, Faber TL, Hoffman JM (2002) Cerebral blood flow during propofol induced sedation. *Mol Imaging Biol* 4: 139-146

Campbell FW, Kulikowski JJ (1966) Orientational selectivity of the human visual system. *J Physiol* 187: 437-445

Casagrande V, Khaytin I, Boyd JD (2007) What the evolution of color vision tells us about the function of parallel visual pathways in primates. In *Evolution of the Nervous System*, Butler A (ed) pp In Press.

Casagrande VA, DeBruyn EJ (1982) The Galago visual system: aspects of normal organization and developmental plasticity. In *An animal model: selected topics*, Haines DE (ed) pp 138-162. CRC Press: Boca Raton, FL

Casagrande VA, Ichida JM (2002) The primary visual cortex. In *Adler's physiology of the eye*, Kaufnan PL, Alm A (eds) pp 669-685. Mosby: St.Louise, MO

Casagrande VA, Joseph R (1980) Morphological effects of monocular deprivation and recovery on the dorsal lateral geniculate nucleus in galago. *J Comp Neurol* 194: 413-426

Casagrande VA, Kaas JH (1994) The afferent, intrinsic, and efferent connection of primary visual cortex in primates. In *Primary Visual Cortex of Primates*, Perers A, Rockland K (eds) pp 201-259. Plenum: New York

Casagrande VA, Norton TT (1991) The lateral geniculate nucleus: A review of its physiology and function. In *The Neural Basis of Visual Function*, Leventhal AG (ed) pp 41-84. MacMillan Press: London

Casagrande VA, Xu X (2004) Parallel visual pathways: a comparative perspective. In *The visual neurosciences.*, Chalupa L, Werner LS (eds) MIT Press: Cambridge, MA

Changizi MA, Shimojo S (2005) Parcellation and area-area connectivity as a function of neocortex size. *Brain Behav Evol* 66: 88-98

Chen, X., Jermakowicz, W. J., Khaytin, I, Bernard, M. R., Bonds, A. B., and Casagrande, V. Dynamics of spatial frequency tuning in primate primary visual cortex (V1). Society for Neuroscience Program No. 436.15/F5. 2006.
Ref Type: Abstract

Chklovskii DB, Koulakov AA (2004) Maps in the brain: what can we learn from them? *Annu Rev Neurosci* 27: 369-392

Coletta NJ, Segu P, Tiana CL (1993) An oblique effect in parafoveal motion perception. *Vision Res* 33: 2747-2756

Collins CE, Lyon DC, Kaas JH (2003) Responses of neurons in the middle temporal visual area after long-standing lesions of the primary visual cortex in adult new world monkeys. *J Neurosci* 23: 2251-2264

Collins CE, Xu X, Khaytin I, Kaskan PM, Casagrande VA, Kaas JH (2005) Optical imaging of visually evoked responses in the middle temporal area after deactivation of primary visual cortex in adult primates. *Proc Natl Acad Sci U S A* 102: 5594-5599

Connolly M, Van Essen D (1984) The representation of the visual field in parvicellular and magnocellular layers of the lateral geniculate nucleus in the macaque monkey. *J Comp Neurol* 226: 544-564

Dacey DM, Peterson BB, Robinson FR, Gamlin PD (2003) Fireworks in the primate retina: in vitro photodynamics reveals diverse LGN-projecting ganglion cell types. *Neuron* 37: 15-27

Das A, Gilbert CD (1995) Long-range horizontal connections and their role in cortical reorganization revealed by optical recording of cat primary visual cortex. *Nature* 375: 780-784

Das A, Gilbert CD (1997) Distortions of visuotopic map match orientation singularities in primary visual cortex. *Nature* 387: 594-598

De Valois RL, Yund EW, Hepler N (1982) The orientation and direction selectivity of cells in macaque visual cortex. *Vision Res* 22: 531-544

DeAngelis GC, Freeman RD, Ohzawa I (1994) Length and width tuning of neurons in the cat's primary visual cortex. *J Neurophysiol* 71: 347-374

DeAngelis GC, Ghose GM, Ohzawa I, Freeman RD (1999) Functional micro-organization of primary visual cortex: receptive field analysis of nearby neurons. *J Neurosci* 19: 4046-4064

DeAngelis GC, Ohzawa I, Freeman RD (1993) Spatiotemporal organization of simple-cell receptive fields in the cat's striate cortex. I. General characteristics and postnatal development. *J Neurophysiol* 69: 1091-1117

DeBruyn EJ, Casagrande VA, Beck PD, Bonds AB (1993) Visual resolution and sensitivity of single cells in the primary visual cortex (V1) of a nocturnal primate (bush baby): correlations with cortical layers and cytochrome oxidase patterns. *J Neurophysiol* 69: 3-18

DeBruyn EJ, Wise VL, Casagrande VA (1980) The size and topographic arrangement of retinal ganglion cells in the galago. *Vision Res* 20: 315-327

DeYoe EA, Van Essen DC (1988) Concurrent processing streams in monkey visual cortex. *Trends Neurosci* 11: 219-226

Dragoi V, Sharma J, Sur M (2000) Adaptation-induced plasticity of orientation tuning in adult visual cortex. *Neuron* 28: 287-298

Dubner R, Zeki SM (1971) Response properties and receptive fields of cells in an anatomically defined region of the superior temporal sulcus in the monkey. *Brain Res* 35: 528-532

Duda RO, Hart PE, Stork DG (2001) *Pattern Classification*. Wiley and Sons, Inc: New York,NY

Elston GN, Rosa MG (1997) The occipitoparietal pathway of the macaque monkey: comparison of pyramidal cell morphology in layer III of functionally related cortical visual areas. *Cereb Cortex* 7: 432-452

Everson RM, Prashanth AK, Gabbay M, Knight BW, Sirovich L, Kaplan E (1998) Representation of spatial frequency and orientation in the visual cortex. *Proc Natl Acad Sci U S A* 95: 8334-8338

Felleman DJ, Kaas JH (1984) Receptive-field properties of neurons in middle temporal visual area (MT) of owl monkeys. *J Neurophysiol* 52: 488-513

Felleman DJ, Van Essen DC (1991) Distributed hierarchical processing in the primate cerebral cortex. *Cereb Cortex* 1: 1-47

Ferrera VP, Nealey TA, Maunsell JH (1994) Responses in macaque visual area V4 following inactivation of the parvocellular and magnocellular LGN pathways. *J Neurosci* 14: 2080-2088

Finlay BL, Schiller PH, Volman SF (1976) Meridional differences in orientation sensitivity in monkey striate cortex. *Brain Res* 105: 350-352

Fiorani M, Jr., Gattass R, Rosa MG, Sousa AP (1989) Visual area MT in the Cebus monkey: location, visuotopic organization, and variability. *J Comp Neurol* 287: 98-118

Florence SL, Casagrande VA (1987) Organization of individual afferent axons in layer IV of striate cortex in a primate. *J Neurosci* 7: 3850-3868

Frazor RA, Albrecht DG, Geisler WS, Crane AM (2004) Visual cortex neurons of monkeys and cats: temporal dynamics of the spatial frequency response function. *J Neurophysiol* 91: 2607-2627

Frostig RD, Lieke EE, Ts'o DY, Grinvald A (1990) Cortical functional architecture and local coupling between neuronal activity and the microcirculation revealed by in vivo high-resolution optical imaging of intrinsic signals. *Proc Natl Acad Sci U S A* 87: 6082-6086

Gallyas F (1979) Silver staining of myelin by means of physical development. *Neurol Res* 1: 203-209

Galuske RA, Schmidt KE, Goebel R, Lomber SG, Payne BR (2002) The role of feedback in shaping neural representations in cat visual cortex. *Proc Natl Acad Sci U S A* 99: 17083-17088

Gattass R, Gross CG (1981) Visual topography of striate projection zone (MT) in posterior superior temporal sulcus of the macaque. *J Neurophysiol* 46: 621-638

Gattass R, Nascimento-Silva S, Soares JG, Lima B, Jansen AK, Diogo AC, Farias MF, Botelho MM, Mariani OS, Azzi J, Fiorani M (2005) Cortical visual areas in monkeys: location, topography, connections, columns, plasticity and cortical dynamics. *Philos Trans R Soc Lond B Biol Sci* 360: 709-731

Gattass R, Sousa AP, Rosa MG (1987) Visual topography of V1 in the Cebus monkey. *J Comp Neurol* 259: 529-548

Girard P, Salin PA, Bullier J (1992) Response selectivity of neurons in area MT of the macaque monkey during reversible inactivation of area V1. *J Neurophysiol* 67: 1437-1446

Grinvald A, Lieke EE, Frostig RD, Hildesheim R (1994) Cortical point-spread function and long-range lateral interactions revealed by real-time optical imaging of macaque monkey primary visual cortex. *J Neurosci* 14: 2545-2568

Gros BL, Blake R, Hiris E (1998) Anisotropies in visual motion perception: a fresh look. *J Opt Soc Am A Opt Image Sci Vis* 15: 2003-2011

Heeley DW, Buchanan-Smith HM (1992) Directional acuity for drifting plaids. *Vision Res* 32: 97-104

Hendry SH, Miller KL (1996) Selective expression and rapid regulation of GABAA receptor subunits in geniculocortical neurons of macaque dorsal lateral geniculate nucleus. *Vis Neurosci* 13: 223-235

Horton JC, Adams DL (2005) The cortical column: a structure without a function. *Philos Trans R Soc Lond B Biol Sci* 360: 837-862

Huang L, Shou T, Chen X, Yu H, Sun C, Liang Z (2006) Slab-like functional architecture of higher order cortical area 21a showing oblique effect of orientation preference in the cat. *Neuroimage* 32: 1365-1374

Hubel DH, Wiesel TN (1962) Receptive fields, binocular interaction and functional architecture in the cat's visual cortex. *J Physiol* 160: 106-154

Hubel DH, Wiesel TN (1968) Receptive fields and functional architecture of monkey striate cortex. *J Physiol* 195: 215-243

Hubel DH, Wiesel TN (1969) Anatomical demonstration of columns in the monkey striate cortex. *Nature* 221: 747-750

Hubel DH, Wiesel TN (1974a) Sequence regularity and geometry of orientation columns in the monkey striate cortex. *J Comp Neurol* 158: 267-293

Hubel DH, Wiesel TN (1974b) Uniformity of monkey striate cortex: a parallel relationship between field size, scatter, and magnification factor. *J Comp Neurol* 158: 295-305

Hubel DH, Wiesel TN (1977) Ferrier lecture. Functional architecture of macaque monkey visual cortex. *Proc R Soc Lond B Biol Sci* 198: 1-59

Hubener M, Shoham D, Grinvald A, Bonhoeffer T (1997) Spatial relationships among three columnar systems in cat area 17. *J Neurosci* 17: 9270-9284

Humphrey AL, Albano JE, Norton TT (1977) Organization of ocular dominance in tree shrew striate cortex. *Brain Res* 134: 225-236

Huntsman MM, Leggio MG, Jones EG (1996) Nucleus-specific expression of GABA(A) receptor subunit mRNAs in monkey thalamus. *J Neurosci* 16: 3571-3589

Hupe JM, James AC, Girard P, Lomber SG, Payne BR, Bullier J (2001) Feedback connections act on the early part of the responses in monkey visual cortex. *J Neurophysiol* 85: 134-145

Hupe JM, James AC, Payne BR, Lomber SG, Girard P, Bullier J (1998) Cortical feedback improves discrimination between figure and background by V1, V2 and V3 neurons. *Nature* 394: 784-787

Ionescu DA, Hassler R (1968) Six cell layers in the lateral geniculate body in the night-active prosimian, Galago crassicaudatus. *Brain Res* 10: 281-284

Issa NP, Trepel C, Stryker MP (2000) Spatial frequency maps in cat visual cortex. *J Neurosci* 20: 8504-8514

Jacobs GH, Neitz M, Neitz J (1996) Mutations in S-cone pigment genes and the absence of colour vision in two species of nocturnal primate. *Proc Biol Sci* 263: 705-710

Kaas JH (1996) What comparative studies of neocortex tell us about the human brain. *Rev Bras Biol* 56 Su 1 Pt 2: 315-322

Kaas JH, Huerta MF, Weber JT, Harting JK (1978) Patterns of retinal terminations and laminar organization of the lateral geniculate nucleus of primates. *J Comp Neurol* 182: 517-553

Kaas JH, Krubitzer LA (1992) Area 17 lesions deactivate area MT in owl monkeys. *Vis Neurosci* 9: 399-407

Kaas JH, Lin CS, Casagrande VA (1976) The relay of ipsilateral and contralateral retinal input from the lateral geniculate nucleus to striate cortex in the owl monkey: a transneuronal transport study. *Brain Res* 106: 371-378

Kaas JH, Lyon DC (2001) Visual cortex organization in primates: theories of V3 and adjoining visual areas. *Prog Brain Res* 134: 285-295

Kaas JH, Lyon DC (2007) Pulvinar contributions to the dorsal and ventral streams of visual processing in primates. *Brain Res Rev* 55: 285-296

Kaskan PM, Kaas JH (2007) Cortical connections of the middle temporal and the middle temporal crescent visual areas in prosimian galagos (Otolemur garnetti). *Anat Rec (Hoboken)* 290: 349-366

Kaskan PM, Lu HD, Dillenburger BC, Roe AW, Kaas JH (2007) Intrinsic-signal optical imaging reveals cryptic ocular dominance columns in primary visual cortex of new world owl monkeys. *Front Neurosci* 1: 67-75

Kawamura S, Kubotera N (2004) Ancestral loss of short wave-sensitive cone visual pigment in lorisiform prosimians, contrasting with its strict conservation in other prosimians. *J Mol Evol* 58: 314-321

Kenet T, Bibitchkov D, Tsodyks M, Grinvald A, Arieli A (2003) Spontaneously emerging cortical representations of visual attributes. *Nature* 425: 954-956

Kennedy C, Des Rosiers MH, Sakurada O, Shinohara M, Reivich M, Jehle JW, Sokoloff L (1976) Metabolic mapping of the primary visual system of the monkey by means of the autoradiographic [14C]deoxyglucose technique. *Proc Natl Acad Sci U S A* 73: 4230-4234

Khaytin I, Chen X, Royal DW, Ruiz O, Jermakowicz WJ, Siegel RM, Casagrande VA (2007) Functional Organization of Temporal Frequency Selectivity in Primate Visual Cortex. *Cereb Cortex*

Krubitzer L, Kaas J (1990) Convergence of processing channels in the extrastriate cortex of monkeys. *Vis Neurosci* 5: 609-613

Lachica EA, Beck PD, Casagrande VA (1992) Parallel pathways in macaque monkey striate cortex: anatomically defined columns in layer III. *Proc Natl Acad Sci U S A* 89: 3566-3570

Lachica EA, Beck PD, Casagrande VA (1993) Intrinsic connections of layer III of striate cortex in squirrel monkey and bush baby: correlations with patterns of cytochrome oxidase. *J Comp Neurol* 329: 163-187

LeVay S, Hubel DH, Wiesel TN (1975) The pattern of ocular dominance columns in macaque visual cortex revealed by a reduced silver stain. *J Comp Neurol* 159: 559-576

LeVay S, Nelson SB (1991) Columnar organization of the visual cortex. In *The neural basis of visual function*, Leventhal AG (ed) pp 266-315. CRC Press: Boston

Levitt JB, Kiper DC, Movshon JA (1994a) Receptive fields and functional architecture of macaque V2. *J Neurophysiol* 71: 2517-2542

Levitt JB, Lund JS (2002) The spatial extent over which neurons in macaque striate cortex pool visual signals. *Vis Neurosci* 19: 439-452

Levitt JB, Yoshioka T, Lund JS (1994b) Intrinsic cortical connections in macaque visual area V2: evidence for interaction between different functional streams. *J Comp Neurol* 342: 551-570

Lin CS, Weller RE, Kaas JH (1982) Cortical connections of striate cortex in the owl monkey. *J Comp Neurol* 211: 165-176

Livingstone M, Hubel D (1988) Segregation of form, color, movement, and depth: anatomy, physiology, and perception. *Science* 240: 740-749

Lu HD, Roe AW (2008) Functional organization of color domains in V1 and V2 of Macaque monkey revealed by optical imaging. *Cereb Cortex* 18: 516-533

Maffei L, Fiorentini A (1977) Spatial frequency rows in the straite visual cortex. *Vision Res* 17: 257-264

Malach R, Schirman TD, Harel M, Tootell RB, Malonek D (1997) Organization of intrinsic connections in owl monkey area MT. *Cereb Cortex* 7: 386-393

Malach R, Tootell RB, Malonek D (1994) Relationship between orientation domains, cytochrome oxidase stripes, and intrinsic horizontal connections in squirrel monkey area V2. *Cereb Cortex* 4: 151-165

Malonek D, Grinvald A (1996) Interactions between electrical activity and cortical microcirculation revealed by imaging spectroscopy: implications for functional brain mapping. *Science* 272: 551-554

Malonek D, Tootell RB, Grinvald A (1994) Optical imaging reveals the functional architecture of neurons processing shape and motion in owl monkey area MT. *Proc Biol Sci* 258: 109-119

Malpeli JG (1983) Activity of cells in area 17 of the cat in absence of input from layer a of lateral geniculate nucleus. *J Neurophysiol* 49: 595-610

Malpeli JG, Baker FH (1975) The representation of the visual field in the lateral geniculate nucleus of Macaca mulatta. *J Comp Neurol* 161: 569-594

Malpeli JG, Lee D, Baker FH (1996) Laminar and retinotopic organization of the macaque lateral geniculate nucleus: magnocellular and parvocellular magnification functions. *J Comp Neurol* 375: 363-377

Malpeli JG, Schiller PH, Colby CL (1981) Response properties of single cells in monkey striate cortex during reversible inactivation of individual lateral geniculate laminae. *J Neurophysiol* 46: 1102-1119

Mansfield RJ (1974) Neural basis of orientation perception in primate vision. *Science* 186: 1133-1135

Mansfield RJ, Ronner SF (1978) Orientation anistropy in monkey visual cortex. *Brain Res* 149: 229-234

Mante V, Carandini M (2005) Mapping of stimulus energy in primary visual cortex. *J Neurophysiol* 94: 788-798

Matthews N, Qian N (1999) Axis-of-motion affects direction discrimination, not speed discrimination. *Vision Res* 39: 2205-2211

Maunsell JH, Nealey TA, DePriest DD (1990) Magnocellular and parvocellular contributions to responses in the middle temporal visual area (MT) of the macaque monkey. *J Neurosci* 10: 3323-3334

Maunsell JH, Van Essen DC (1983) The connections of the middle temporal visual area (MT) and their relationship to a cortical hierarchy in the macaque monkey. *J Neurosci* 3: 2563-2586

Mazer JA, Vinje WE, McDermott J, Schiller PH, Gallant JL (2002) Spatial frequency and orientation tuning dynamics in area V1. *Proc Natl Acad Sci U S A* 99: 1645-1650

Merigan WH, Byrne CE, Maunsell JH (1991a) Does primate motion perception depend on the magnocellular pathway? *J Neurosci* 11: 3422-3429

Merigan WH, Katz LM, Maunsell JH (1991b) The effects of parvocellular lateral geniculate lesions on the acuity and contrast sensitivity of macaque monkeys. *J Neurosci* 11: 994-1001

Merigan WH, Maunsell JH (1990) Macaque vision after magnocellular lateral geniculate lesions. *Vis Neurosci* 5: 347-352

Merigan WH, Maunsell JH (1993) How parallel are the primate visual pathways? *Annu Rev Neurosci* 16: 369-402

Mignard M, Malpeli JG (1991) Paths of information flow through visual cortex. *Science* 251: 1249-1251

Montero VM (1980) Patterns of connections from the striate cortex to cortical visual areas in superior temporal sulcus of macaque and middle temporal gyrus of owl monkey. *J Comp Neurol* 189: 45-59

Moore BD, Alitto HJ, Usrey WM (2005) Orientation tuning, but not direction selectivity, is invariant to temporal frequency in primary visual cortex. *J Neurophysiol* 94: 1336-1345

Movshon JA, Adelson EH, Gizzi MS, Newsome WT (1985) The analysis of moving visual patterns. In *Pattern Recognition Mechanisms*, Chagas C, Gattass R, Gross C (eds) pp 117-151. Vatican Press: Rome

Munk MH, Nowak LG, Girard P, Chounlamountri N, Bullier J (1995) Visual latencies in cytochrome oxidase bands of macaque area V2. *Proc Natl Acad Sci U S A* 92: 988-992

Myerson J, Manis PB, Miezin FM, Allman JM (1977) Magnification in striate cortex and retinal ganglion cell layer of owl monkey: a quantitative comparison. *Science* 198: 855-857

Nassi JJ, Lyon DC, Callaway EM (2006) The parvocellular LGN provides a robust disynaptic input to the visual motion area MT. *Neuron* 50: 319-327

Nealey TA, Maunsell JH (1994) Magnocellular and parvocellular contributions to the responses of neurons in macaque striate cortex. *J Neurosci* 14: 2069-2079

Norden JJ (1979) Some aspects of the organization of the lateral geniculate nucleus in Galago senegalensis revealed by using horseradish peroxidase to label relay neurons. *Brain Res* 174: 193-206

Norton TT, Casagrande VA (1982) Laminar organization of receptive-field properties in lateral geniculate nucleus of bush baby (Galago crassicaudatus). *J Neurophysiol* 47: 715-741

Norton TT, Casagrande VA, Irvin GE, Sesma MA, Petry HM (1988) Contrast-sensitivity functions of W-, X-, and Y-like relay cells in the lateral geniculate nucleus of bush baby, Galago crassicaudatus. *J Neurophysiol* 59: 1639-1656

O'Keefe LP, Levitt JB, Kiper DC, Shapley RM, Movshon JA (1998) Functional organization of owl monkey lateral geniculate nucleus and visual cortex. *J Neurophysiol* 80: 594-609

Ogawa K, Uema T, Motohashi N, Nishikawa M, Takano H, Hiroki M, Imabayashi E, Ohnishi T, Inoue T, Takayama Y, Takeda M, Matsuda H, Andoh T, Yamada Y (2003) Neural mechanism of propofol anesthesia in severe depression: a positron emission tomographic study. *Anesthesiology* 98: 1101-1111

Orbach HS, Cohen LB, Grinvald A (1985) Optical mapping of electrical activity in rat somatosensory and visual cortex. *J Neurosci* 5: 1886-1895

Orban GA, Kennedy H (1981) The influence of eccentricity on receptive field types and orientation selectivity in areas 17 and 18 of the cat. *Brain Res* 208: 203-208

Ordy JM, Samorajski T (1968) Visual acuity and ERG-CFF in relation to the morphologic organization of the retina among diurnal and nocturnal primates. *Vision Res* 8: 1205-1225

Payne BR, Lomber SG, Villa AE, Bullier J (1996) Reversible deactivation of cerebral network components. *Trends Neurosci* 19: 535-542

Perry VH, Cowey A (1985) The ganglion cell and cone distributions in the monkey's retina: implications for central magnification factors. *Vision Res* 25: 1795-1810

Perry VH, Oehler R, Cowey A (1984) Retinal ganglion cells that project to the dorsal lateral geniculate nucleus in the macaque monkey. *Neuroscience* 12: 1101-1123

Pessoa VF, Abrahao JC, Pacheco RA, Pereira LC, Magalhaes-Castro B, Saraiva PE (1992) Relative sizes of cortical visual areas in marmosets: functional and phylogenetic implications. *Exp Brain Res* 88: 459-462

Pinon MC, Gattass R, Sousa AP (1998) Area V4 in Cebus monkey: extent and visuotopic organization. *Cereb Cortex* 8: 685-701

Poggio GF, Fischer B (1977) Binocular interaction and depth sensitivity in striate and prestriate cortex of behaving rhesus monkey. *J Neurophysiol* 40: 1392-1405

Polimeni JR, Granquist-Fraser D, Wood RJ, Schwartz EL (2005) Physical limits to spatial resolution of optical recording: clarifying the spatial structure of cortical hypercolumns. *Proc Natl Acad Sci U S A* 102: 4158-4163

Ponce CR, Lomber SG, Born RT (2008) Integrating motion and depth via parallel pathways. *Nat Neurosci* 11: 216-223

Purpura K, Kaplan E, Shapley RM (1988) Background light and the contrast gain of primate P and M retinal ganglion cells. *Proc Natl Acad Sci U S A* 85: 4534-4537

Purushothaman G, Bradley DC (2005) Neural population code for fine perceptual decisions in area MT. *Nat Neurosci* 8: 99-106

Purushothaman, G., Khaytin, I., and Casagrande, V. A. Detection and classification methods for optical imagies. Abstract Viewer 451.3. 2007.
Ref Type: Abstract

Ramsden BM, Hung CP, Roe AW (2001) Real and illusory contour processing in area V1 of the primate: a cortical balancing act. *Cereb Cortex* 11: 648-665

Rao SC, Toth LJ, Sur M (1997) Optically imaged maps of orientation preference in primary visual cortex of cats and ferrets. *J Comp Neurol* 387: 358-370

Ratzlaff EH, Grinvald A (1991) A tandem-lens epifluorescence macroscope: hundred-fold brightness advantage for wide-field imaging. *J Neurosci Methods* 36: 127-137

Reid RC, Alonso JM (1996) The processing and encoding of information in the visual cortex. *Curr Opin Neurobiol* 6: 475-480

Ringach DL, Hawken MJ, Shapley R (1997) Dynamics of orientation tuning in macaque primary visual cortex. *Nature* 387: 281-284

Rockland KS (1992) Laminar distribution of neurons projecting from area V1 to V2 in macaque and squirrel monkeys. *Cereb Cortex* 2: 38-47

Rockland KS, Pandya DN (1979) Laminar origins and terminations of cortical connections of the occipital lobe in the rhesus monkey. *Brain Res* 179: 3-20

Rodman HR, Gross CG, Albright TD (1989) Afferent basis of visual response properties in area MT of the macaque. I. Effects of striate cortex removal. *J Neurosci* 9: 2033-2050

Rodman HR, Gross CG, Albright TD (1990) Afferent basis of visual response properties in area MT of the macaque. II. Effects of superior colliculus removal. *J Neurosci* 10: 1154-1164

Roe AW, Fritsches K, Pettigrew JD (2005) Optical imaging of functional organization of V1 and V2 in marmoset visual cortex. *Anat Rec A Discov Mol Cell Evol Biol* 287: 1213-1225

Rolls ET, Cowey A (1970) Topography of the retina and striate cortex and its relationship to visual acuity in rhesus monkeys and squirrel monkeys. *Exp Brain Res* 10: 298-310

Rosa MG (1997) Visuotopic organization of primate extrastriate cortex. In *Cerebral Cortex Vol 12: Extrastriate Cortex in Primates*,

Rosa MG, Casagrande VA, Preuss T, Kaas JH (1997) Visual field representation in striate and prestriate cortices of a prosimian primate (Galago garnetti). *J Neurophysiol* 77: 3193-3217

Rosa MG, Soares JG, Fiorani M, Jr., Gattass R (1993) Cortical afferents of visual area MT in the Cebus monkey: possible homologies between New and Old World monkeys. *Vis Neurosci* 10: 827-855

Rosa MG, Tweedale R, Elston GN (2000) Visual responses of neurons in the middle temporal area of new world monkeys after lesions of striate cortex. *J Neurosci* 20: 5552-5563

Rose D, Blakemore C (1974) An analysis of orientation selectivity in the cat's visual cortex. *Exp Brain Res* 20: 1-17

Rowe MH, Benevento LA, Rezak M (1978) Some observations on the patterns of segregated geniculate inputs to the visual cortex in New World primates: an autoradiographic study. *Brain Res* 159: 371-378

Sakas DE, Charnvises K, Borges LF, Zervas NT (1990) Biologically inert synthetic dural substitutes. Appraisal of a medical-grade aliphatic polyurethane and a polysiloxane-carbonate block copolymer. *J Neurosurg* 73: 936-941

Sandell JH, Schiller PH (1982) Effect of cooling area 18 on striate cortex cells in the squirrel monkey. *J Neurophysiol* 48: 38-48

Sceniak MP, Hawken MJ, Shapley R (2001) Visual spatial characterization of macaque V1 neurons. *J Neurophysiol* 85: 1873-1887

Sceniak MP, Ringach DL, Hawken MJ, Shapley R (1999) Contrast's effect on spatial summation by macaque V1 neurons. *Nat Neurosci* 2: 733-739

Schein SJ, de Monasterio FM (1987) Mapping of retinal and geniculate neurons onto striate cortex of macaque. *J Neurosci* 7: 996-1009

Schiller PH, Finlay BL, Volman SF (1976) Quantitative studies of single-cell properties in monkey striate cortex. I. Spatiotemporal organization of receptive fields. *J Neurophysiol* 39: 1288-1319

Schiller PH, Logothetis NK, Charles ER (1990) Functions of the colour-opponent and broad-band channels of the visual system. *Nature* 343: 68-70

Shaw C, Cynader M (1986) Laminar distribution of receptors in monkey (Macaca fascicularis) geniculostriate system. *J Comp Neurol* 248: 301-312

Shipp S, Zeki S (1989) The Organization of Connections between Areas V5 and V1 in Macaque Monkey Visual Cortex. *Eur J Neurosci* 1: 309-332

Shmuel A, Korman M, Sterkin A, Harel M, Ullman S, Malach R, Grinvald A (2005) Retinotopic axis specificity and selective clustering of feedback projections from V2 to V1 in the owl monkey. *J Neurosci* 25: 2117-2131

Shoham D, Hubener M, Schulze S, Grinvald A, Bonhoeffer T (1997) Spatio-temporal frequency domains and their relation to cytochrome oxidase staining in cat visual cortex. *Nature* 385: 529-533

Siegel RM, Duann JR, Jung TP, Sejnowski T (2007) Spatiotemporal dynamics of the functional architecture for gain fields in inferior parietal lobule of behaving monkey. *Cereb Cortex* 17: 378-390

Siegel RM, Raffi M, Phinney RE, Turner JA, Jando G (2003) Functional architecture of eye position gain fields in visual association cortex of behaving monkey. *J Neurophysiol* 90: 1279-1294

Silveira LC, Picanco-Diniz CW, Sampaio LF, Oswaldo-Cruz E (1989) Retinal ganglion cell distribution in the cebus monkey: a comparison with the cortical magnification factors. *Vision Res* 29: 1471-1483

Sincich LC, Park KF, Wohlgemuth MJ, Horton JC (2004) Bypassing V1: a direct geniculate input to area MT. *Nat Neurosci*

Sirovich L, Uglesich R (2004) The organization of orientation and spatial frequency in primary visual cortex. *Proc Natl Acad Sci U S A* 101: 16941-16946

Skeen LC, Humphrey AL, Norton TT, Hall WC (1978) Deoxyglucose mapping of the orientation column system in the striate cortex of the tree shrew, Tupaia glis. *Brain Res* 142: 538-545

Slovin H, Arieli A, Hildesheim R, Grinvald A (2002) Long-term voltage-sensitive dye imaging reveals cortical dynamics in behaving monkeys. *J Neurophysiol* 88: 3421-3438

Stepniewska I, Qi HX, Kaas JH (1999) Do superior colliculus projection zones in the inferior pulvinar project to MT in primates? *Eur J Neurosci* 11: 469-480

Stevens CF (2001) An evolutionary scaling law for the primate visual system and its basis in cortical function. *Nature* 411: 193-195

Stiers P, Peeters R, Lagae L, Van Hecke P, Sunaert S (2006) Mapping multiple visual areas in the human brain with a short fMRI sequence. *Neuroimage* 29: 74-89

Swindale NV (2004) How different feature spaces may be represented in cortical maps. *Network* 15: 217-242

Swindale NV, Shoham D, Grinvald A, Bonhoeffer T, Hubener M (2000) Visual cortex maps are optimized for uniform coverage. *Nat Neurosci* 3: 822-826

Timney BN, Muir DW (1976) Orientation anisotropy: incidence and magnitude in Caucasian and Chinese subjects. *Science* 193: 699-701

Tolhurst DJ, Dean AF, Thompson ID (1981) Preferred direction of movement as an element in the organization of cat visual cortex. *Exp Brain Res* 44: 340-342

Tolhurst DJ, Thompson ID (1982) Organization of neurones preferring similar spatial frequencies in cat striate cortex. *Exp Brain Res* 48: 217-227

Tootell RB, Hamilton SL, Silverman MS (1985) Topography of cytochrome oxidase activity in owl monkey cortex. *J Neurosci* 5: 2786-2800

Tootell RB, Hamilton SL, Silverman MS, Switkes E (1988a) Functional anatomy of macaque striate cortex. I. Ocular dominance, binocular interactions, and baseline conditions. *J Neurosci* 8: 1500-1530

Tootell RB, Hamilton SL, Switkes E (1988b) Functional anatomy of macaque striate cortex. IV. Contrast and magno-parvo streams. *J Neurosci* 8: 1594-1609

Tootell RB, Silverman MS, De Valois RL (1981) Spatial frequency columns in primary visual cortex. *Science* 214: 813-815

Tootell RB, Silverman MS, Hamilton SL, De Valois RL, Switkes E (1988c) Functional anatomy of macaque striate cortex. III. Color. *J Neurosci* 8: 1569-1593

Tootell RB, Silverman MS, Hamilton SL, Switkes E, De Valois RL (1988d) Functional anatomy of macaque striate cortex. V. Spatial frequency. *J Neurosci* 8: 1610-1624

Tootell RB, Switkes E, Silverman MS, Hamilton SL (1988e) Functional anatomy of macaque striate cortex. II. Retinotopic organization. *J Neurosci* 8: 1531-1568

Toth LJ, Rao SC, Kim DS, Somers D, Sur M (1996) Subthreshold facilitation and suppression in primary visual cortex revealed by intrinsic signal imaging. *Proc Natl Acad Sci U S A* 93: 9869-9874

Ts'o DY, Frostig RD, Lieke EE, Grinvald A (1990) Functional organization of primate visual cortex revealed by high resolution optical imaging. *Science* 249: 417-420

Ts'o DY, Roe AW, Gilbert CD (2001) A hierarchy of the functional organization for color, form and disparity in primate visual area V2. *Vision Res* 41: 1333-1349

Ungerleider LG, Desimone R (1986) Cortical connections of visual area MT in the macaque. *J Comp Neurol* 248: 190-222

Van Essen DC, Maunsell JH (1980) Two-dimensional maps of the cerebral cortex. *J Comp Neurol* 191: 255-281

Van Essen DC, Maunsell JH, Bixby JL (1981) The middle temporal visual area in the macaque: myeloarchitecture, connections, functional properties and topographic organization. *J Comp Neurol* 199: 293-326

Van Essen DC, Newsome WT, Maunsell JH (1984) The visual field representation in striate cortex of the macaque monkey: asymmetries, anisotropies, and individual variability. *Vision Res* 24: 429-448

Van Hooser SD, Heimel JA, Chung S, Nelson SB (2006) Lack of Patchy Horizontal Connectivity in Primary Visual Cortex of a Mammal without Orientation Maps. *Journal of Neuroscience* 26: 7680-7692

Van Hooser SD, Heimel JA, Chung S, Nelson SB, Toth LJ (2005) Orientation selectivity without orientation maps in visual cortex of a highly visual mammal. *J Neurosci* 25: 19-28

Vandenbussche E, Orban GA (1983) Meridional variations in the line orientation discrimination of the cat. *Behav Brain Res* 9: 237-255

Vandenbussche E, Vogels R, Orban GA (1986) Human orientation discrimination: changes with eccentricity in normal and amblyopic vision. *Invest Ophthalmol Vis Sci* 27: 237-245

Vanduffel W, Payne BR, Lomber SG, Orban GA (1997) Functional impact of cerebral connections. *Proc Natl Acad Sci U S A* 94: 7617-7620

Vidyasagar TR, Kulikowski JJ, Lipnicki DM, Dreher B (2002) Convergence of parvocellular and magnocellular information channels in the primary visual cortex of the macaque. *Eur J Neurosci* 16: 945-956

Wall JT, Symonds LL, Kaas JH (1982) Cortical and subcortical projections of the middle temporal area (MT) and adjacent cortex in galagos. *J Comp Neurol* 211: 193-214

Walls GL (1953) The lateral geniculate nucleus and visual histophysiology. *Univ Calif Publs Physiol* 9: 1-100

Wassle H, Grunert U, Rohrenbeck J, Boycott BB (1989) Cortical magnification factor and the ganglion cell density of the primate retina. *Nature* 341: 643-646

Wassle H, Grunert U, Rohrenbeck J, Boycott BB (1990) Retinal ganglion cell density and cortical magnification factor in the primate. *Vision Res* 30: 1897-1911

Weliky M, Bosking WH, Fitzpatrick D (1996) A systematic map of direction preference in primary visual cortex. *Nature* 379: 725-728

Weller RE, Kaas JH (1983) Retinotopic patterns of connections of area 17 with visual areas V-II and MT in macaque monkeys. *J Comp Neurol* 220: 253-279

Weller RE, Wall JT, Kaas JH (1984) Cortical connections of the middle temporal visual area (MT) and the superior temporal cortex in owl monkeys. *J Comp Neurol* 228: 81-104

Westheimer G (2003) The distribution of preferred orientations in the peripheral visual field. *Vision Res* 43: 53-57

Wikler KC, Rakic P (1990) Distribution of photoreceptor subtypes in the retina of diurnal and nocturnal primates. *J Neurosci* 10: 3390-3401

Wilson JR, Sherman SM (1976) Receptive-field characteristics of neurons in cat striate cortex: Changes with visual field eccentricity. *J Neurophysiol* 39: 512-533

Xu X, Anderson TJ, Casagrande VA (2007) How do functional maps in primary visual cortex vary with eccentricity? *J Comp Neurol* 501: 741-755

Xu X, Bosking W, Sary G, Stefansic J, Shima D, Casagrande V (2004a) Functional organization of visual cortex in the owl monkey. *J Neurosci* 24: 6237-6247

Xu X, Bosking WH, White LE, Fitzpatrick D, Casagrande VA (2005) Functional Organization of Visual Cortex in the Prosimian Bush Baby Revealed by Optical Imaging of Intrinsic Signals. *J Neurophysiol*

Xu, X., Boyd, J. D., Gallucci, M., Emeric, E., Barahimi, B., Stefansic, J., Shima, D., Melzer, P., Allison, J. D., Bonds, A. B., and Casagrande, V. A. Spatial frequency preference maps of primate visual cortex revealed by optical imaging of intrinsic signals. J Vision 3[9]. 2003.
Ref Type: Abstract

Xu X, Collins CE, Kaskan PM, Khaytin I, Kaas JH, Casagrande VA (2004b) Optical imaging of visually evoked responses in prosimian primates reveals conserved features of the middle temporal visual area. *Proc Natl Acad Sci U S A* 101: 2566-2571

Xu X, Collins CE, Khaytin I, Kaas JH, Casagrande VA (2006) Unequal representation of cardinal vs. oblique orientations in the middle temporal visual area. *Proc Natl Acad Sci U S A* 103: 17490-17495

Xu X, Ichida J, Shostak Y, Bonds AB, Casagrande VA (2002) Are primate lateral geniculate nucleus (LGN) cells really sensitive to orientation or direction? *Vis Neurosci* 19: 97-108

Yabuta NH, Sawatari A, Callaway EM (2001) Two functional channels from primary visual cortex to dorsal visual cortical areas. *Science* 292: 297-300

Yamada ES, Marshak DW, Silveira LC, Casagrande VA (1998) Morphology of P and M retinal ganglion cells of the bush baby. *Vision Res* 38: 3345-3352

Zeki S, Shipp S (1988) The functional logic of cortical connections. *Nature* 335: 311-317